

# Optical, electrical, and X-ray-structural studies on Verneuil-grown SrTiO<sub>3</sub> single crystal: Annealing study

S. Mochizuki<sup>a,\*</sup>, F. Fujishiro<sup>a</sup>, K. Shibata<sup>a</sup>, A. Ogi<sup>b</sup>, T. Konya<sup>b</sup>, K. Inaba<sup>b</sup>

<sup>a</sup>Department of Physics, College of Humanities and Sciences, Nihon University, 3–25–40 Sakurajosui, Setagaya-ku, Tokyo 156–8550, Japan

<sup>b</sup>Rigaku Corporation, 3–9–12 Matsubara-cho, Akishima, Tokyo 196–8666, Japan

## Abstract

In order to clarify crystal defect effects on the physical phenomena observed for a SrTiO<sub>3</sub> single crystal grown by Verneuil method, the optical density and photoluminescence spectra, complex impedance spectra, and crystal structure were fully studied for the as-grown crystal boule. The as-grown crystal boule consists of a shell (which is colorless transparent and electrically good insulator) and a core (which is dark blue and has a high electrical conductivity ( $>10^{-3}\Omega^{-1}\text{cm}^{-1}$ ), and a colossal static dielectric constant ( $>10^6$ ) at room temperature). The as-grown single crystal was then annealed at 973 K in an Ar–H<sub>2</sub> gas stream. With the progressing of annealing, the as-grown single crystal becomes colorless-transparent insulator and the static dielectric constant decreases down to approximately 300 at room temperature. The X-ray crystallographic studies indicate that the crystallinity is almost independent of the annealing, while the dielectric property is considerably affected by the annealing. A model on the basis of a (Ti<sup>3+</sup>–oxygen vacancy) complex defect is proposed for explaining the observed properties of SrTiO<sub>3</sub>.

© 2007 Elsevier B.V. All rights reserved.

**Keywords:** Oxygen defect; Non-stoichiometry; X-ray topograph; Photoluminescence; Quantum paraelectricity

## 1. Introduction

There has been a considerable number of experimental research on the quantum paraelectricity [1,2], photo-excitation [3–5] and photo-induced phenomena [3,5] in SrTiO<sub>3</sub>. Like cases for other transition metal oxides, a SrTiO<sub>3</sub> single crystal contains crystal defects which affect considerably its physical properties. For example, we have frequently observed specimen-dependent-static dielectric constant, photoluminescence (PL) spectra in its shape and intensity. Most of the recent workers use commercially available colorless transparent SrTiO<sub>3</sub> crystals as specimens. The crystals are usually prepared as follows. Using nominally pure SrTiO<sub>3</sub> powder (approximately 99.99%) as a starting material, a SrTiO<sub>3</sub> single crystal boule is grown by the Verneuil method. The obtained single crystal boule is black at a glance. After annealing at about 1000 K in a

reducing gas atmosphere, the crystal boule becomes colorless transparent [6]. The annealed crystal boule is cut into several parallel plates followed by mechanical polishing to optical flats, which is supplied to many workers as a substrate crystal for thin film deposition and as a specimen for different studies. The purity of starting material powder, the crystal growth apparatus, and the cutting and polishing processes depend on the crystal manufacture company. Such differences are thought to be the main causes for the observed specimen-dependent properties of real SrTiO<sub>3</sub> single crystals. Crystal defects may also affect the photoelectric and photodielectric properties. For instance, photo-generated carriers (electrons and holes) tend to stay and to accumulate around crystal defects, and they may display apparent phenomena, which are not present in a perfect SrTiO<sub>3</sub> single crystal. Such specimen-dependent properties and extrinsic phenomena have led many researchers astray. In the present study, we study systematically the annealing effects on the structural, electrical, and optical properties of as-grown SrTiO<sub>3</sub> crystal.

\*Corresponding author. Tel.: +81 3 5317 9771; fax: +81 3 5317 9771.

E-mail address: [motizuki@physics.chs.nihon-u.ac.jp](mailto:motizuki@physics.chs.nihon-u.ac.jp) (S. Mochizuki).

## 2. Experimental

The optical density (OD) and PL spectra were measured by two optical multi-channel analyzer systems. The optical measurement systems are previously described in Ref. [3]. The complex impedance measurements were performed with a LCR meter (Kokuyo LC-605). Advanced Thin film X-ray Diffractometer (Rigaku ATX-E) and Curved IP 2-Dimensional X-ray Diffractometer (Rigaku D/MAX RAPID) were used for X-ray diffraction studies.

## 3. Results and discussion

Fig. 1(a) shows the side view of a  $\text{SrTiO}_3$  single crystal boule grown by the Verneuil method. The chemical purity of the starting material  $\text{SrTiO}_3$  powder was 99.99%.

Main impurities are Al, Ca, Ba, Fe, and Cu. Since Ba is volatile at high temperature, the concentration of Ba in the boule is smaller than that in the starting material powder. The boule looks black. When the  $\text{SrTiO}_3$  boule was cut perpendicular to the growth axis [100] using a wire saw, the boule tends to fracture. The brittleness is due to a thermal stress whose magnitude depends on the crystal growth condition. Fig. 1(b) shows one of the fractured surfaces of the fragment, as a typical result. We can see a colorless transparent shell, which is electrically insulating ( $\sigma < 10^{-8} \Omega^{-1}\text{cm}^{-1}$ ) and a dark blue core which is conductive ( $\sigma \geq 10^{-3} \Omega^{-1}\text{cm}^{-1}$ ). The thickness of the shell was about 2 mm for this boule. Both the degree of such blue-color unevenness and the shell thickness also depend on the crystal growth condition. The blue color thins down with leaving from the core center. The electrical conductivity also tends to decrease with leaving from the core center.

The complex impedance ( $Z = \text{Re } Z + i \text{Im } Z$ ) was measured for an as-grown  $\text{SrTiO}_3$  single crystal with Au electrodes. It is found that both the real part of the conductivity,  $\text{Re } \sigma$ , and the real part of the dielectric constant,  $\text{Re } \epsilon$ , tend to decrease with leaving from the core

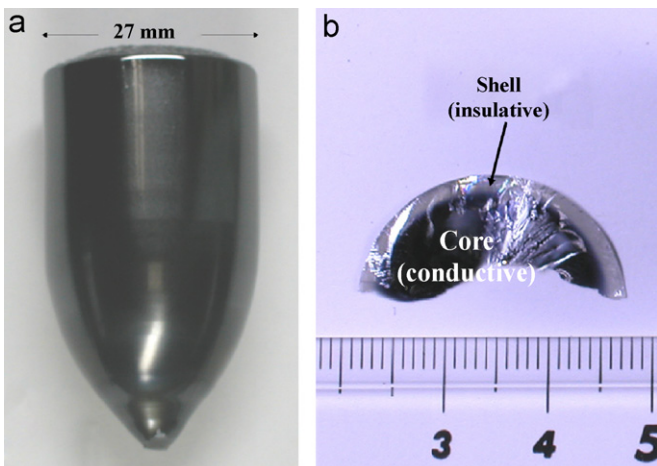


Fig. 1. The as-grown  $\text{SrTiO}_3$  single crystal boule: (a) side view and (b) fractured surface.

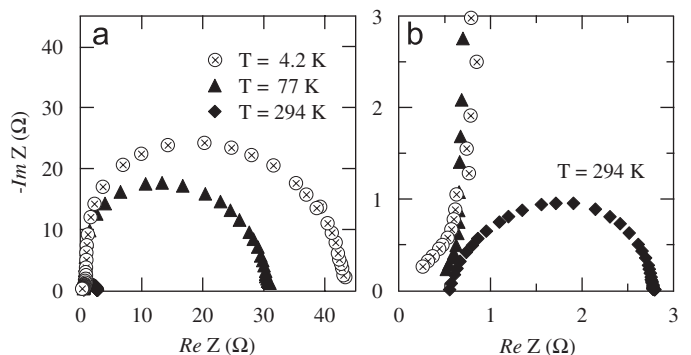


Fig. 2. Impedance complex plane plots for the as-grown  $\text{SrTiO}_3$  crystal at different temperatures.

center. Fig. 2(a) shows the impedance complex plane plots for a highly conductive as-grown  $\text{SrTiO}_3$  single crystal plate at 294, 77, and 4.2 K. Each curve is not a perfect semicircle but an elliptical arc without the zero intercept, which implies that the impedance curve consists of some components of arc. This suggests that the equivalent circuit should be considered as two parallel capacitance  $C$ -resistance  $R$  elements connected in serial at least. Fig. 2(b) shows the expanded view of the high frequency  $Z$  data near the origin. As seen in the left-hand side of the arc, the impedance plot shifts to the origin (the high frequency limit) with decreasing temperature, growing an extra arc at the high frequency side. The  $\text{Re } \epsilon$  and  $\text{Re } \sigma$  at 294 K are  $1.2 \times 10^6$  and  $1.3 \times 10^{-2} \Omega^{-1}\text{cm}^{-1}$  at 1 kHz, respectively. Similar colossal dielectric constant ( $\geq 10^5$ ) has been already observed for oxygen-deficient  $\text{BaTiO}_3$  which is conductive [7]. The complex impedance plot has been carried out for a colorless transparent  $\text{SrTiO}_3$  crystal at 294 K. This crystal was obtained by fully annealing at 973 K in Ar-H<sub>2</sub> mixture gas stream, which is almost the same crystal as the commercially available one. The  $\text{Re } \epsilon$  and  $\text{Re } \sigma$  of this crystal at 1 kHz are 342 and  $1.6 \times 10^{-9} \Omega^{-1}\text{cm}^{-1}$ , respectively. The results obtained for the as-grown and fully annealed  $\text{SrTiO}_3$  crystals indicate that the ellipticity of the  $Z$  curve relates to oxygen deficiency in the as-grown  $\text{SrTiO}_3$  crystal.

The as-grown crystal plates cut from the core were annealed at 973 K in a Ar-H<sub>2</sub> mixture gas stream for desired times. The silver was evaporated on both sides of the plate surfaces as electrodes. The cross-section and thickness of the specimens are  $1\text{cm}^2$  and 0.5 mm, respectively. At different stages of annealing, the complex impedance was measured at room temperature in a frequency range 42 Hz–1 MHz. The results of  $R$  and  $C$  at 1 kHz are shown in Fig. 3.

These results suggest that the enhanced conductivity and colossal dielectric constant are closely connected to crystal defects. Through the annealing study, it is found that fully annealed transparent crystal has different values of  $\text{Re } \sigma$  and  $\text{Re } \epsilon$ , depending on the original position in the crystal boule. Incidentally, the ferroelectric-like hysteresis loop has been clearly observed for the as-grown crystal and it comes

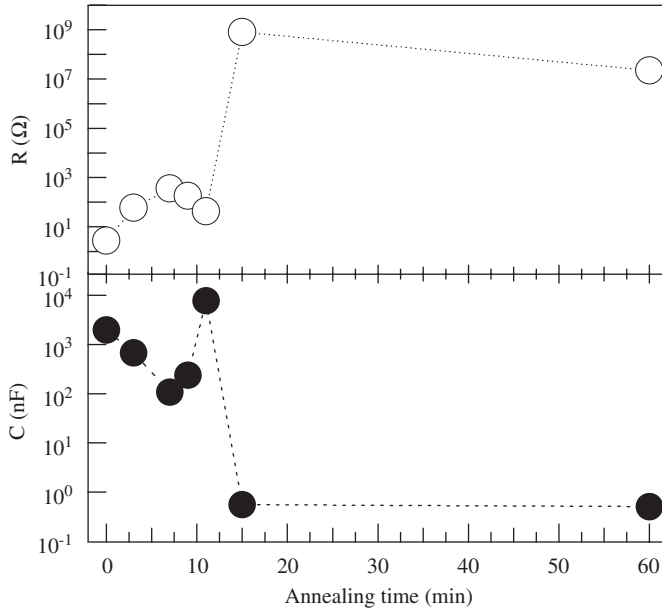


Fig. 3. Annealing time dependence of the  $C$  and  $R$  for the as-grown  $\text{SrTiO}_3$  crystal. The crystals were sputtered with Au electrodes.

to disappear at the early stage of annealing. Such strange changes seem to be similar to the self-healing phenomenon of  $\text{Re}\sigma$  during thermal reduction of a colorless transparent  $\text{SrTiO}_3$  crystal [8]. It is interpreted the phenomenon to be related to the redistribution of Sr and/or  $\text{SrO}$  complexes in close neighborhoods at the surfaces and subsequent solid state reactions leading to a chemical inhomogeneous microscopic near-surface region which is characterized by non-Perovskite phases.

The OD and PL spectra were also measured at different temperatures as a function of annealing time: preliminary results were reported in Ref. [6]. The spectra for the as-grown crystal and fully annealed one are shown in Fig. 4. Below the energy gap of 3.2 eV, OD spectrum of the as-grown crystal shows many absorptions due to in-gap states which can act as luminescence center. The oxygen defects (for example,  $\text{Ti}^{3+}$ –oxygen vacancy complex) act as PL center and some portion of them may remain even in fully annealed crystal. In the complex,  $\text{Ti}^{3+}$  ions act as hole trap, while oxygen vacancies act as electron trap. Thus, complex defects are responsible for the Stokes-shifted greenish white luminescence observed in  $\text{SrTiO}_3$  crystal [3].

Using a 3.8 eV laser light, we have measured the photoenhancement effect on the complex impedance at 4.2 K for the as-grown crystal and different annealed single crystals. Two Au electrodes with a gap of about 1 mm were sputtered on the one side of each crystal surface. The applied voltage between the surface electrodes was 3 V. The laser light fluence was at least  $1.2 \text{ W/cm}^2$ . The as-grown crystal and crystals annealed for less than 2 h in  $\text{Ar}-\text{H}_2$  gas stream did not exhibit any enhancement of the capacitance by light irradiation, as shown in Fig. 5(a). However, after a subsequent annealing at 973 K in air for 12 h, this crystal showed considerable photoenhancement, as shown in

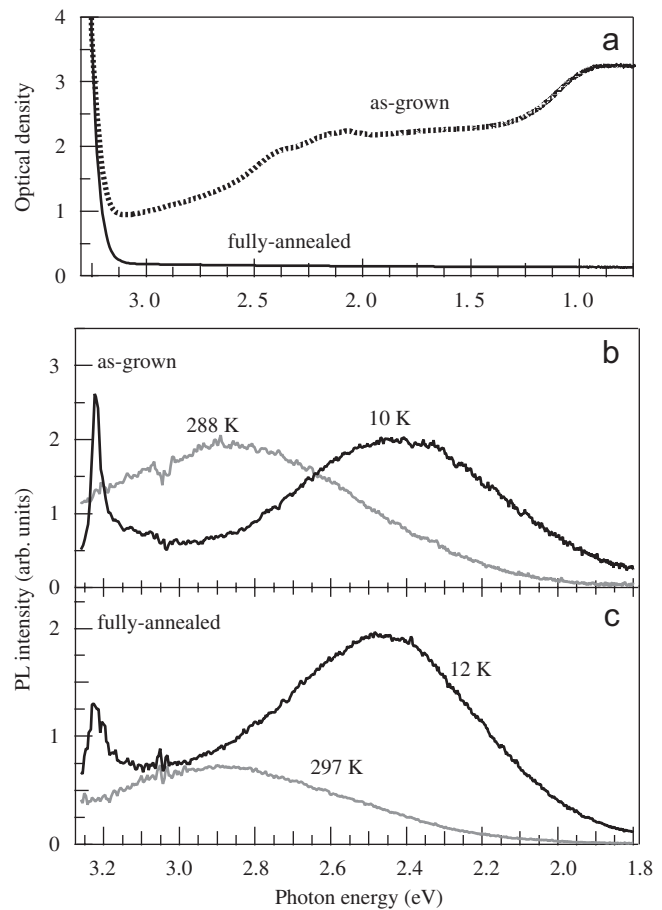


Fig. 4. The OD and PL spectra of the as-grown and fully annealed  $\text{SrTiO}_3$  crystals.

Fig. 5(b). A result for the fully annealed crystal is shown in Fig. 5(c). The subsequent annealing in air may enhance photocarrier accumulation around crystal defects (for example,  $\text{Ti}^{3+}$ –oxygen vacancy complex).

The X-ray fluorescence spectroscopic analysis has shown that the oxygen content of as-grown crystal is smaller by 0.2% than that of fully annealed crystal. The X-ray diffraction pattern, rocking curve, X-ray reflectivity, and X-ray topograph were measured for the as-grown and fully annealed crystals. The lattice parameters of the both crystals are almost same, which are 0.390498 and 0.390497 nm, respectively. The half-widths of (0 0 5) line of the both crystals are also almost identical,  $0.0501^\circ$  and  $0.0498^\circ$ . Non-Perovskite line, for instance, Ruddlesden–Popper phases  $\text{Sr}_{n+1}\text{Ti}_n\text{O}_{3n+1}$  ( $n = 1–5$ ) [9] are not observed.

Figs. 6(a) and (b) are the X-ray topographs of the as-grown crystal and fully annealed one, respectively. These topographs were obtained by the  $\omega$  scan around the center of the (1 2 3) diffraction line. The  $\omega$  value is given by each topograph. Although the  $\omega$  dependence (uneven coloring) seen in the topographs indicates the structural inhomogeneity at their crystal surfaces, the crystallinity is almost independent of annealing. The two-dimensional

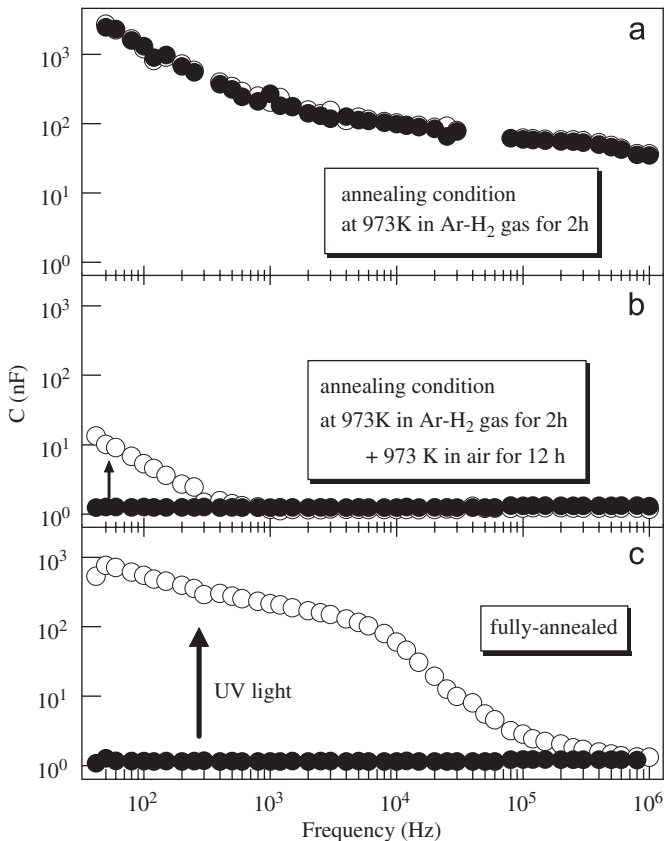


Fig. 5. Photoenhancement of the  $C$  of different  $\text{SrTiO}_3$  crystals: (a) crystal annealed at 973 K in  $\text{Ar}-\text{H}_2$  gas stream for 2 h, (b) (a)+annealed at 973 K in air for 12 h, (c) the fully annealed crystal. Solid circle and open circle denote the  $C$  with and without UV light, respectively.

rocking-curve mapping study also proves that the crystallinity is almost independent of the annealing, regardless of remarkable differences on the electrical and optical properties. Namely, the annealing decreases oxygen defect in number and reduces microscopic semiconducting domain in both number and size. The Maxwell–Wagner relaxation [10] at the interfaces between an insulating stoichiometric domain and a semiconducting non-stoichiometric one is thus suppressed by annealing, which extinguishes the colossal dielectric constant.

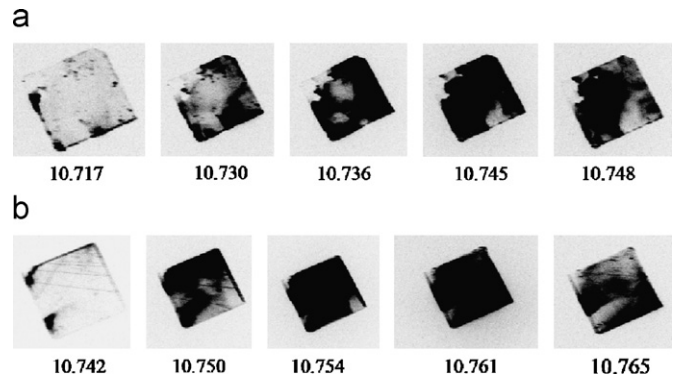


Fig. 6. X-ray topographs of the as-grown  $\text{SrTiO}_3$  crystal (a) and fully annealed  $\text{SrTiO}_3$  crystal (b). The  $\omega$  value is given by each topograph.

## Acknowledgements

This work was partially supported by a Grant-in-Aid for Scientific Research from the Ministry of Education, Science, Sport Culture, and Technology, Japan. This work is supported by an Interdisciplinary General Joint Research Grant (Nihon University). This work is also partially supported by a Research Grant from the College of Humanities and Sciences (Nihon University).

## References

- [1] K.A. Müller, H. Burkard, Phys. Rev. B 19 (1979) 3593.
- [2] K.A. Müller, W. Berlinger, E. Toatti, Z. Phys. B 84 (1991) 277.
- [3] S. Mochizuki, F. Fujishiro, S. Minami, J. Phys.: Condens. Matter 17 (2005) 923.
- [4] T. Hasegawa, M. Shirai, K. Tanaka, J. Lumin. 87–89 (2000) 1217.
- [5] S. Mochizuki, S. Minami, F. Fujishiro, J. Lumin. 112 (2005) 267.
- [6] S. Mochizuki, F. Fujishiro, K. Ishiwata, K. Shibata, Physica B 376 (2006) 816.
- [7] J. Yu, P.F. Paradis, T. Ishikawa, S. Yoda, Appl. Phys. Lett. 85 (2004) 2899.
- [8] K. Szot, W. Speier, R. Carius, U. Zastrow, W. Beyer, Phys. Rev. Lett. 88 (2002) 075508.
- [9] K. Szot, W. Speier, Phys. Rev. B 60 (1999) 5909.
- [10] R. von Hippel, Dielectrics and Waves, MIT Press, Cambridge, MA, 1954.

# Photo-induced defects of metal oxides: MgO and rutile TiO<sub>2</sub>

S. Mochizuki<sup>a,\*</sup>, F. Fujishiro<sup>a</sup>, A. Iino<sup>a</sup>, K. Shibata<sup>a</sup>, H. Yamamoto<sup>b</sup>

<sup>a</sup>Department of Physics, College of Humanities and Sciences, Nihon University, 3-25-40 Sakurajosui, Setagaya-ku, Tokyo 156-8550, Japan

<sup>b</sup>Department of Electronics and Computer Science, College of Science and Technology, Nihon University, 7-24-1 Narashinodai, Funabashi-shi, Chiba 274-8501, Japan

## Abstract

When MgO and rutile TiO<sub>2</sub> are irradiated with ultraviolet laser light ( $\lambda = 325 \text{ nm}$ ,  $h\nu = 3.81 \text{ eV}$ ) in vacuum, their photoluminescence spectra change in intensity and/or in spectral structure with increasing irradiation time. By irradiating with the same laser light at room temperature in O<sub>2</sub> gas, their original photoluminescence re-appear. Such reversible phenomena are results of photo-induced oxygen desorption and adsorption at surfaces. The mechanism and dynamics of the observed photo-induced spectral transitions are discussed on the basis of the exciton theory.

© 2007 Elsevier B.V. All rights reserved.

**Keywords:** Photo-induced phenomena; Oxygen defect; Exciton instability; Oxygen desorption; Photoluminescence

## 1. Introduction

The photo-induced oxygen desorption and adsorption of metal oxides have attracted much interest, since these phenomena may be used for a crystallinity improvement and for searching new functional materials. For 10 years, we have studied these phenomena for different metal oxides, using the bulk single crystal, ceramics, film and nanocrystal specimens [1–7]. When metal oxides are irradiated with ultraviolet (UV) laser light in vacuum, their photoluminescence (PL) spectra change in intensity and/or in spectral structure with increasing irradiation time  $t_{\text{ir}}$ . After removing the laser light, these PL properties are retained for long times at room temperature under room light, regardless of any changes of atmosphere. By irradiating with the same laser light at room temperature in O<sub>2</sub> gas, their original PL re-appear. Some of the results are collectively shown in Fig. 1 for BaTiO<sub>3</sub> single crystal, Eu<sub>2</sub>O<sub>3</sub> ceramics, KTaO<sub>3</sub> single crystal, SiO<sub>2</sub> glass, Sm<sub>2</sub>O<sub>3</sub> ceramics, SrTiO<sub>3</sub> single crystal, anatase TiO<sub>2</sub> ceramics,

Y<sub>2</sub>O<sub>3</sub> ceramics and ZnO ceramics. All the measurements were carried out at room temperature. The  $t_{\text{ir}}$  (in min) of laser light ( $\lambda = 325 \text{ nm}$ ,  $h\nu = 3.81 \text{ eV}$ ) is given by arrows which indicate the direction of the spectral change. Each oxide shown in this figure shows a similar spectral change for bulk single crystal, ceramic, film and nanocrystal specimens. Such reversible phenomena are the results of photo-induced oxygen desorption and adsorption at surfaces, which also creates/annihilates oxygen defects, and they may well yield materials for white-light emitting devices and erasable optical storage. The photo-induced phenomena are observed also at low temperatures and therefore they may be not phonon-assisted phenomena but purely electronic ones. Incidentally, the incident photon energy ( $h\nu = 3.81 \text{ eV}$ ) is smaller than the band gap energies of Eu<sub>2</sub>O<sub>3</sub>, SiO<sub>2</sub> glass, Sm<sub>2</sub>O<sub>3</sub> and Y<sub>2</sub>O<sub>3</sub>. It indicates that there are other electronic oxygen desorption and adsorption processes other than interband electronic excitation in bulk. Recently, many workers have been re-considering the photo-induced oxygen desorption from MgO surface taking into account the surface atomic and electronic structures in detail [8]. Recently, we observed remarkable photo-induced spectral change at room temperature under a 3.81 eV-laser-light irradiation. In the present paper, results of MgO are presented comparing with those of rutile.

\*Corresponding author. Tel./fax: +81 3 5317 9771.

E-mail address: [motizuki@physics.chs.nihon-u.ac.jp](mailto:motizuki@physics.chs.nihon-u.ac.jp) (S. Mochizuki).

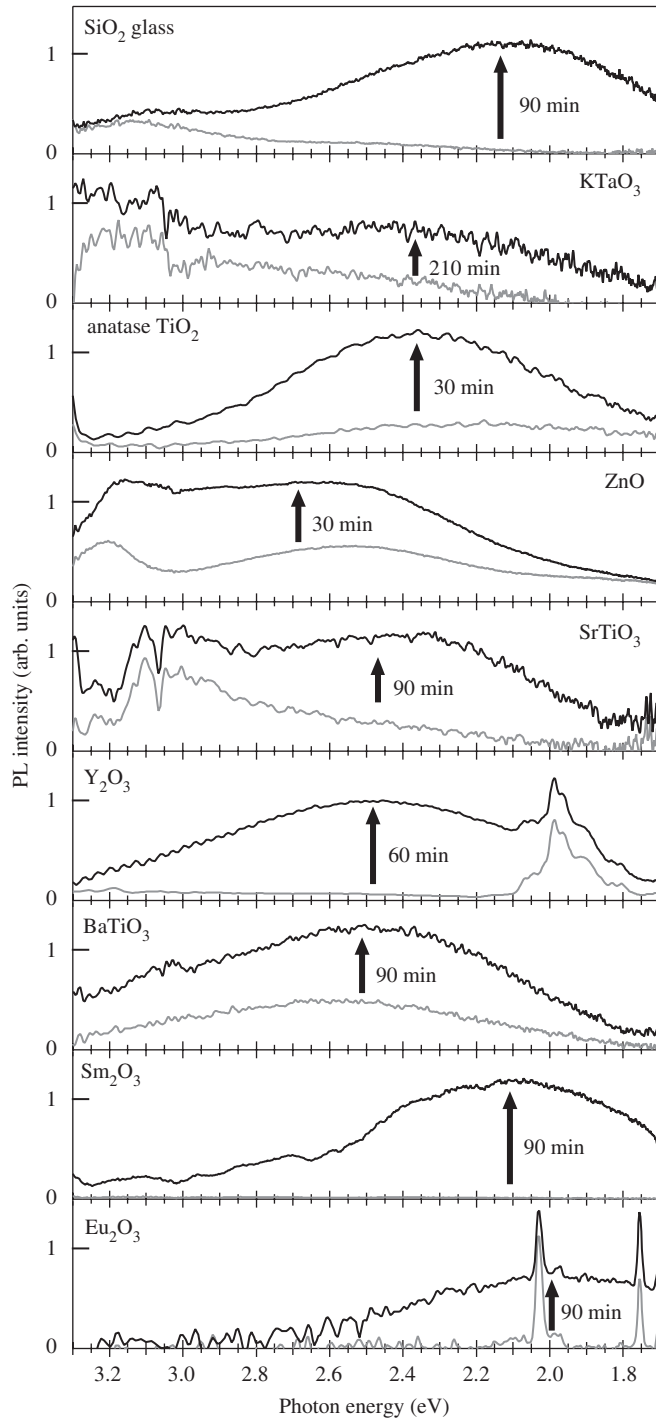


Fig. 1. Photo-induced PL spectral changes of different oxides at room temperature. The irradiation was carried out with a UV laser light ( $\lambda = 325 \text{ nm}$ ,  $h\nu = 3.81 \text{ eV}$ ) in vacuum.

## 2. Experimental

$\text{MgO}$  single crystal (99.98% purity) was grown by the arc-melting method at Tateho Chem. Co.  $\text{MgO}$  ceramics was prepared by pressing  $\text{MgO}$  powder (Wako Pure Chemical Industry Ltd., 99.9% purity) under a pressure of 0.2 GPa at room temperature for 1 h followed by sintering at 1673 K in air for 100 h. Rutile  $\text{TiO}_2$  single

crystal (99.99% purity) was grown by the Verneuil method at Nakazumi Crystal Co. Rutile ceramics was prepared by pressing rutile powder (Wako Pure Chemical Industry Ltd., 99% purity) under a pressure of 0.2 GPa for 15 min at room temperature followed by sintering at 673 K in air for 100 h. Irradiation is carried out with a continuous wave of a He–Cd laser line ( $\lambda = 325 \text{ nm}$ ,  $h\nu = 3.81 \text{ eV}$ ) with power densities between 31 and  $840 \text{ kW/m}^2$ . The illumination area is between  $2.54 \times 10^{-6}$  and  $1.13 \times 10^{-8} \text{ m}^2$ . The He–Cd laser line also excites luminescence. Emitted light is dispersed and detected by using a grating spectrograph equipped with a multichannel photodetection system.

## 3. Results and discussion

Figs. 2(a) and (b) show the 3.81 eV-laser-light-induced PL spectral changes of  $\text{MgO}$  (100) single crystal at room temperature in vacuum and  $\text{O}_2$  gas atmosphere, respectively.

The PL spectrum consists of at least two components above 3.0 eV and around 2.5 eV. The intense PL due to  $\text{Cr}^{3+}$  impurities is observed below 1.9 eV. Like for other oxides shown in Fig. 1, the PL intensity of  $\text{MgO}$  single crystal is enhanced by a 3.81 eV-laser-light irradiation in vacuum, while the PL spectrum returns to the original one under a 3.81 eV-laser-light irradiation in  $\text{O}_2$  gas. The observed reversible photo-induced PL spectral change in between vacuum and  $\text{O}_2$  gas for  $\text{MgO}$  single crystal indicates that oxygen desorption and absorption can occur even by photons of lower energy than the bulk  $\text{MgO}$  band gap (7.7 eV). The difference between the curve at  $t_{\text{ir}} = 0 \text{ min}$  and that at  $t_{\text{ir}} = 60 \text{ min}$  in Fig. 2(a), is shown in Fig. 3.

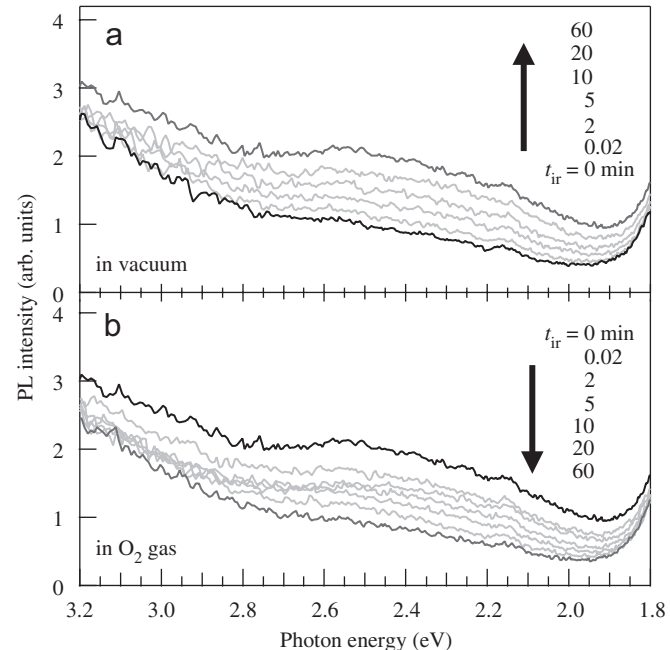


Fig. 2. UV-laser-light-induced PL spectral changes of  $\text{MgO}$  single crystal at room temperature: (a) in vacuum and (b) in  $\text{O}_2$  gas.

As shown in this figure, a broad band around 2.5 eV, accompanied by unresolved shoulder luminescence above 2.8 eV, appears. Coluccia [9] and Spoto observed the luminescence band at 3.3 eV under 5.7 and 4.6 eV excitations for MgO powder [10]. We have also carried out the same photo-induced experiments for MgO ceramics. The results are shown in Fig. 4.

It is noted that the PL intensity and speed of spectral change for MgO ceramics are larger than those for MgO single crystal. The same photo-induced experiments are also carried out for rutile TiO<sub>2</sub> single crystal, which is shown in Fig. 5.

The difference between the curve at  $t_{ir} = 0$  min and that at  $t_{ir} = 8$  h in Fig. 5(a), is shown in Fig. 6.

The spectral components between 2.5 and 1.6 eV are due to oxygen desorption. The spectral change is very similar to that of anatase TiO<sub>2</sub>, which is shown in Fig. 1 and Ref. [11]. It is found that the spectral changes shown in

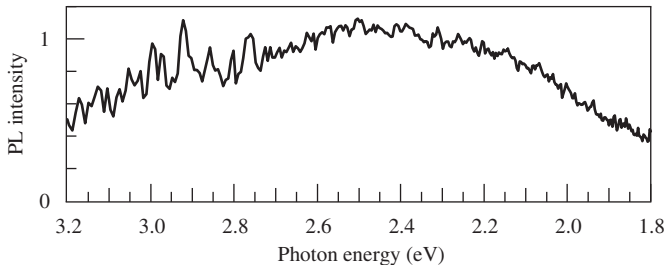


Fig. 3. Difference spectrum between the curve at  $t_{ir} = 0$  min and that at  $t_{ir} = 60$  min in Fig. 2(a).

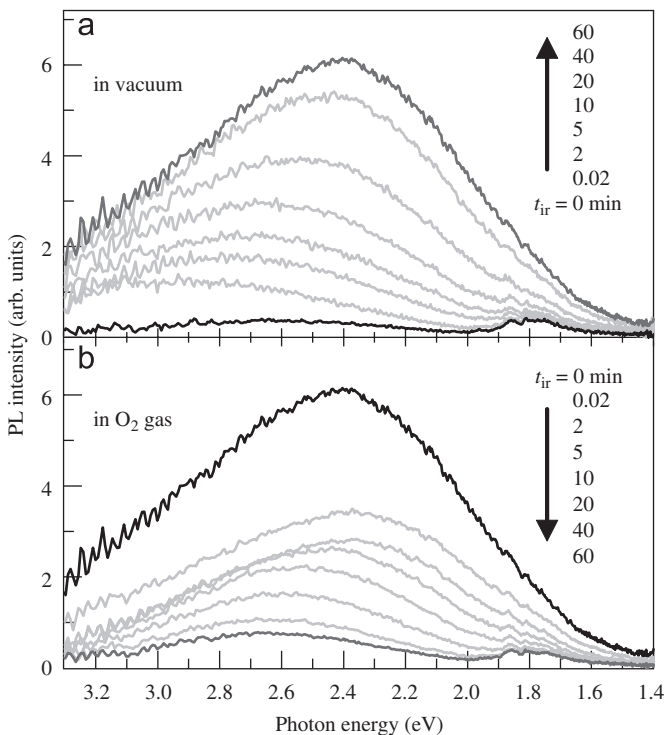


Fig. 4. UV-laser-light-induced PL spectral changes of MgO ceramics at room temperature: (a) in vacuum and (b) in O<sub>2</sub> gas.

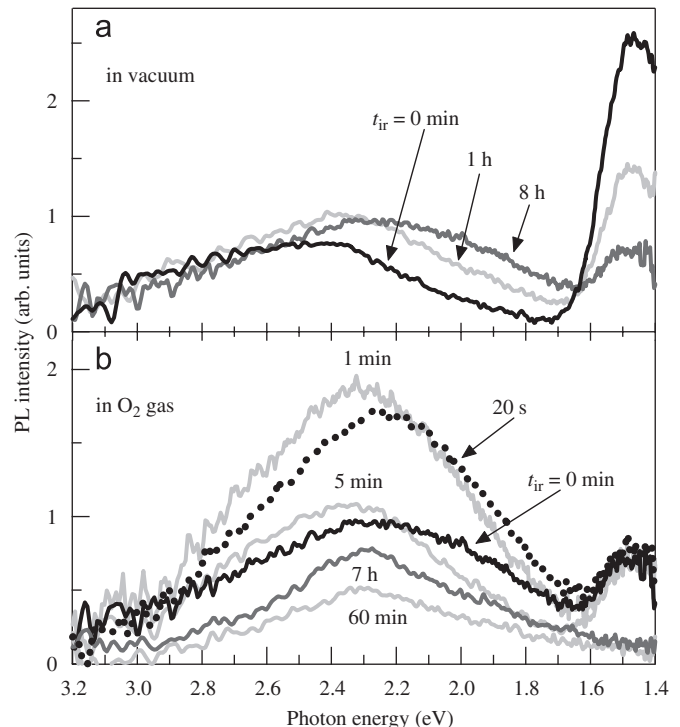


Fig. 5. UV-laser-light-induced PL spectral changes of rutile TiO<sub>2</sub> single crystal at room temperature: (a) in vacuum and (b) in O<sub>2</sub> gas.

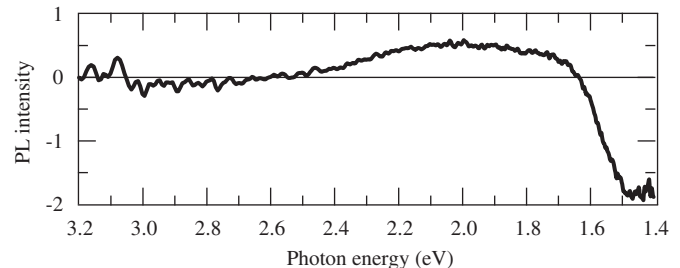


Fig. 6. Difference spectrum between the curve at  $t_{ir} = 0$  min and that at  $t_{ir} = 8$  h in Fig. 5(a).

Figs. 5(a) and (b) are hard to be induced by photons with energies lower than the band gap (3.0 eV) of rutile. Therefore, it may be concluded that oxygen desorption from rutile surface can be induced only by the interband electronic excitation. We have also carried out the same photo-induced experiments for rutile TiO<sub>2</sub> ceramics. Fig. 7 shows the photo-induced PL spectral change of rutile ceramics in vacuum.

It is noted that, like the case of MgO, the PL intensity and speed of spectral change of rutile ceramics are larger than those of rutile single crystal.

#### 4. Exciton model of photo-induced oxygen defect and photo-enhanced white luminescence

For MgO, conventional optical absorption measurements do not exhibit any absorption at photon energies below 7.7 eV (which is the band gap of MgO). However, it has been theoretically concluded that the surface oxygen

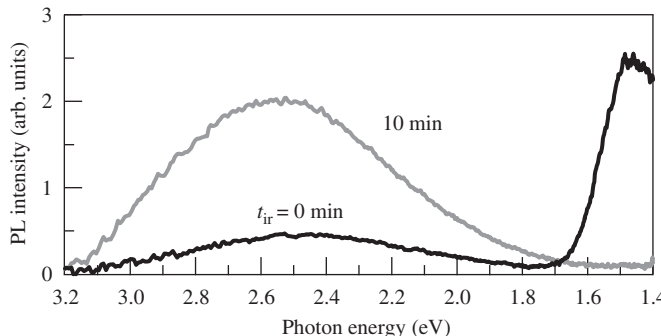


Fig. 7. UV-laser-light-induced PL spectral change of rutile  $\text{TiO}_2$  ceramics at room temperature in vacuum.

atomic structures (steps, kinks and corners) with low crystal symmetry, which are regarded as clusters, create in-gap states. The energy calculation of such surface clusters gives the highest occupied molecular orbital (HOMO)—the lowest unoccupied molecular orbital (LUMO) gap energy smaller than 7.7 eV, for example, 4.5 eV [12]. Since a 3.81 eV ( $\lambda = 325 \text{ nm}$ ) laser photon can induce oxygen desorption, there is a HOMO–LUMO gap of 3.81 eV. The HOMO state is mainly localized on the surface oxygen, while the LUMO state is delocalized over the adjacent  $\text{Mg}^{2+}$  ions. The optical transition from the HOMO to the LUMO creates  $\text{O}^{-1}$  ion at surfaces. This does not result in spontaneous oxygen emission. However, if the lifetime of the excited state is long and photon fluence is high, the second excitation of oxygen ion ( $\text{O}^{-1} \rightarrow \text{O}^0 + \text{e}^-$ ) may occur and result in spontaneous oxygen desorption and oxygen defect formation.

On the other hand, rutile  $\text{TiO}_2$  can be excited by the 3.81 eV-laser light. After such photoexcitation, some of the photo-produced electrons and holes recombine directly, displaying luminescence with a short lifetime. Another portion of photo-produced electrons may move itinerantly, undergoing repeated collisions by phonons and trapping by oxygen defects. When some portion of photo-produced electrons and holes are trapped at distant traps, luminescence arises from accidental recombination of shallowly trapped electrons with distant holes localized around defects, exhibiting a long-lasting luminescence. Possible oxygen defects in rutile include a complex defect,  $\text{Ti}^{3+}$ —(oxygen vacancy)— $\text{Ti}^{3+}$ , and a point defect, (oxygen vacancy)  $+ 2\text{e}^-$ . In the complex defect,  $\text{Ti}^{3+}$  ions act as

hole trap, while oxygen vacancies act as electron trap. Toyozawa [13] proposed three types of symmetry-breaking instabilities of excitons in the phonon field. According to this theory, if the electron and the hole have deformation potentials of opposite sign, the decomposition into a pair of self-trapped particles occur. In other words, electron ( $\text{e}$ ) and hole ( $\text{h}$ ) combine, forming a trapped electron ( $\text{S}_e$ ) and a trapped hole ( $\text{S}_h$ ) on adjoining sites, i.e.  $\text{S}_e + \text{S}_h$  state. In this case, the  $(\text{e} + \text{S}_h)$  and  $(\text{h} + \text{S}_e)$  states are thought to be unstable, so that this exciton instability may result in oxygen desorption and oxygen defect formation at rutile surface, like the case discussed for photo-induced breaking of Si–O bond in silica [14]. In both  $\text{MgO}$  and rutile  $\text{TiO}_2$ , the oxygen defects act as luminescence centres.

## Acknowledgements

This work was partially supported by a Grant-in-Aid for Scientific Research from the Ministry of Education, Science, Sport Culture and Technology, Japan. This work is supported by an Interdisciplinary General Joint Research Grant (Nihon University). This work is also partially supported by a Research Grant from the College of Humanities and Sciences (Nihon University).

## References

- [1] S. Mochizuki, T. Nakanishi, Y. Suzuki, K. Ishi, Appl. Phys. Lett. 79 (2001) 3785.
- [2] S. Mochizuki, F. Fujishiro, T. Mochizuki, H. Yamamoto, Phys. Status Solidi C 4 (2007) 518.
- [3] S. Mochizuki, Physica B 340–342 (2003) 944.
- [4] S. Mochizuki, H. Araki, Physica B 340–342 (2003) 969.
- [5] S. Mochizuki, F. Fujishiro, S. Minami, J. Phys.: Condens. Matter 17 (2005) 923.
- [6] S. Mochizuki, S. Minami, F. Fujishiro, J. Lumin. 112 (2005) 267.
- [7] F. Fujishiro, S. Mochizuki, J. Phys.: Conf. Ser. 21 (2005) 142.
- [8] W.P. Hess, A.G. Joly, K.M. Beck, M. Henyk, P.V. Sushko, P.E. Trevisanutto, A.L. Shluger, J. Phys. Chem. B 109 (2005) 19563.
- [9] S. Coluccia, Stud. Surf. Sci. Catal. 21 (1985) 59.
- [10] G. Spoto, E.N. Gribov, G. Ricchiardi, A. Damin, D. Scarano, S. Bordiga, C. Lamberti, A. Zecchina, Prog. Surf. Sci. 76 (2004) 71.
- [11] S. Mochizuki, T. Shimizu, F. Fujishiro, Physica B 340–342 (2003) 956.
- [12] P.E. Trevisanutto, P.V. Sushko, A.L. Shluger, K.M. Beck, M. Henyk, A.G. Joly, W.P. Hess, Sur. Sci. 593 (2005) 210.
- [13] Y. Toyozawa, Physica B+C 117&118 (1983) 23.
- [14] A. Shluger, E. Stefanovich, Phys. Rev. B 42 (1990) 9664.

**Optical and dielectric studies on nanoparticles  
and atomically-engineered surfaces of superparaelectric SrTiO<sub>3</sub>**

**Shosuke Mochizuki and Fumito Fujishiro**

Department of Physics, College of Humanities and Sciences, Nihon University,  
3-25-40 Sakurajosui, Setagaya-ku, Tokyo 156-8550, Japan

Received 30 July 2006, revised 10 August 2006, accepted 10 August 2006  
Published online 7 February 2007

**PACS** 68.35.-p, 77.84.Dy, 78.55.Kz

In order to find useful surface properties of SrTiO<sub>3</sub> (STO) crystal, the photoluminescence and dielectric properties of STO nanoparticles and STO bulk single crystal with nanometer steps have been measured at different temperatures. The obtained results are compared with those obtained for STO bulk single crystal.

phys. stat. sol. (c) **4**, No. 2, 515–517 (2007) / DOI 10.1002/pssc.200673302



**WILEY-VCH**

**REPRINT**

## Optical and dielectric studies on nanoparticles and atomically-engineered surfaces of superparaelectric SrTiO<sub>3</sub>

Shosuke Mochizuki\* and Fumito Fujishiro

Department of Physics, College of Humanities and Sciences, Nihon University,  
3-25-40 Sakurajosui, Setagaya-ku, Tokyo 156-8550, Japan

Received 30 July 2006, revised 10 August 2006, accepted 10 August 2006

Published online 7 February 2007

PACS 68.35.-p, 77.84.Dy, 78.55.Kz

In order to find useful surface properties of SrTiO<sub>3</sub> (STO) crystal, the photoluminescence and dielectric properties of STO nanoparticles and STO bulk single crystal with nanometer steps have been measured at different temperatures. The obtained results are compared with those obtained for STO bulk single crystal.

© 2007 WILEY-VCH Verlag GmbH & Co. KGaA, Weinheim

**1 Introduction** Strontium titanate (SrTiO<sub>3</sub>, STO) is a well-known quantum paraelectrics. STO bulk-crystal has a large dielectric constant [1], excellent optical transparency and remarkable photo-induced effects [2, 3]. On the other hand, STO is also a well-known photocatalyst and the surface property has attracted great attention. The nanosized particles and engineered nanosized-surface of STO are particularly interesting for the development of novel optoelectronic devices. We pointed out previously an important role of (Ti<sup>3+</sup>-oxygen vacancy-Ti<sup>3+</sup>) complex defects in the optical properties of STO single crystal [3, 4]. Recently, we have studied the photoluminescence and dielectric properties of STO nanoparticles and STO single crystal with molecular layer steps on the surfaces. Here, we report the results.

**2 Experimental** The surface of a molecular-layer-step (MLS) STO single crystals were supplied by Sinkosya Co. They consist of a flat terrace (200 nm in width) and molecular layer steps (0.4 nm in height). STO nanoparticle specimens were prepared by compressing nominally pure STO nanoparticle powder (99.9 % in purity and 50–90 nm in diameter), under 0.4 GPa for 10 min at room temperature. They were then treated by 2.4 GHz microwave in air for 5 min. X-ray diffraction analysis shows that STO specimens are a cubic perovskite phase STO. The experimental setup for photoluminescence measurements is presented in detail elsewhere [3].

**3 Results and discussion** Figure 1(a) shows the photoluminescence (PL) spectra of pristine STO single crystal without any engineering at 13 K under different photoexcitation intensities. The photoexcitation is carried out with a 355 nm laser light from a Nd<sup>3+</sup>-YAG laser and the intensity (mJ/cm<sup>2</sup>) is given by each curve. Under weak excitation, only a white luminescence around 2.45 eV is observed. With increasing laser fluence, the white luminescence intensity increases monotonously and a near-band-edge luminescence (NBE luminescence) around 3.23 eV appears. On the laser fluence further increasing up to 4 mJ/cm<sup>2</sup>, the white luminescence attains a maximum, while both the NBE luminescence and a broad blue luminescence between the NBE luminescence and the white one become prominent. We have already clarified, for one-photon excitation PL, that the white luminescence arises mainly from oxygen

\* Corresponding author: e-mail: motizuki@physics.chs.nihon-u.ac.jp, Phone: +81 3 5317 9771, Fax: +81 3 5317 9771

defects at the crystal surfaces [3], and the blue luminescence and the NBE luminescence are the free-carrier-enhanced defect luminescence and the free-carrier-enhanced band edge emission, respectively. On laser fluence exceeding  $4 \text{ mJ/cm}^2$ , the white luminescence intensity begins to decrease monotonously, while both the NBE luminescence band and the blue luminescence band continue to grow more, deteriorating the white luminescence band. Incidentally, we have found that the white luminescence intensity maximum appeared at  $0.4 \text{ mJ/cm}^2$  for the sintered STO powder (several hundreds micrometres in size) compact. This suggests that most of the white-luminescence centres are at specimen surface [3]. The same measurement was carried out for the MLS STO single crystal. The result is shown in figure 1(b).

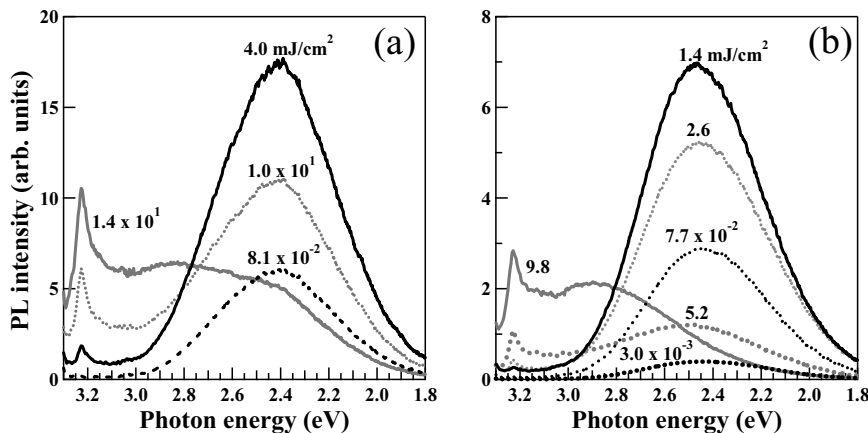


**Fig. 1** The excitation light intensity dependence of the PL spectra of different STO single crystals: (a) Pristine STO at 13 K, (b) MLS STO at 10 K. The excitation laser light wavelength is 355 nm.

As seen in this figure, the white luminescence intensity maximum appears at  $1.4 \text{ mJ/cm}^2$  which is smaller than that ( $4.0 \text{ mJ/cm}^2$ ) of the pristine STO single crystal. Clear white-blue luminescence colour change is observed at an intensity of  $8 \text{ mJ/cm}^2$  with the naked eye. The white luminescence observed for both the STO single crystals almost disappears above 40 K.

Figure 2(a) shows the photoexcitation intensity dependence of the PL spectrum of STO nanoparticles at 10 K. Photoexcitation was carried out with a 355 nm laser light. In Fig. 2(b), after normalizing the spectra in intensity, the spectrum under intense excitation is compared with that under weak excitation.

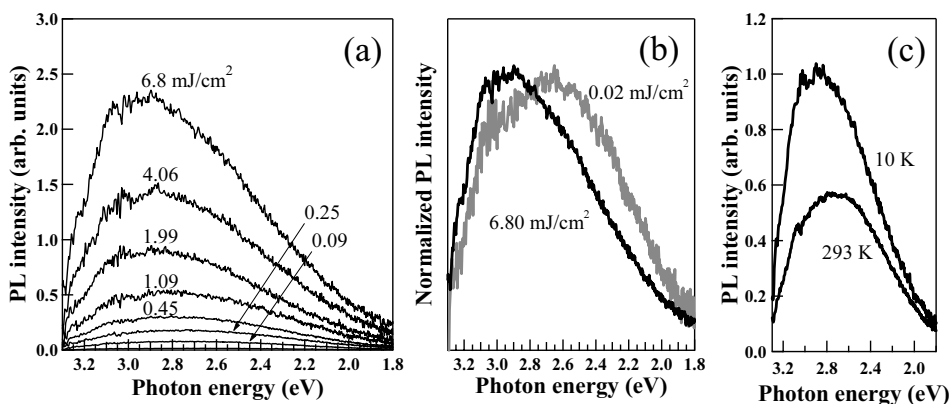


**Fig. 2** The excitation light intensity dependence of the PL spectrum of STO nanoparticle specimen at 10 K: (a), (b) comparison of the spectra under intense excitation with that under weak excitation, (c) temperature dependence of PL spectrum.

As seen from this figure, the white luminescence is merged in the blue luminescence band, which suggests that the white luminescence maximum intensity appears at lower excitation intensity than  $0.02 \text{ mJ/cm}^2$ . The NBE luminescence is faintly seen at the high energy side of the blue luminescence as a shoulder. It is found that, at room temperature, the blue-luminescence intensity of the STO nanoparticles is three times larger than that of the STO bulk single crystal. This suggests that the free carrier as an activator of the blue-luminescence and/or the defect as a luminescence centre increase in number. Incidentally, a relatively high electrical conductivity ( $> 10^{-3} \text{ S/m}$ ) has been observed for the STO nanoparticle specimen. Figure 3(c) shows the PL spectra of the STO nanoparticles at 10 and 293 K. Unlike the pristine STO single crystal and MLS one, the temperature dependence of the blue luminescence is small.

As discussed in the previous paper [3], the one-photon-excitation PL of the pristine STO single crystal is explained as follows. Most of the photo-generated holes may be deeply trapped at  $\text{Ti}^{3+}$  sites of the complexes. Unlike such holes, photo-generated electrons may move itinerantly, experiencing repeatedly collisions by phonons and trapping by oxygen defects. When some portion of photo-generated holes and -electrons are trapped at distant complexes, the white luminescence arises from accidental recombination of shallowly trapped electrons with distant holes localized around the defects, exhibiting a long-lasting white luminescence. With increasing laser fluence, the numbers of photo-generated electrons and holes increase and then the PL intensity may increase. At further increasing laser fluence, photo-generated electrons and holes become diffused more rapidly inside crystal (bulk), and therefore the PL intensity decreases. This is a reason why the white PL intensity maximum appears. In other word, this means that most of the defect luminescence centres ( $(\text{Ti}^{3+}\text{-oxygen vacancy-}\text{Ti}^{3+})$  complex defects) are at the specimen surface. In the complex, the  $\text{Ti}^{3+}$  ions act as hole traps, while the vacancy tends to trap electron. Since nanoparticle has large specific surface area, the STO nanoparticle specimen may exhibit a PL intensity maximum at the laser fluence smaller than that of the bulk single crystal specimen. In addition to these defect effects, it should be taken into the consideration that, at higher laser fluence, direct recombination of photo-generated carriers enhances the NBE and blue luminescence, deteriorating the white luminescence. Assuming the nonradiative multiphonon relaxation, the observed small temperature dependence of the blue luminescence intensity indicates that the height of an average potential barrier separating the luminescent state from ground state in STO nanoparticles is small compared with that of STO bulk crystals.

The dielectric constants ( $\epsilon$ ) of the three types of STO specimens were also measured with an impedance meter in a frequency range between 0.01 Hz and 3 MHz. The  $\epsilon$  (1 kHz) of both the pristine STO single crystal and the MLS STO one are about 300 at room temperature, while  $\epsilon$  (1 kHz) of STO nanoparticle specimens are between 340 and 300, regardless of a high porosity (about 50%). Such the enhanced  $\epsilon$  may be due to the polar ( $(\text{Ti}^{3+}\text{-oxygen vacancy-}\text{Ti}^{3+})$  complex defects at nanoparticle surfaces or due to the Maxwell-Wagner effect [5] contributed by the heterogeneity within nanoparticles, or due to the Maxwell-Wagner effect contributed by the depletion layer between electrode and nanoparticle.

**Acknowledgements** This work was partially supported by a Grant-in-Aid for Scientific Research from the Ministry of Education, Science, Sport Culture and Technology, Japan. This work is supported by an Interdisciplinary General Joint Research Grant (Nihon University). This work is also partially supported by a Research Grant from the College of Humanities and Sciences (Nihon University), and by a Collaboration Research Grant from the Institute of Natural Science (Nihon University).

## References

- [1] K. A. Müller and H. Burkard, Phys. Rev. B **19**, 3593 (1979).
- [2] H. Katsu, H. Tanaka, and T. Kawai, J. Appl. Phys. **90**, 4578 (2001).
- [3] S. Mochizuki, F. Fujishiro, and S. Minami, J. Phys.: Condens. Matter **17**, 923. (2005).
- [4] S. Mochizuki, F. Fujishiro, K. Shibata, and K. Ishiwata, Physica B **376/377**, 816 (2006).
- [5] J. Yu, P. F. Paradis, T. Ishikawa, and S. Yoda, Appl. Phys. Lett. **85**, 2899 (2004).

## Erasable photomemory phenomena in $\text{Eu}_2\text{O}_3$ -, $\text{Y}_2\text{O}_3$ - and $\text{SrTiO}_3$ nanoparticles at room temperature

**Shosuke Mochizuki<sup>1</sup>, Fumito Fujishiro<sup>1</sup>, Teruyuki Mochizuki<sup>2</sup>, and Hiroshi Yamamoto<sup>3</sup>**

<sup>1</sup> Department of Physics, College of Humanities and Sciences, Nihon University, 3-25-40 Sakurajosui, Setagaya-ku, Tokyo 156-8550, Japan

<sup>2</sup> Material Design Division, G. P. I. Japon, 271-12 Kunugida, Hachioji, Tokyo 193-0942, Japan

<sup>3</sup> Department of Electronics and Computer Science, College of Science and Technology, Nihon University, 7-24-1, Narashinodai, Funabashi-shi, 274-8501, Japan

Received 30 July 2006, revised 25 September 2006, accepted 25 September 2006

Published online 7 February 2007

**PACS** 71.35.-y, 78.55.Kz, 78.67.Bf, 81.40.Tv

Reversible ultraviolet-laser-light-induced spectral changes have been observed for  $\text{Eu}_2\text{O}_3$ -,  $\text{Y}_2\text{O}_3$ - and  $\text{SrTiO}_3$  nanocrystal specimens at room temperature. Comparing with their bulk specimens, the speed of the changes in the nanoparticle specimens tend to increase. The transitions are explained by photo-induced reduction and photo-induced oxidation at nanocrystal surfaces due to exciton instability.

phys. stat. sol. (c) 4, No. 2, 518–520 (2007) / DOI 10.1002/pssc.200673303

## Erasable photomemory phenomena in $\text{Eu}_2\text{O}_3$ -, $\text{Y}_2\text{O}_3$ - and $\text{SrTiO}_3$ nanoparticles at room temperature

Shosuke Mochizuki<sup>\*, 1</sup>, Fumito Fujishiro<sup>1</sup>, Teruyuki Mochizuki<sup>2</sup>, and Hiroshi Yamamoto<sup>3</sup>

<sup>1</sup> Department of Physics, College of Humanities and Sciences, Nihon University, 3-25-40 Sakurajosui, Setagaya-ku, Tokyo 156-8550, Japan

<sup>2</sup> Material Design Division, G. P. I. Japon, 271-12 Kunugida, Hachioji, Tokyo 193-0942, Japan

<sup>3</sup> Department of Electronics and Computer Science, College of Science and Technology, Nihon University, 7-24-1, Narashinodai, Funabashi-shi, 274-8501, Japan

Received 30 July 2006, revised 25 September 2006, accepted 25 September 2006

Published online 7 February 2007

PACS 71.35.-y, 78.55.Kz, 78.67.Bf, 81.40.Tv

Reversible ultraviolet-laser-light-induced spectral changes have been observed for  $\text{Eu}_2\text{O}_3$ -,  $\text{Y}_2\text{O}_3$ - and  $\text{SrTiO}_3$  nanocrystal specimens at room temperature. Comparing with their bulk specimens, the speed of the changes in the nanoparticle specimens tend to increase. The transitions are explained by photo-induced reduction and photo-induced oxidation at nanocrystal surfaces due to exciton instability.

© 2007 WILEY-VCH Verlag GmbH & Co. KGaA, Weinheim

**1 Introduction** Several years ago, we found a reversible photo-induced spectral change in  $\text{Eu}_2\text{O}_3$  at room temperature [1, 2]. When  $\text{Eu}_2\text{O}_3$  ceramic and film are irradiated with a 325 nm laser light in vacuum, their photoluminescence (PL) spectrum changes from a red sharp-line structure to a white broad band, which can be clearly seen with the naked eye. After removing the ultraviolet (UV) laser light, the white PL state was stored for several years at room temperature under room light, regardless of any changes of atmosphere. By irradiating with the same UV laser light at room temperature under  $\text{O}_2$  gas atmosphere, the original red PL state re-appears. Such reversible phenomenon may well yield materials for white-light-emitting devices and erasable optical storage. Expecting the improvement in the speed of such spectral change due to reduction of system size, we have studied the reversible UV-laser-light-induced spectral change in several kinds of oxide nanoparticle specimens. In the present paper, we report upon the results of  $\text{Eu}_2\text{O}_3$  nanoparticles,  $\text{Y}_2\text{O}_3$  nanoparticles and  $\text{SrTiO}_3$  nanoparticles.

**2 Experimental**  $\text{Eu}_2\text{O}_3$  fine particles (several nanometers in size) were deposited on a room-temperature silica substrate in  $\text{O}_2$  gas of a pressure (5.1 Pa) by laser ablation method with a pulsed Nd<sup>3+</sup>-YAG laser light (wavelength  $\lambda = 355$  nm). X-ray diffraction (XRD) shows that the as-deposited film displays halo XRD pattern which is reproduced by broadening the B-form- and C-form  $\text{Eu}_2\text{O}_3$  XRD lines. The particle size is several ten nanometers.  $\text{Y}_2\text{O}_3$  and  $\text{SrTiO}_3$  nanocrystal specimens are prepared by pressing nominally pure  $\text{Y}_2\text{O}_3$  nanocrystal powder (99.9 % in purity and 27 nm in average size) and nominally pure  $\text{SrTiO}_3$  nanocrystal powder (99.9 % in purity and 50-90 nm in diameter), respectively, under 0.4 GPa for 10 min at room temperature. The XRD analysis shows that  $\text{Y}_2\text{O}_3$  specimen and  $\text{SrTiO}_3$  one are a cubic phase  $\text{Y}_2\text{O}_3$  and a cubic perovskite phase  $\text{SrTiO}_3$ , respectively. UV-laser-light irradiation is carried out with a continuous wave of a He-Cd laser line ( $\lambda = 325$  nm) with a power of 30 mW. The irradiated optic area is about  $3 \times 10^{-6} \text{ m}^2$ . The same laser light excites luminescence. Emitted light is

\* Corresponding author: e-mail: motizuki@physics.chs.nihon-u.ac.jp, Phone: +81 3 5317 9771, Fax: +81 3 5317 9771

dispersed and detected using a grating spectrograph equipped with an image-intensified photodetection system. To avoid oil-vapour effects, the evacuation of the specimen chamber is carried out with an oil-free vacuum pumping system.

**3 Results and discussion** Figure 1(a) shows the luminescence of the  $\text{Eu}_2\text{O}_3$  nanoparticle film which was fully-irradiated with a 325 nm laser light in  $\text{O}_2$  gas of  $1.01 \times 10^5 \text{ Pa}$  for 1h. The red colour is due to the luminescent  ${}^5\text{D}_0 - {}^7\text{F}_J$  ( $J = 0, 1, 2, \dots$ ) transitions in  $\text{Eu}^{3+}$  ion. Under irradiation of the laser light, the specimen chamber was then evacuated below  $1.33 \times 10^{-4} \text{ Pa}$  and the red luminescence changes gradually to white one. Figure 1(b) shows the luminescence of the same film irradiated with the same laser light in vacuum for 1h. The measured spectral changes under the irradiation in vacuum and in  $\text{O}_2$  gas are shown in Fig. 1(c) and Fig. 1(d), respectively. The irradiation time  $t_{\text{ir}}$  is given by each curve in min.

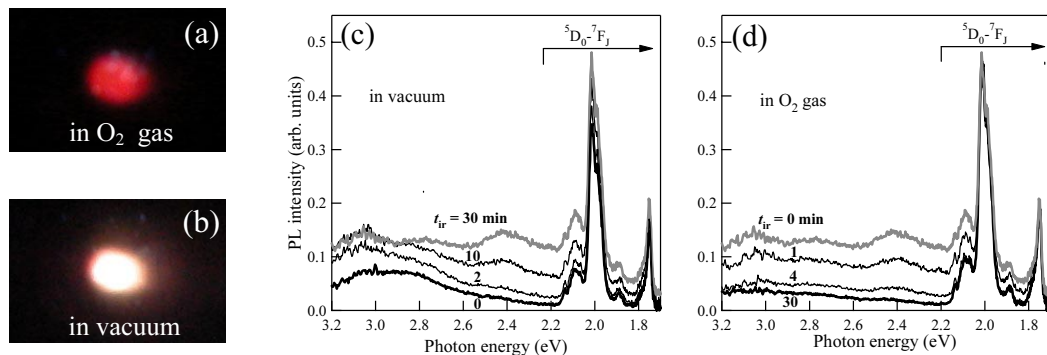
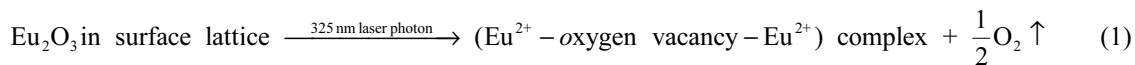


**Fig. 1** 325 nm-laser-light-induced photoluminescence changes of  $\text{Eu}_2\text{O}_3$  nanoparticle specimen: (a) and (b) show the colour change, (c) and (d) show the spectral changes in vacuum and in  $\text{O}_2$  gas, respectively.

It is found that, after removing the 325 nm laser light, the white PL state is stored for more than several years at room temperature under room light, regardless of any changes of atmosphere. As seen in Fig. 1(c), the PL due to the  ${}^5\text{D}_0 - {}^7\text{F}_2$  transition decreases in intensity with irradiation time. The red-white luminescence change arises from a photo-induced detachment of oxygen near film surface. The photo-induced oxygen detachment may be accompanied both by the valence number change ( $\text{Eu}^{3+} \rightarrow \text{Eu}^{2+}$ ) and by oxygen defect, as follows.



In the complex, the  $\text{Eu}^{2+}$  ions act as hole traps ( $S_h$ ), while the oxygen vacancies behave as electron traps ( $S_e$ ). Toyozawa [3] proposed three types of symmetry-breaking instabilities of excitons in the phonon field and, when the electron and the hole have deformation potentials of opposite sign, the decomposition into a pair of self-trapped particles occur. Therefore, such exciton instability may result in oxygen desorption at  $\text{Eu}_2\text{O}_3$  surfaces. The laser photon energy is close to the charge transfer exciton energy of  $\text{Eu}_2\text{O}_3$ . In the present  $\text{Eu}_2\text{O}_3$  specimens, the seeds of the observed photo-induced spectral change may be the defects which had already existed at particle surfaces and can absorb 325 nm laser photons.

Figures 2(a) and (b) show the 325 nm-laser-light-induced spectral change of  $\text{Y}_2\text{O}_3$  nanoparticle specimen in vacuum and  $\text{O}_2$  gas, respectively. The irradiation time is given by each curve in min. A reversible photo-induced spectral change of the white PL has been clearly observed. The intense PL state created under 325 nm laser light irradiation is found to be stored for at least several days at room temperature, regardless of any changes of atmosphere. The spectral changes are accompanied by some spectral red-shift. It is found that the spectral change speed of  $\text{Y}_2\text{O}_3$  nanoparticle specimen is about three times larger than that of  $\text{Y}_2\text{O}_3$  bulk crystal. Since the energy gap of  $\text{Y}_2\text{O}_3$  crystal is about 5 eV [4] which is larger than the incident photon energy (3.81 eV), the optical absorption due to surface defects should be considered.

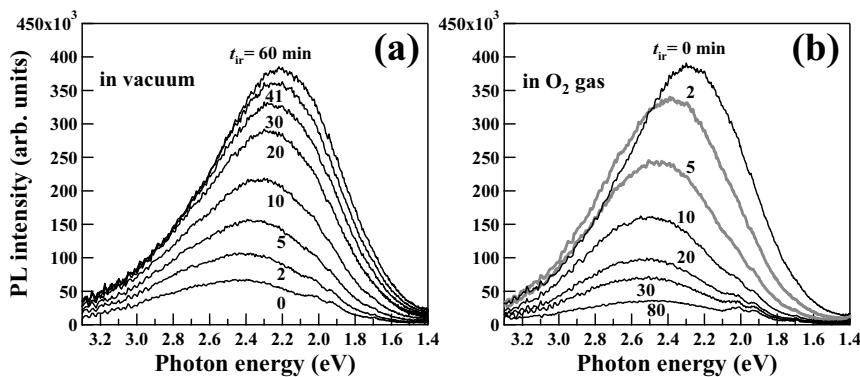


**Fig. 2** 325 nm-laser-light-induced photoluminescence spectral change of  $Y_2O_3$  nanoparticle specimen.

Quite similar photo-induced spectral changes have been observed for  $SrTiO_3$  nanoparticle specimen. Figures 3(a) and (b) show the spectral changes of  $SrTiO_3$  nanoparticle specimen at room temperature.

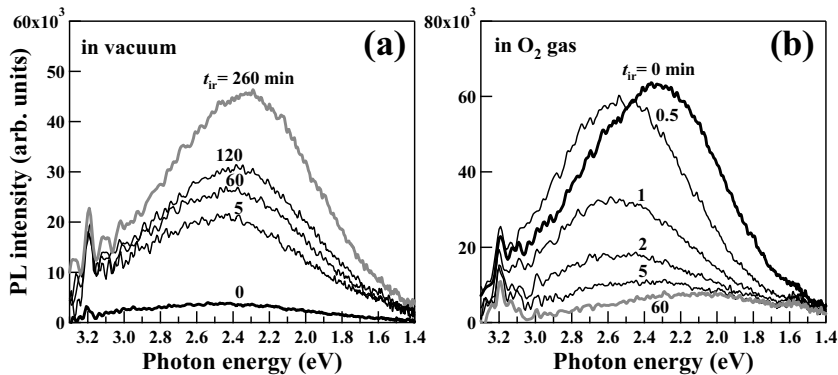


**Fig. 3** 325 nm-laser-light-induced photoluminescence spectral change of  $SrTiO_3$  nanoparticle specimen.

It is noted that, unlike  $Eu_2O_3$ - and  $Y_2O_3$  nanoparticles, the fully-photo-reduced  $SrTiO_3$  nanoparticles became more luminescent by introducing  $O_2$  gas (compare the uppermost curve in Fig. 3(a) with the uppermost one in Fig. 3(b)). This suggests that a successive photoreduction-photooxidation treatment removes nonradiative traps. As pointed out previously for  $SrTiO_3$  bulk single crystal [5], ( $Ti^{3+}$ -oxygen vacancy- $Ti^{3+}$ ) complex defects at surfaces are luminescence centres. It is found that the speed of the spectral change is larger than that of  $SrTiO_3$  single bulk crystal [5].

**Acknowledgements** This work was partially supported by a Grant-in-Aid for Scientific Research from the Ministry of Education, Science, Sport Culture and Technology, Japan. This work was supported by an Interdisciplinary General Joint Research Grant (Nihon University). This work is also partially supported by a Research Grant from the College of Humanities and Sciences (Nihon University).

## References

- [1] S. Mochizuki, T. Nakanishi, Y. Suzuki, and K. Ishi, *Appl. Phys. Lett.* **70**, 3785 (2001).
- [2] S. Mochizuki, Y. Suzuki, T. Nakanishi, and K. Ishi, *Physica B* **308-310**, 1046 (2001).
- [3] Y. Toyozawa, *Physica B+C* **117-118**, 23 (1983).
- [4] J. Robertson, *J. Vac. Sci. Technol. B* **18**, 1785 (2000).
- [5] S. Mochizuki, F. Fujishiro, and S. Minami, *J. Phys.: Condens. Matter* **17**, 923 (2005).

**Structural and optical properties of as-deposited and annealed SrTiO<sub>3</sub> films prepared by laser ablation**

**Ken'ichiro Ishiwata and Shosuke Mochizuki**

Department of Physics, College of Humanities and Science, Nihon University,  
3-25-40 Sakurajosui, Setagaya-ku, Tokyo 156-8550, Japan

Received 20 June 2006, revised 18 July 2006, accepted 21 July 2006  
Published online 2 November 2006

**PACS** 68.55.-a, 78.20.Ci, 78.55.Hx, 81.15.Fg, 81.40.Ef

In order to clarify the large band gap energy reported for thin SrTiO<sub>3</sub> film (of which thickness is smaller than 200 nm) and to examine the optical properties reported for bulk SrTiO<sub>3</sub> crystals, different thick SrTiO<sub>3</sub> films were prepared by a pulsed laser ablation method. The morphology and structure of the as-deposited and annealed films were studied with the optical- and scanning electron microscopes and with an x-ray diffraction method. The optical absorption and photoluminescence properties of the films are then measured at temperatures between 6.5 and 300 K. A large band gap energy (about 4.0 eV) has been observed even for thick amorphous SrTiO<sub>3</sub> films (of which thicknesses are approximately 1.3 μm).

phys. stat. sol. (c) 3, No. 10, 3516–3519 (2006) / DOI 10.1002/pssc.200672127

## Structural and optical properties of as-deposited and annealed SrTiO<sub>3</sub> films prepared by laser ablation

Ken'ichiro Ishiwata\* and Shosuke Mochizuki

Department of Physics, College of Humanities and Science, Nihon University,  
3-25-40 Sakurajosui, Setagaya-ku, Tokyo 156-8550, Japan

Received 20 June 2006, revised 18 July 2006, accepted 21 July 2006

Published online 2 November 2006

PACS 68.55.-a, 78.20.Ci, 78.55.Hx, 81.15.Fg, 81.40.Ef

In order to clarify the large band gap energy reported for thin SrTiO<sub>3</sub> film (of which thickness is smaller than 200 nm) and to examine the optical properties reported for bulk SrTiO<sub>3</sub> crystals, different thick SrTiO<sub>3</sub> films were prepared by a pulsed laser ablation method. The morphology and structure of the as-deposited and annealed films were studied with the optical- and scanning electron microscopes and with an x-ray diffraction method. The optical absorption and photoluminescence properties of the films are then measured at temperatures between 6.5 and 300 K. A large band gap energy (about 4.0 eV) has been observed even for thick amorphous SrTiO<sub>3</sub> films (of which thicknesses are approximately 1.3 μm).

© 2006 WILEY-VCH Verlag GmbH & Co. KGaA, Weinheim

**1 Introduction** Strontium titanate (SrTiO<sub>3</sub>, STO) crystal is a well-known perovskite-type paraelectric oxide with a large dielectric constant (300 at 300 K, 10<sup>4</sup> at 10 K) [1]. In view of the large dielectric constant, excellent optical transparency and remarkable photo-induced effects [2, 3], a thin STO film has many important applications in the field of semiconductor device. So far, various growth techniques have been applied to prepare thin STO films and several workers [4, 5] reported excessively large optical band-gap energy  $E_g$  (3.4 eV <  $E_g$  < 3.8 eV) of thin STO films, while the  $E_g$  of a bulk STO crystal is approximately 3.2 eV. However, the cause of such a large  $E_g$  of the thin films has been not fully elucidated. Recently, we have prepared different thick STO films and observed also excessively large  $E_g$  and intense luminescence. The morphology, crystal structure and optical (absorption and photoluminescence) properties have been studied before and after thermal annealing. The obtained results are compared with those reported for thin STO films.

**2 Experimental** STO films were prepared on different kinds of optically-flat substrates (silica glass, Au-coated silica glass, and C-cut sapphire) by a pulsed laser ablation method. The conditions of the laser ablation are shown in Table 1.

**Table 1** Conditions of the laser ablation.

laser	third-harmonic wave ( $\lambda = 355$ nm) of Nd <sup>3+</sup> -YAG laser
target	as-grown STO single crystal grown by Verneuil method
substrate temperature	room temperature
atmosphere	vacuum
substrates	silica glass, Au-coated silica glass, and C-cut sapphire
spacing between target and substrate	110 mm

\* Corresponding author: e-mail: ishiwata@phys.chs.nihon-u.ac.jp, Phone: +81 3 5317 9771, Fax: +81 3 5317 9771

After deposition, the half pieces of the as-deposited films were annealed at 873 K in air for 6 h. The surface morphology of the films was studied with an optical microscope (OM) (Nano Scale Hybrid Microscope, KEYENCE VN-8000), an atomic force microscope (AFM) (Nano Scale Hybrid Microscope, KEYENCE VN-8000) and a scanning electron microscope (SEM) (3D real surface microscope, KEYENCE VE-9800). The structural data of the films were gathered at 300 K using an x-ray diffraction (XRD) system with Cu  $\text{K}\alpha_1$  radiation. The optical absorption, the transmittance and the reflectance of the films were measured using an optical multi-channel analyser (OMA). The photoluminescence (PL) and PL-excitation spectra were measured another OMA equipped with an image-intensified photodiode-array detector. A He-Cd laser ( $\lambda = 325$  nm) and a Nd<sup>3+</sup>-YAG laser were used as excitation sources. A He-closed-cycle-refrigerator-type cryostat was used to control sample temperature.

**3 Results and discussion** The morphologic and structural studies were carried out at room temperature on all of the fabricated films with the above-described three microscopes and the XRD apparatus. The results were almost independent of the kinds of substrates. As typical results, the SEM images and XRD patterns of the as-deposited and annealed STO films on the silica glass substrate are shown in Fig. 1. As seen from these figures, the as-deposited film is a smooth-surface amorphous film, while the annealed film is a STO crystalline film consisting of grains. The grain sizes are characterized to be several hundreds nanometers by the SEM observations with a higher resolution. The lattice constant of the annealed film is estimated to be  $0.390 \pm 0.001$  nm (which is close to the bulk crystal value) from the XRD pattern. On the other hand, the XRD pattern of the as-deposited film can be reproduced by broadening and shifting the XRD pattern of the annealed film to lower angles, indicating that the average atomic separation of the as-deposited film is increased. It is also seen that the thermal annealing process makes many crevices in the uniform film layer and divides it into domains of several ten micrometers sizes, indicating that the strain in the film is almost released by creating crevices. Some large particles (whose sizes are between several hundreds nanometers and several micrometers) are also observed. They may be explosively spouted out from the STO target crystal during the laser ablation.

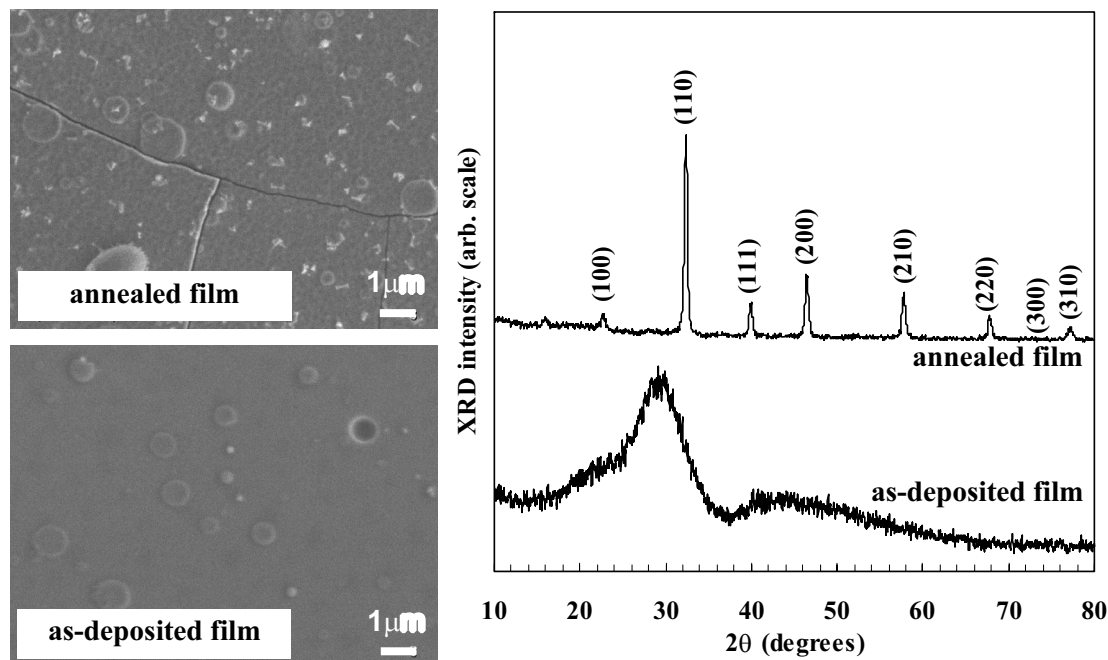


**Fig. 1** The SEM images and X-ray diffraction patterns of the as-deposited and annealed STO films.

The optical density (OD) and PL spectra of all the fabricated STO films were measured at temperatures between 6.5 and 300 K. As typical results, the OD spectra of the as-deposited and annealed STO film on the silica glass and sapphire substrates at room temperature are shown in Fig. 2. The film thicknesses  $d$  estimated from the interference fringes are given by each curves. It is noted that the absorption edge of the as-deposited film is blue-shifted to about 4.0 eV (which was estimated by plotting the square of the OD against photon energy) and then it is red-shifted to about 3.3 eV (which is close to the  $E_g$  of STO bulk crystal [6]) by thermal annealing. Such behaviour is independent of the kind of substrate material.

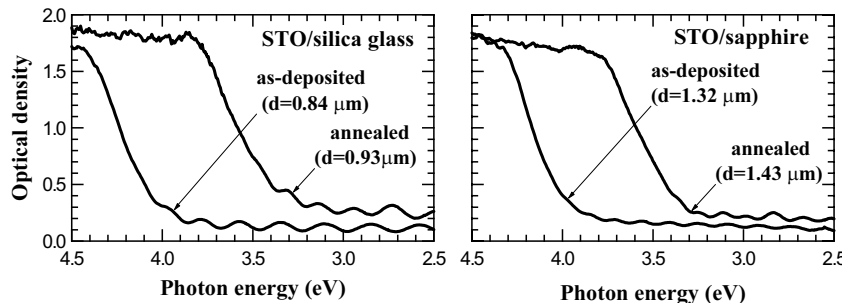


**Fig. 2** The OD spectra of the as-deposited and annealed STO films on different kinds of substrates at 300 K.

Although it has been believed that the  $E_g$  of STO film shows a strong dependence on film thickness and there is a critical film thickness (about 200 nm) [4, 5], the present results on the thick films clarify that, even if it is thick film, the STO film exhibiting a halo-XRD pattern has always large band gap energy.

We have measured the PL spectra of all the fabricated films at different temperatures between 7.4 and 300 K. The PL spectra of the as-deposited and annealed STO films on the silica glass, Au-coated silica glass and sapphire substrates at several temperatures are shown in Fig. 3. In this figure, the PL intensities of the as-deposited STO films on the silica glass are tripled. A 325 nm laser light was used for the excitation. It is found that the PL intensity is nearly proportional to the excitation light intensity. The time-resolved PL measurements showed that all the PL components have the lifetimes of about 10 ns.

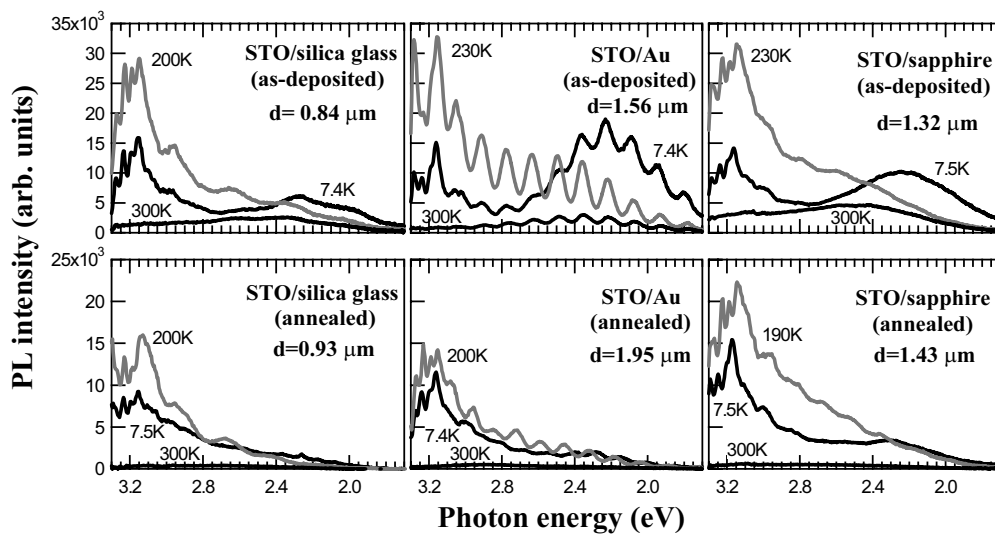


**Fig. 3** The PL spectra of different STO film specimens at several temperatures.

The observed PL spectral features are summarized as follows.

- (1) The PL spectra of the as-deposited films consist of several ultraviolet (UV) components between 3.3 and 2.8 eV and several white luminescence components between 2.7 and 2.0 eV.
- (2) The PL intensity is decreased by thermal annealing. Especially, the intensity decrease of the white luminescence at low temperatures ( $< 8$  K) is remarkable.
- (3) The white luminescence components of the as-deposited STO films remain at room temperature, while those of the annealed films almost disappears at room temperature.
- (4) With increasing temperature from 7.5 K to about 180 K, the PL intensity monotonously decreases. With further increasing temperature, the PL components above 2.8 eV begin to increase in intensity. The PL intensity of each specimen attains each maximum at an intermediate temperature range between 190 and 230 K. On further increasing temperature to 300 K, all of the PL components decrease in intensity.

Similar UV luminescence and white one were observed for a bulk STO single crystal [7, 8], but the white luminescence of the bulk specimen almost disappears above 50 K. Pontes et al. [9] found an intense white luminescence band centred at 2.3 eV at room temperature in highly disordered STO films and the luminescence disappeared with progressing thermal annealing (which induces crystallization). The behaviour is very similar to the features (2) and (3). They tried to assign the white luminescence to non-bridging oxygen defect centres. In the previous paper [8, 10], we pointed out the important role of oxygen defects (for example,  $(\text{Ti}^{3+}\text{-oxygen vacancy-Ti}^{3+})$  complex) for the white luminescence observed for STO bulk single crystal. The temperature-enhanced luminescence at the intermediate temperature range, which is given in the feature (4), may be due to some thermal release of trapped electrons. Comparing the considerably-blue-shifted optical absorption edge energies (see Fig. 2) with the excitation laser photon energy (3.81 eV), a basic problem is raised about the PL of the as-deposited films. How does a 325 nm (= 3.81 eV) laser photon excite the luminescence of the as-deposited films having large band gap ( $> 3.8$  eV)? A possible mechanism is the photoexcitation of mid-gap states due to structural defects and/or surface defects which are missed in a conventional optical transmission measurement. On the other hand, since the interband excitation is effectively achieved in the annealed films by the 325 nm laser photon, the PL components of the annealed films may be assigned to the recombination luminescence of the electron and hole trapped around crystal defects (which decrease in number by annealing).

Finally, though the blue-shifted energy gap of the film (which displays a halo XRD pattern) has been frequently attributed to the quantum-size effect or the amorphous structures, the present study suggests that the blue-shift originates mainly from large interatomic spacing in amorphous structure which contains a large number of oxygen defects. The PL spectra before and after annealing procedure clarify that the crystal defects in STO films act as the white-luminescence centres. More detailed analysis of the experimental data shown in the present paper is now in progress. The results will be reported in a separate paper.

## References

- [1] K. A. Müller and H. Burkard, Phys. Rev. B **19**, 3593 (1979).
- [2] H. Katsu, H. Tanaka, and T. Kawai, J. Appl. Phys. **90**, 4578 (2001).
- [3] T. Hasegawa, S. Mouri, Y. Yamada, and K. Tanaka, J. Phys. Soc. Jpn. **72**, 41 (2003).
- [4] D. Bao, X. Yao, N. Wakiya, K. Shinozaki, and N. Mizutani, Appl. Phys. Lett. **79**, 3767 (2001).
- [5] Y. Gao, Y. Masuda, and K. Koumoto, J. Korean Ceram. Soc. **40**(3), 213 (2003).
- [6] M. Cardona, Phys. Rev. **140**, A651 (1965).
- [7] T. Hasegawa, M. Shirai, and K. Tanaka, J. Lumin. **87-89**, 1217 (2000).
- [8] S. Mochizuki, F. Fujishiro, and S. Minami, J. Phys.: Condens. Matter **17**, 923 (2005).
- [9] E. M. Pontes, E. Longo, E. R. Leite, E. J. H. Lee, J. A. Varela, P. S. Pizani, C. E. M. Campos, F. Lanciotti, V. Mastellaro, and C. D. Pinheiro, Mater. Chem. Phys. **77**, 598 (2002).
- [10] S. Mochizuki, F. Fujishiro, K. Shibata, and K. Ishiwata, Physica B **376/377**, 816 (2006).

## **Excitons in pristine silver iodide crystals**

**Shosuke Mochizuki and Fumito Fujishiro**

Department of Physics, College of Humanities and Sciences, Nihon University, 3-25-40 Sakurajosui, Setagaya-ku, Tokyo 156-8550, Japan

Received 7 June 2006, revised 14 July 2006, accepted 17 July 2006  
Published online 2 November 2006

**PACS** 61.72.Nn, 71.35.-y, 78.55.Hx

We prepared the film and bulk specimens of chemically-pure pristine silver iodide and their crystal structures were investigated by the x-ray diffraction method. The photoluminescence properties of these specimens were measured at different temperatures under different excitation powers. The luminescence due to the radiative decay of free exciton is observed at about 2.936 eV. Several specimen-dependent luminescence components (which increase sublinearly in intensity with increasing excitation power) are also observed and they are discussed in the light of the x-ray diffraction data.

phys. stat. sol. (c) 3, No. 10, 3586–3591 (2006) / DOI 10.1002/pssc.200672144



**WILEY-VCH**

**REPRINT**

## Excitons in pristine silver iodide crystals

Shosuke Mochizuki\* and Fumito Fujishiro

Department of Physics, College of Humanities and Sciences, Nihon University, 3-25-40 Sakurajosui, Setagaya-ku, Tokyo 156-8550, Japan

Received 7 June 2006, revised 14 July 2006, accepted 17 July 2006  
Published online 2 November 2006

PACS 61.72.Nn, 71.35.-y, 78.55.Hx

We prepared the film and bulk specimens of chemically-pure pristine silver iodide and their crystal structures were investigated by the x-ray diffraction method. The photoluminescence properties of these specimens were measured at different temperatures under different excitation powers. The luminescence due to the radiative decay of free exciton is observed at about 2.936 eV. Several specimen-dependent luminescence components (which increase sublinearly in intensity with increasing excitation power) are also observed and they are discussed in the light of the x-ray diffraction data.

© 2006 WILEY-VCH Verlag GmbH & Co. KGaA, Weinheim

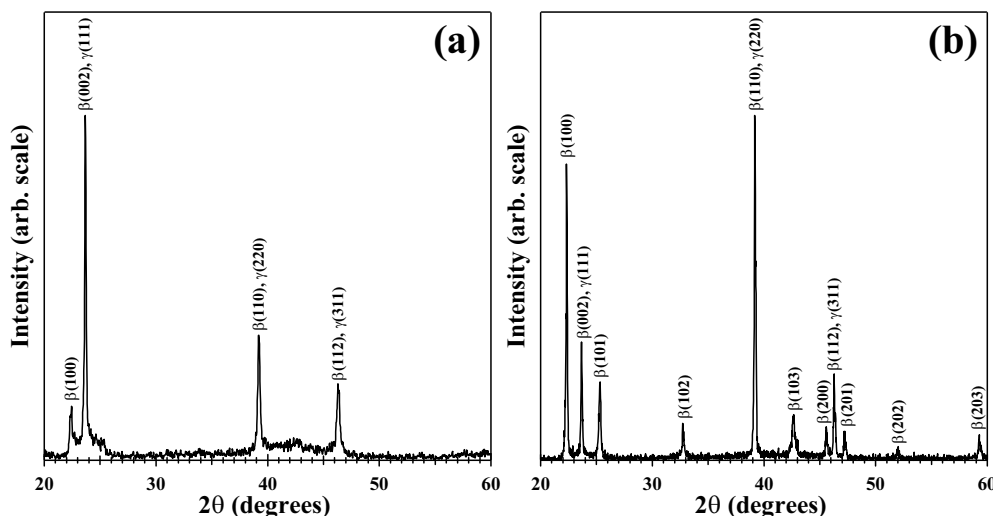
**1 Introduction** Silver iodide (AgI) crystal has three phases designated as  $\alpha$ ,  $\beta$  and  $\gamma$  at normal pressure in the order of decreasing temperature [1], and it is a well-known superionic conductor and a solid-battery material. It is known that the dispersion of oxide fine particles into AgI enhances considerably the ionic conductivity [2, 3]. A special basic problem about the AgI-based composites is raised. What are the atomic and electronic structures of the AgI/oxide particle interfaces? Since constituent material AgI shows clear exciton spectra even above room temperature [4] and the spectra are very sensitive to the environment in which excitons are moving, the optical spectra due to excitons may provide useful information about the structure of the AgI/oxide particle interfaces [3]. However, the information on the structural and optical-spectral characteristics of pristine AgI remains somewhat fragmentary. Cardona [5] reported the optical absorption spectra of  $\gamma$ - and  $\beta$ AgI films. As seen from his spectrum (Fig. 1), the spectrum of  $\gamma$ AgI film contains the spectral component of  $\beta$ AgI, and therefore the detailed structure near absorption edge of AgI remains to be clarified. Mochizuki and Ohta [4] measured the optical absorption and photoluminescence (PL) spectra of AgI films at different temperatures from 7 K, through the superionic phase transition point (419 K), to 472 K, for the first time. The observed low-temperature exciton spectra were still affected by crystal defects and impurities. To date, the detailed optical study on the well-characterised  $\gamma$ - and  $\beta$ AgI crystals has been not reported. Although  $\beta$ AgI crystal can be easily grown from a saturated solution, the crystal displays very complicated PL spectra. Very recently, we fabricated purer AgI crystals by the AgI-I<sub>2</sub> composite technique and the melt-growth one, and studied both their crystal structures and their PL properties. In the present paper, we report the results and clarify the exciton nature of pristine AgI, taking account of their structural properties.

**2 Experimental** AgI powder of 99.999 % purity was produced by Alpha Aesar (U. S. A). Detected impurities are B (1 ppm) and Si (4 ppm). The AgI powder was evaporated onto a low-temperature optically-flat sapphire substrate (R-cut) in vacuum to grow an AgI-I<sub>2</sub> composite film, and the film was annealed at room temperature. The detail of the film fabrication has been reported previously [6]. Two

\* Corresponding author: e-mail: motizuki@physics.chs.nihon-u.ac.jp, Phone: +81 3 5317 9771, Fax: +81 3 5317 9771

types of bulk AgI crystals were prepared as follows. The powder was fully melted in a lidded alumina crucible at 873 K for 12 h. The melt was cooled by the rapidly-cooling method with a twin roller. The cooling speed was approximately 100 K/s. We call this specimen ‘the rapidly-cooled AgI’. Another cooling method was also used. The melt was naturally cooled to room temperature in a furnace. We call this specimen ‘the naturally-cooled AgI’. The obtained crystals were characterized by a conventional x-ray diffraction (XRD) method using a Cu  $\text{K}\alpha_1$  radiation. The PL spectra were measured by an optical multi-channel analyser consisting of a grating monochromator (focal length = 32 cm) and an intensified diode-array detector (gate time  $\geq 5$  ns). A Q-switched Nd<sup>3+</sup>-YAG laser ( $\lambda = 355$  nm, pulse width  $< 5$  ns, repetition frequency = 10 Hz) was used as an excitation source. The PL excitation spectra were also measured by varying the excitation-light wavelength. A closed-cycle helium refrigerator equipped with a temperature controller was used for changing specimen temperature between 10 and 300 K.

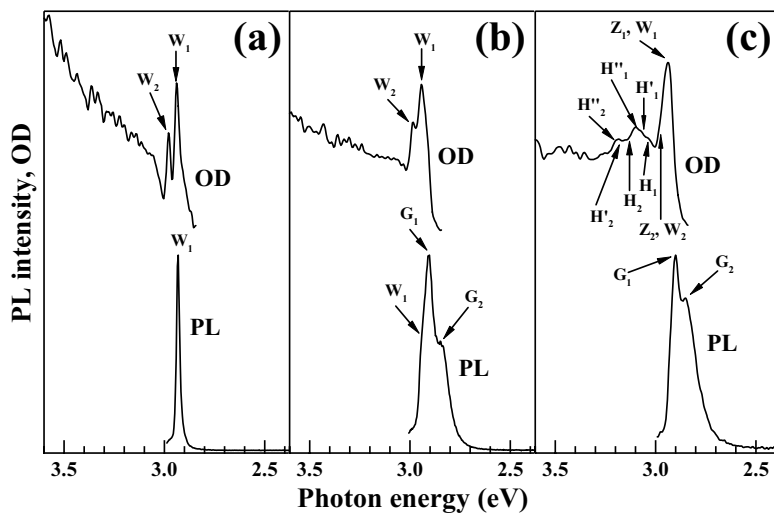
**3 Results and discussion** Figures 1(a) and (b) show the room-temperature XRD patterns of the naturally-cooled AgI and rapidly-cooled one, respectively. All of the diffraction lines observed for the rapidly-cooled AgI are assigned to those of the hexagonal AgI ( $\beta\text{AgI}$ ). As seen in these figures, the XRD pattern of the naturally-cooled AgI differs from that of the rapidly-cooled one. The  $(h0l)$  lines related to the hexagonal stacking are weaken and broadened, which indicates the stacking disorder in the  $\beta\text{AgI}$  structure. It is also noted that extra diffractions appear between 38 and 48 degrees, creating a broad background band. Several periodically-stacking faults (for example, 4H, 7H, 8H, 12H, 16H, 80H polytypes) of AgI were reported [7] for  $\beta\text{AgI}$ . The wurtzite structure of  $\beta\text{AgI}$  (2H) and zincblende structure of the metastable  $\gamma\text{AgI}$  (3C) differ in the stacking sequence, and they can be regarded as different polytypes.



**Fig. 1** X-ray diffraction patterns: (a) the naturally-cooled AgI and (b) rapidly-cooled one.

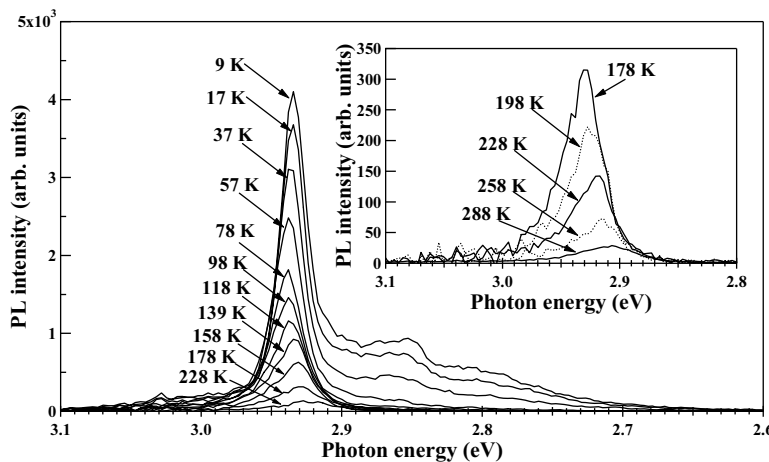
So-called  $\gamma\text{AgI}$  film displays almost the same XRD pattern observed for the naturally-cooled AgI, except for weak  $\beta(100)$  line. Real  $\gamma\text{AgI}$  film contains more or less stacking disorder, exhibiting traces of the  $\beta(100)$  line and the extra diffractions between 38 and 48 degrees. It is said that  $\gamma$  phase is stabilized by nonstoichiometry and strain due to a difference in the thermal expansion coefficients between the AgI film and substrate. The naturally-cooled AgI is thin reddish, suggesting iodine deficiency, while the rapidly-cooled AgI is thin yellowish. The naturally-cooled AgI is more iodine-deficient than the rapidly-cooled one, becoming reddish, since the former AgI was heated at high temperature for longer time (about 10 h) than the latter one. This view agrees with the known result that a silver-rich AgI solution crystallizes in the  $\gamma$  phase. Anyway, the naturally-cooled AgI should be designated as  $\gamma\text{AgI}$ .

We show first the optical spectra of different AgI films and look over the exciton structure of AgI. Figures 2(a), (b) and (c) show the optical density and PL spectra of three different AgI films at about 12 K. The three films were evaporated on the sapphire substrates of different substrate temperatures  $T_s$ : (a)  $T_s = 200$  K, (b)  $T_s = 109$  K and (c)  $T_s = 300$  K. The spectra shown in Fig. 2(a) correspond to the wurtzite phase ( $\beta\text{AgI}$ ). Near the band edge of AgI, sharp  $W_1$ - and  $W_2$  exciton absorption bands, and a very sharp luminescence band due to the radiative decay of the  $W_1$  exciton, appear. With introducing stacking disorder, the  $W_1$ - and  $W_2$  exciton bands become broaden as shown in Fig. 2(b). With further introducing stacking disorder, several polytype-structure-related  $H_j$  ( $j = 1, 2$ ) and  $H'_j$  ( $j = 1, 2$ ) exciton absorptions, and two  $Z_1$  and  $Z_2$  exciton absorptions [8] also appear, as shown in Fig. 2(c). It is also noted that, with introducing stacking disorder, new luminescence bands,  $G_1$  and  $G_2$ , appear, merging with the  $W_1$  exciton band. The  $G_1$  and  $G_2$  luminescence bands may be assigned to the radiative decays of excitons trapped at different stacking faults. As discussed previously [6, 8], three types of the spectral structures shown here may arise mainly from iodine deficiency and/or thermal strain.



**Fig. 2** Optical spectra of different AgI films at about 12 K.

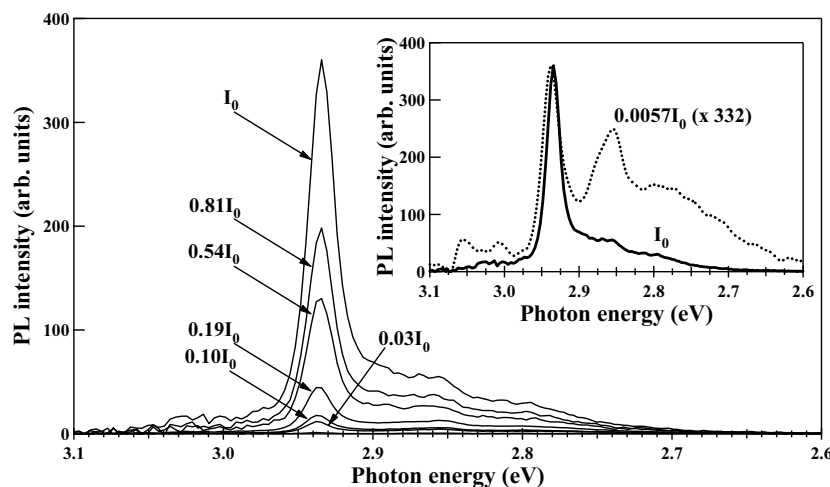
Figure 3 shows the PL spectra of the naturally-cooled AgI bulk at different temperatures between 9 and 288 K. The PL spectra at different temperatures above 178 K are also shown in the inset.



**Fig. 3** Photoluminescence spectra of the naturally-cooled AgI at different temperatures.

The PL spectrum at 9 K is characterized by an intense luminescence centred at 2.936 eV. This luminescence is on a skirt extending up to about 3.1 eV, and it is also accompanied by several shoulder components. The peak energy of 2.936 eV is higher than the  $Z_{1,2}$  exciton energy (2.919 eV) determined from the optical absorption spectrum of  $\gamma$ AgI (zincblende structure). The peak energy is close to the  $Z_1$  exciton energy and  $W_1$  exciton one determined from the optical absorption and reflection spectra [4–6, 8, 9]. With increasing temperature, the free exciton luminescence decreases in intensity, shifting toward 2.938 eV. With further increasing temperature above 78 K, the centre energy begins to red-shift and then it attains 2.907 eV at 288 K. This energy is very close to the optical absorption peak energy of  $\gamma$ AgI film at 4 K [4, 6]. Through the PL excitation measurements, it is found that the PL components below 2.9 eV follow the free exciton formation. This suggests that the naturally-cooled AgI contains several kinds of shallow exciton traps.

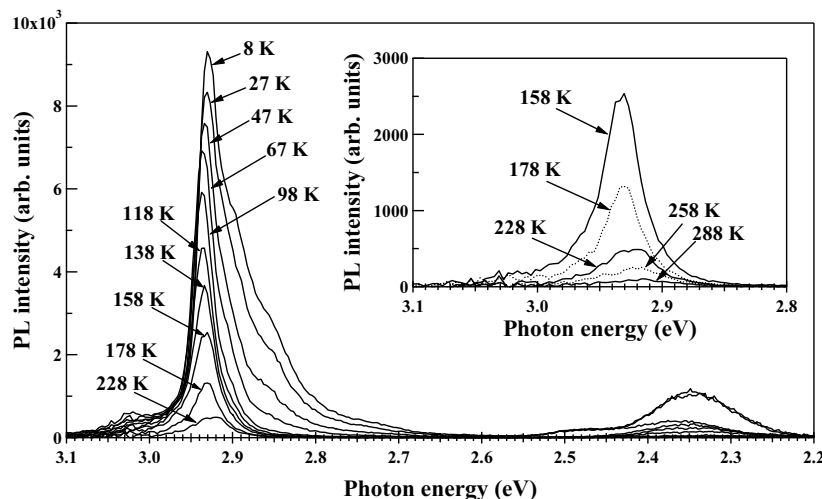
Figure 4 shows the PL spectra of the naturally-cooled AgI at 9 K under different excitation powers. In the inset, the spectra obtained under  $I_0$  and  $0.0057I_0$  are shown. The maximum power  $I_0$  is  $50 \mu\text{J} (\sim 0.7 \text{ mJ/cm}^2)$ . The PL intensity at 2.936 eV increases linearly with increasing excitation intensity up to  $0.8I_0$ , while the PL components below 2.9 eV increase sublinearly in intensity. In the inset, after rescaling, the PL spectrum under the maximum excitation power is compared with that under the minimum one. This indicates that the PL components below 2.9 eV arise from finite number of luminescence centres (for example, crystal defects and residual impurities). On further increasing excitation power from  $0.8I_0$ , the PL intensity at 2.936 eV has become superlinearly increased and narrowed in spectral shape. In general, a superlinearly-dependent exciton luminescence is explained by the stimulated emission due to the exciton-exciton collision process [10, 11] or by the amplified spontaneous emission (so-called ASE), as reported for PbS films [12] and polymer film [13]. Since the observed lower-energy shift is too small to explain the result by such exciton-exciton collision process, both the observed superlinear dependence and the observed spectral narrowing may be assigned to the amplified spontaneous emission process. The threshold pump intensity is estimated to be about  $0.57 \text{ mJ/cm}^2$ . The skirt extending up to 3.1 eV remains even at the highest photoexcitation and it may be ascribed to the bound exciton background due to crystal imperfections (for example, stacking faults) or several combinations of exciton and phonons. The LO and TO phonon energies of AgI are 15.4 and 13.2 meV, respectively [14]. In particular, the higher energy portion of the skirt overlaps in energy of the  $W_1$  exciton absorption, polytype-related exciton absorptions [6, 8] and  $Z_2$  exciton absorption. Therefore, the higher energy portion (of which intensity is decreased by reabsorptions) may consist of several kinds of free-exciton luminescence components and it may be assigned to the radiative decays of these excitons. We carried out also the time-resolved PL measurements.



**Fig. 4** Photoluminescence spectra of the naturally-cooled AgI at 9 K under different excitation powers.

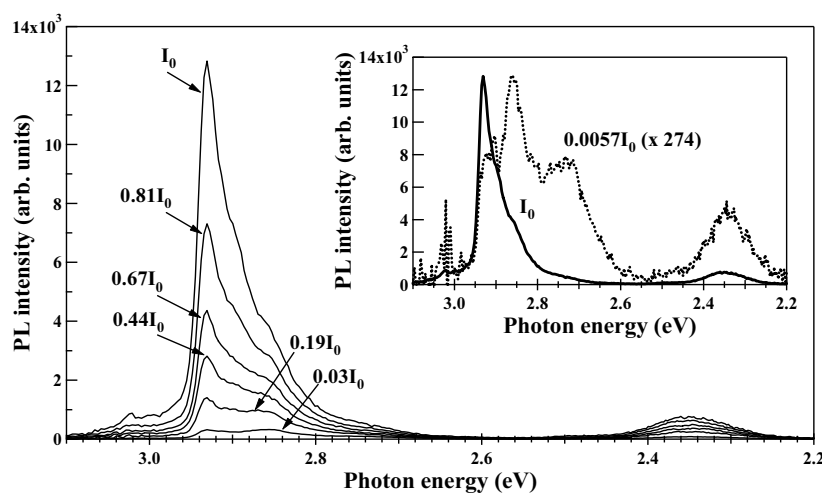
It is found that the free exciton luminescence decays within several nanoseconds, while the PL components below 2.9 eV remain after 30 ns. This suggests that the PL components below 2.9 eV arise from excitons trapped at crystal defects or/and impurities.

Figure 5 shows the PL spectra of the rapidly-cooled AgI ( $\beta$ -AgI) at different temperatures. A sharp luminescence appears at 2.930 eV, which is slightly lower than that of the naturally-cooled AgI. With increasing temperature up to 118 K, the luminescence decreases in intensity and it shifts slightly toward 2.937 eV and, on further increasing temperature, the luminescence begins to red-shift, which suggests a coexistence of the heavy-hole exciton and light-hole one.



**Fig. 5** Photoluminescence spectra of the rapidly-cooled AgI at different temperatures

Like as the naturally-cooled AgI, the sharp luminescence is accompanied by several PL components below 2.9 eV. With further increasing temperature, the PL components also decrease in intensity. Unlike the naturally-cooled AgI, a broad luminescence appears at 2.35 eV. Through the PL excitation measurements, it is found that all the PL components below 2.9 eV follow the free exciton formation. This suggests that the rapidly-cooled AgI contains deeply exciton traps due to excessively high cooling rate.



**Fig. 6** Photoluminescence spectra of the rapidly-cooled AgI at 8 K under different excitation power.

Figure 6 shows the PL spectra of the rapidly-cooled AgI under different excitation powers at 8 K. The maximum intensity  $I_0$  is 50  $\mu\text{J}$  ( $\sim 0.7 \text{ mJ/cm}^2$ ). The 2.931 eV peak intensity increases linearly with increasing excitation power up to  $0.7I_0$  and, on further increasing excitation power, it becomes to increase superlinearly, which suggests the onset of an amplified spontaneous emission. On the other hand, the PL components below 2.9 eV increase sublinearly with increasing excitation power. Like as the naturally-cooled AgI, the result indicates that the PL components below 2.9 eV arise from finite number of luminescence centres (crystal defects and impurities). It is noted that the PL spectra are almost independent of the cooling rate, though their crystal structure and absorption spectra differ each other. We carried out also the time-resolved PL measurements at 8 K for the rapidly-cooled AgI. It is found that the PL components above 2.8 eV disappear within several nanoseconds, while the 2.35 eV luminescence remains after 20 ns.

In conclusion, we prepared different chemically-pure film- and bulk AgI specimens and we have studied their structures and optical properties. The followings are found.

- (i) Depending on the preparation methods, AgI crystallizes in a wurtzite structure ( $\beta\text{AgI}$ ) or zincblende-like one ( $\gamma\text{AgI}$ ) which is stabilized by stacking faults, leading to several kinds of polytype structures.
- (ii) The spectral structures of optical absorption and the photoluminescence properties (temperature- and excitation-power dependencies of the photoluminescence spectra) clarify the intrinsic exciton nature and crystal-defect-induced exciton one in real AgI specimens. The stacking faults lead to the splitting of the degenerated  $Z_{1,2}$  exciton state and the creation of new polytype-structure-related  $H_J$  and  $H'_J$  exciton states.
- (iii) The enhanced luminescence and spectral narrowing have been observed at high excitation powers ( $> 0.56 \text{ mJ/cm}^2$ ) for the AgI bulk crystals. It can be explained by the amplified spontaneous emission process.

Finally, we would like to draw an attention to similar splitting of the  $Z_{1,2}$  exciton state for AgI micro-crystal [15]. One of the causes for the  $Z_{1,2}$  splitting in AgI microcrystal is some crystal-field change at the crystallite surfaces. The iodine deficiency may affect on the crystal structure (namely, crystal filed around  $\text{Ag}^+$  ion) of AgI, as discussed in the present paper.

**Acknowledgements** This work was partially supported by a Grant-in-Aid for Scientific Research from the Ministry of Education, Science, Sport Culture and Technology, Japan. This work is supported by an Interdisciplinary General Joint Research Grand (Nihon University). This work is also partially supported by a Research Grant from the College of Humanities and Sciences (Nihon University).

## References

- [1] P. V. Smith, J. Phys. Chem. Solids **37**, 589 (1976).
- [2] J.-S. Lee, S. Adams, and J. Maier, J. Electrochem. Soc. **147**, 2407 (2000).
- [3] S. Mochizuki and F. Fujishiro, J. Phys.: Condens. Matter **15**, 5057 (2003).
- [4] S. Mochizuki and Y. Ohta, J. Lumin. **87–89**, 299 (2000).
- [5] M. Cardona, Phys. Rev. **129**, 69 (1963).
- [6] S. Mochizuki and F. Fujishiro, J. Phys.: Condens. Matter **16**, 3239 (2004).
- [7] P. R. Prager and P. Krishna, Crystal Growth and Characterization of Polytype Structures (Pergamon, Oxford, 1983), p. 451.
- [8] S. Mochizuki, Physica B **308–310**, 1042 (2001).
- [9] M. Bettini, S. Suga, and R. Hanson, Solid State Commun. **15**, 1885 (1974).
- [10] C. Klingshirn, phys. stat. sol. (b) **74**, 547 (1975).
- [11] I. Tanaka and M. Nakayama, J. Appl. Phys. **92**, 3511 (2002).
- [12] V. Sukhovatkin, S. Musikhin, I. Gorelikov, S. Cauchi, L. Bakueva, E. Kumacheva, and E. H. Sargent, Opt. Lett. **30**, 171 (2005).
- [13] M. D. McGehee, R. Gupta, S. Veenstra, E. K. Miller, M. A. Diaz-Garcia, and A. J. Heeger, Phys. Rev. B **58**, 7035 (1998).
- [14] G. L. Bottger and C. V. Damsgard, J. Chem. Phys. **57**, 1215 (1972).
- [15] S. Mochizuki and K. Umezawa, Phys. Lett. A **228**, 111 (1997).

## **Excitons in AgI–oxide particle composites: AgI–SrTiO<sub>3</sub>**

**Fumito Fujishiro and Shosuke Mochizuki**

Department of Physics, College of Humanities and Sciences, Nihon University, 3–25–40 Sakurajosui, Setagaya-ku, Tokyo 156–8550, Japan

Received 7 June 2006, revised 8 July 2006, accepted 8 July 2006  
Published online 2 November 2006

PACS 71.35.-y, 72.80.Tm, 78.55.Hx

We fabricated (x)AgI–(1–x)SrTiO<sub>3</sub> fine particle composites over a wide composition range of 0–100 mol % AgI. It is found that the dispersion of SrTiO<sub>3</sub> fine particles enhances the ionic conductivity and (0.6)AgI–(0.4)SrTiO<sub>3</sub> has the highest ionic conductivity ( $1.68 \times 10^{-4}$  S/cm which is two hundreds times in comparison with that of pristine AgI), for the first time. In order to clarify such ionic conductivity enhanced by dispersing SrTiO<sub>3</sub> fine particles into AgI, the photoluminescence measurements were carried out at different temperatures between 10 K and room temperature under different photoexcitation intensities, together with the structural and morphological studies (X-ray diffractometry, scanning electron microscopy and energy dispersive X-ray fluorescence spectroscopy). The spectra consist of free exciton luminescence band and several broad luminescence bands due to the excitons trapped at crystal defects and residual impurities. The free exciton luminescence band almost disappears at  $x = 0.6$ , which may suggest the existence of considerable number of non-radiative traps (crystal defects) at the AgI/SrTiO<sub>3</sub> particle interfaces. Such crystal defects may act as ionic pathways. The structural and morphological studies confirm the randomly-stacked  $\gamma$ AgI/ $\beta$ AgI heterostructures at the AgI/SrTiO<sub>3</sub> particle interfaces.

phys. stat. sol. (c) 3, No. 10, 3592–3597 (2006) / DOI 10.1002/pssc.200672112

## Excitons in AgI–oxide particle composites: AgI–SrTiO<sub>3</sub>

Fumito Fujishiro\* and Shosuke Mochizuki

Department of Physics, College of Humanities and Sciences, Nihon University, 3–25–40 Sakurajosui, Setagaya-ku, Tokyo 156–8550, Japan

Received 7 June 2006, revised 8 July 2006, accepted 8 July 2006  
Published online 2 November 2006

PACS 71.35.-y, 72.80.Tm, 78.55.Hx

We fabricated  $(x)\text{AgI}-(1-x)\text{SrTiO}_3$  fine particle composites over a wide composition range of 0–100 mol % AgI. It is found that the dispersion of SrTiO<sub>3</sub> fine particles enhances the ionic conductivity and  $(0.6)\text{AgI}-(0.4)\text{SrTiO}_3$  has the highest ionic conductivity ( $1.68 \times 10^{-4}$  S/cm) which is two hundreds times in comparison with that of pristine AgI, for the first time. In order to clarify such ionic conductivity enhanced by dispersing SrTiO<sub>3</sub> fine particles into AgI, the photoluminescence measurements were carried out at different temperatures between 10 K and room temperature under different photoexcitation intensities, together with the structural and morphological studies (X-ray diffractometry, scanning electron microscopy and energy dispersive X-ray fluorescence spectroscopy). The spectra consist of free exciton luminescence band and several broad luminescence bands due to the excitons trapped at crystal defects and residual impurities. The free exciton luminescence band almost disappears at  $x = 0.6$ , which may suggest the existence of considerable number of non-radiative traps (crystal defects) at the AgI/SrTiO<sub>3</sub> particle interfaces. Such crystal defects may act as ionic pathways. The structural and morphological studies confirm the randomly-stacked  $\gamma\text{AgI}/\beta\text{AgI}$  heterostructures at the AgI/SrTiO<sub>3</sub> particle interfaces.

© 2006 WILEY-VCH Verlag GmbH & Co. KGaA, Weinheim

**1 Introduction** It is known that a dispersion of oxide fine particles into silver iodide (AgI) (which is well known as a typical superionic conductor) enhances considerably its ionic conductivity at room temperature by several orders of magnitude, in comparison with that of pristine AgI. Theoretically, in the composites, cations (which are the component of the ionic crystal) are adsorbed at the oxide surfaces, creating the space charge layer at the ionic conductor/oxide particle interfaces and enhancing the electrical conductivity and, moreover, the smaller particle enhances more ionic conductivity and the oxide having the higher dielectric constant does also [1]. To date, many studies on the conductivity enhancement have been reported for AgI-based composites. In particular, AgI– $\gamma\text{Al}_2\text{O}_3$  composites were widely investigated. A polytype structure and stacking disorder in the AgI domain were confirmed by X-ray diffraction (XRD) and differential scanning calorimetry, which also accounts for the observed electrical properties of the composites [2]. A special basic problem about AgI-based composites is raised. What are the atomic and electronic structures of the AgI/oxide particle interfaces? Fortunately, constituent material AgI shows clear optical absorption and photoluminescence (PL) spectra due to excitons even at room temperature [3–5]. Moreover the exciton behaviour is very sensitive to the environments in which excitons are moving, and therefore the exciton spectra may provide useful information about the microscopic structure at the AgI/oxide particle interfaces. Previously, we fabricated several kinds of AgI–oxide fine particle composites and observed considerable conductivity enhancement. In addition to measurements of the XRD patterns and electrical conductivities, we measured the optical spectra due to excitons and discussed the pathway for the mobile Ag<sup>+</sup> ion (for example, AgI–anatase TiO<sub>2</sub> composites [6]). Inciden-

\* Corresponding author: e-mail: fumito@phys.chs.nihon-u.ac.jp, Phone: +81 3 5317 9771, Fax: +81 3 5317 9771

tally, strontium titanate ( $\text{SrTiO}_3$ ) is known as the quantum paraelectrics [7] and has a high dielectric constant (300) at room temperature. In addition,  $\text{SrTiO}_3$  particles tend to contain oxygen defects (a point defect as an oxygen vacancy and a complex defect represented as the  $\text{Ti}^{3+}$ –oxygen vacancy– $\text{Ti}^{3+}$ ) and show a catalysis. Therefore, the dispersion of  $\text{SrTiO}_3$  particles into  $\text{AgI}$  may easily affect the electronic and atomic structure at/near the  $\text{AgI}/\text{SrTiO}_3$  particle interfaces and hence we can anticipate a large conductivity enhancement for the  $\text{AgI}-\text{SrTiO}_3$  fine particle composites.

In present paper, we show the results of the structural, electrical and optical measurements for the  $\text{AgI}-\text{SrTiO}_3$  composites and discuss the structure and exciton behaviour based on the data obtained.

**2 Experimental** The  $\text{AgI}-\text{SrTiO}_3$  composites,  $(x)\text{AgI}-(1-x)\text{SrTiO}_3$ , were prepared by fully mixing  $\text{AgI}$  powder (Alfa Aesar, 99.999%) with  $\text{SrTiO}_3$  nanoparticles (Aldrich, 99.5%) in air. The mixture was uniaxially compressed under 0.2 GPa for 30 minutes at room temperature to fabricate pellets, and then the pellets were heated in the lidded crucible at 673 K for 12 h in air. The pristine  $\text{SrTiO}_3$  ( $x = 0$ ) and pristine  $\text{AgI}$  ( $x = 1$ ) pellets were prepared by the same method.

The composites were characterized at 295 K by XRD analysis with  $\text{Cu K}\alpha_1$  radiation. The morphology of the composites was analyzed by using a scanning electron microscope (SEM). Distribution maps of Ag, I, Sr, Ti and O atoms in the composites were obtained by means of a SEM with an energy dispersive X-ray (EDX) fluorescence spectrophotometer. The electrical conductivity was measured by using the complex impedance method with silver electrodes evaporated onto both sides of the pellets. The PL spectra were measured by an optical multi-channel analyzer consisting of a grating monochromator (focal length = 32 cm) and an image-intensified diode-array detector (gate time  $\geq 5$  ns). A CW He–Cd laser ( $\lambda = 325$  nm) and a  $\text{Nd}^{3+}:\text{YAG}$  laser ( $\lambda = 355$  nm, pulse width  $\leq 5$  ns, repetition frequency = 10 Hz) were used as the excitation source. A closed cycle helium-gas refrigerator equipped with a temperature controller was used for changing specimen temperature between 10 K and 288 K.

**3 Results and discussion** The electrical conductivity variation against  $\text{AgI}$  content is shown in Fig. 1. There is the conductivity enhancement, which shows a maximum (about  $1.68 \times 10^{-4}$  S/cm) at  $x = 0.6$ . Since the conductivity for pristine  $\text{AgI}$  ( $x = 1$ ) is about  $8.04 \times 10^{-7}$  S/cm, the conductivity at  $x = 0.6$  is enhanced about two hundreds times in comparison with that of pristine  $\text{AgI}$ .

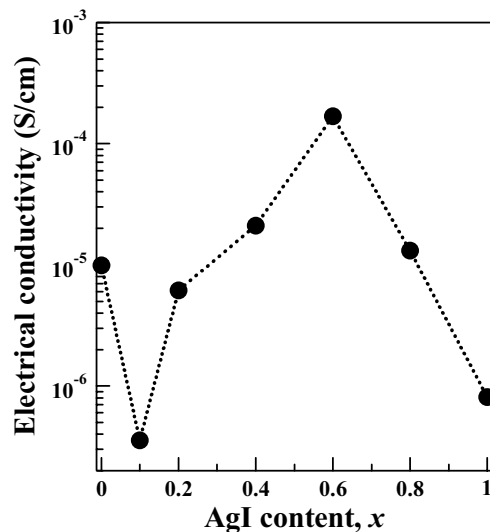


**Fig. 1** Electrical conductivity for different  $(x)\text{AgI}-(1-x)\text{SrTiO}_3$  composites at room temperature.

This conductivity enhancement may be caused by  $\text{Ag}^+$  ion conduction through the randomly-stacked  $\gamma\text{AgI}/\beta\text{AgI}$  heterogeneity at/near the  $\text{AgI}/\text{SrTiO}_3$  particle interfacial region [8]. However,  $(0.1)\text{AgI}-$

(0.9)SrTiO<sub>3</sub> shows the conductivity decrease. Since SrTiO<sub>3</sub> is an electronic conductor, dopant AgI is thought to be an electronic-carrier scattering centre.

We performed observations of the fractured surfaces of (x)AgI–(1–x)SrTiO<sub>3</sub> composites with a SEM attached with an EDX fluorescence analyser. The low- and high-resolution-SEM images of the (0.6)AgI–(0.4)SrTiO<sub>3</sub> are shown in Figs. 2(a) and (b), respectively, as typical results.

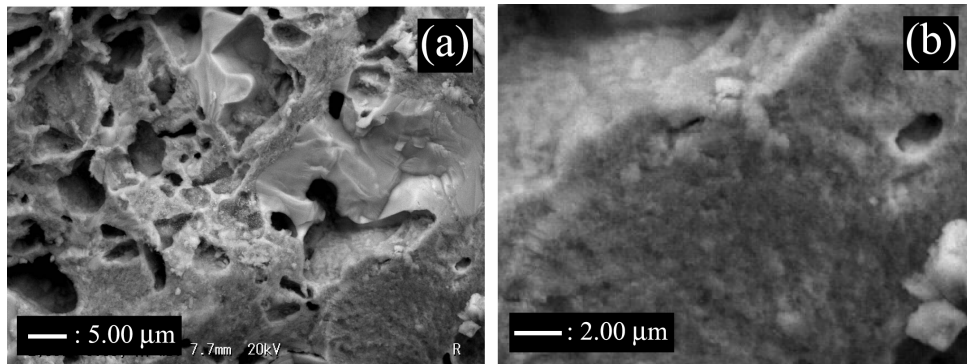


**Fig. 2** Scanning electron microscope images of the (0.6)AgI–(0.4)SrTiO<sub>3</sub>: (a) low- and (b) high resolution.

Rough-face blocks, smooth-face them and voids are seen in these figures. The rough-face blocks contain fine particles which aggregate to make larger domain. From the EDX measurement, we found that AgI and SrTiO<sub>3</sub> fine particles distributed uniformly over both the rough-face blocks and smooth-face them. This indicates that the rough-face blocks are the fractured surfaces of the smooth-face blocks, and SrTiO<sub>3</sub> particles are densely packed within the large AgI blocks, which makes the three-dimensionally networks, as the AgI–anatase TiO<sub>2</sub> composites [6].

Figures 3(a) and (b) show the XRD patterns for different (x)AgI–(1–x)SrTiO<sub>3</sub> composites at 295 K. All XRD patterns in Fig. 3(a) are normalized in intensity.

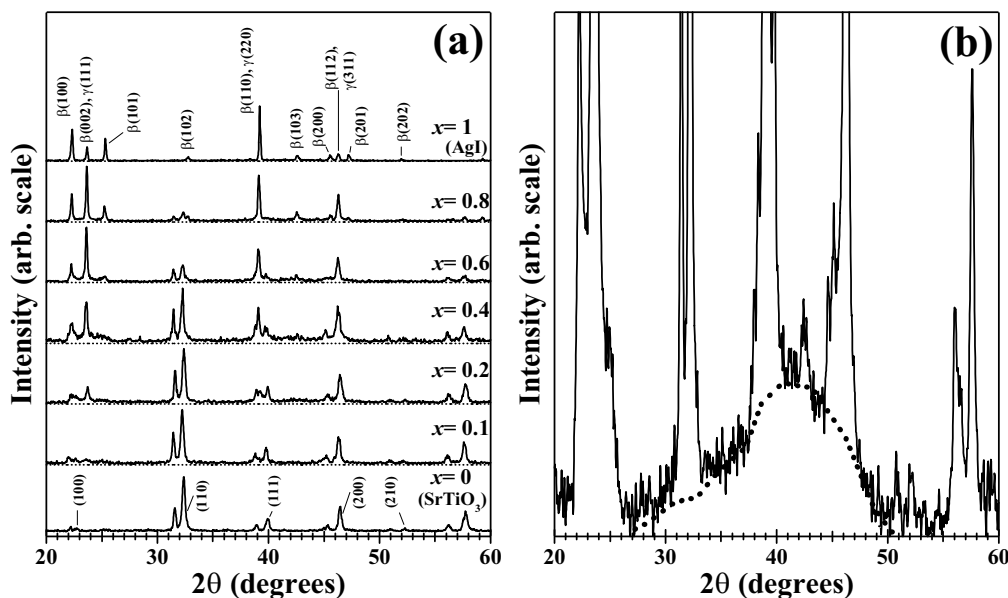


**Fig. 3** X-ray diffraction patterns at 295 K: (a) for different (x)AgI–(1–x)SrTiO<sub>3</sub> composites and (b) of the (0.6)AgI–(0.4)SrTiO<sub>3</sub>.

It is found that the full width at half maximum of the diffraction lines due to  $\text{SrTiO}_3$  hardly changes with increasing  $\text{AgI}$  contents, which indicates that the average size of  $\text{SrTiO}_3$  particles is not changed in the composites. Pristine  $\text{AgI}$  shows clear lines due to  $\beta\text{AgI}$  (wurtzite structure), and with decreasing  $x$ , the  $(h0l)$  lines due to the stacking sequence of the hexagonal  $\beta\text{AgI}$  are weakened in intensity and widened. In small  $x$  region, the diffraction lines related to  $\text{AgI}$  become  $\gamma\text{AgI}$ -like them. The diffraction profile is similar to that of Type II  $\text{AgI}$  crystal reported by Lee *et al.* [9]. Thus, it is found that, with increasing  $\text{SrTiO}_3$  content, an amount of  $\gamma\text{AgI}$  component increases and some stacking faults of  $\beta\text{AgI}$  are created, in addition to the preferential orientation of the crystallites. It is also noted that a broad background (which is shown by a dotted curve ranging from 27 to 52 degrees) grows in middle  $x$  region, as shown for  $(0.6)\text{AgI}-(0.4)\text{SrTiO}_3$  in Fig. 3(b). Unlike to the present  $\text{AgI}-\text{SrTiO}_3$  composites, several diffraction lines related to the 7H-polytype  $\text{AgI}$  were clearly observed for  $\text{AgI}-\gamma\text{Al}_2\text{O}_3$  composites [2] in the same  $2\theta$  range. The 7H- $\text{AgI}$  is partially composed of the stacking sequence of  $\gamma$ - and  $\beta\text{AgI}$  [10]. Although the XRD pattern does not give the information about the microstructure at the interfaces but about the macroscopically-averaged structure, we can assume that the amorphous like  $\text{AgI}$  domain and stacking disordered  $\text{AgI}$  one exist in the  $\text{AgI}/\text{SrTiO}_3$  particle interfacial region. Such stacking disorder may induce some randomly stacked heterogeneities consisting of  $\beta\text{AgI}$  crystallites and  $\gamma\text{AgI}$  them, creating ionic pathways.

Figure 4 shows the PL spectra for different  $(x)\text{AgI}-(1-x)\text{SrTiO}_3$  composites at 10 K. The specimens were excited with a 325 nm laser light (intensity is 0.3 W/cm<sup>2</sup>). All curves in this figure are normalized at the each peak intensity. The rescaling factor is given by each curve.

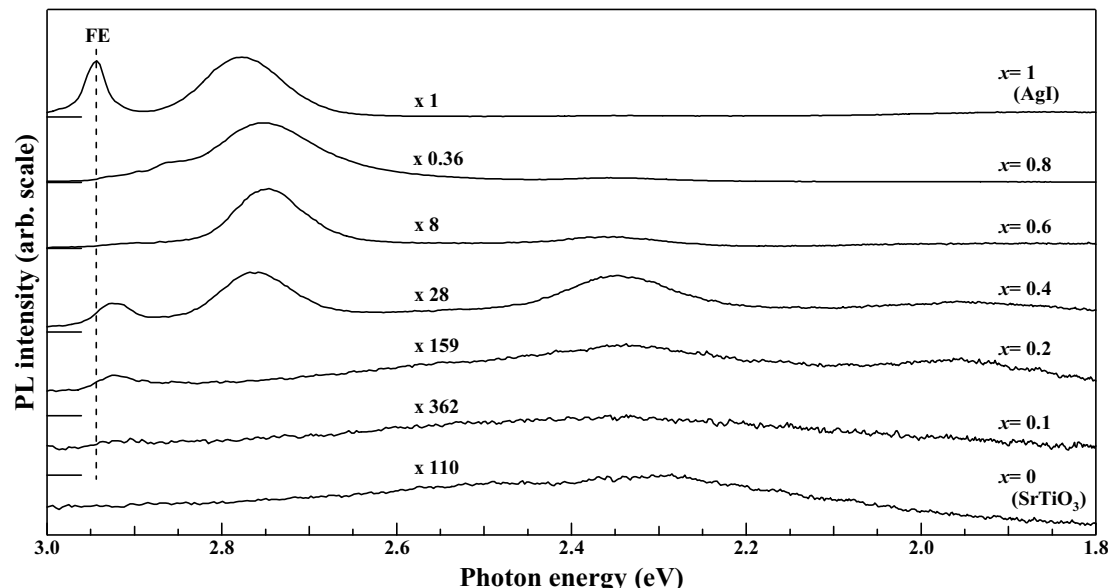


**Fig. 4** Photoluminescence spectra for different  $(x)\text{AgI}-(1-x)\text{SrTiO}_3$  composites at 10 K.

As seen from this figure, the sharp free exciton (FE) luminescence band due to the wurtzite phase  $\text{AgI}$  appears at about 2.94 eV for pristine  $\text{AgI}$ . A broad luminescence band is also observed at 2.78 eV and it may be assigned to the radiative decay of excitons trapped at crystal defects, because most of the pristine  $\text{AgI}$  bulk specimens show specimen-dependent luminescence components in energies between 2.9 and 2.6 eV [4, 11]. With adding  $\text{SrTiO}_3$  particles of 20 mol % ( $x = 0.8$ ), the FE luminescence intensity decreases considerably. The broad luminescence band shifts toward lower energy side, enhancing intensity, and at least two shoulders are observed at the high energy side between 2.94 and 2.82 eV. At  $x = 0.6$  (this composite has a maximum ionic conductivity), the FE luminescence band almost disappears and a new

band begins to appear at 2.34 eV. The depression of the FE luminescence suggests a creation of the non-radiative traps at/near the AgI/SrTiO<sub>3</sub> particle interfaces. A candidate for the non-radiative traps is an amorphous structure. Possible amorphous structure is the randomly-stacked γAgI/βAgI heterostructures which is already shown in the XRD components ranging from 27 to 52 degrees (Fig. 3(b)). On the other hand, since the luminescence intensity at 2.34 eV is higher than that of pristine SrTiO<sub>3</sub> (note the rescaling factor), the origin of the luminescence band may be related to the AgI/SrTiO<sub>3</sub> particle interfaces. With further adding SrTiO<sub>3</sub> particles, a new luminescence band appears at 2.92 eV (see the spectra of  $x = 0.4$  and 0.2). For pristine SrTiO<sub>3</sub>, the luminescence components centred at about 2.29 and 2.49 eV are assigned to oxygen defect structures, for example (Ti<sup>3+</sup>–oxygen vacancy–Ti<sup>3+</sup>) complex. Another luminescence band is seen around 1.95 eV at  $x = 0.4$  and 0.2. Since this luminescence band is not observed for pristine AgI and pristine SrTiO<sub>3</sub>, it is also assigned to the radiative decay of the exciton trapped at the AgI/SrTiO<sub>3</sub> particle interfaces.

We measured the PL spectra for different  $(x)\text{AgI}-(1-x)\text{SrTiO}_3$  composites under more intense pulsed 355 nm laser light at different temperatures between 10 and 288 K. PL spectra at 10 K are shown in Fig. 5. Solid curves are the spectra measured under laser intensity of 0.5 mJ/cm<sup>2</sup> ( $\sim 10^5 \text{ W/cm}^2$ ) and dotted curves are the spectra measured by attenuating the laser light intensity.

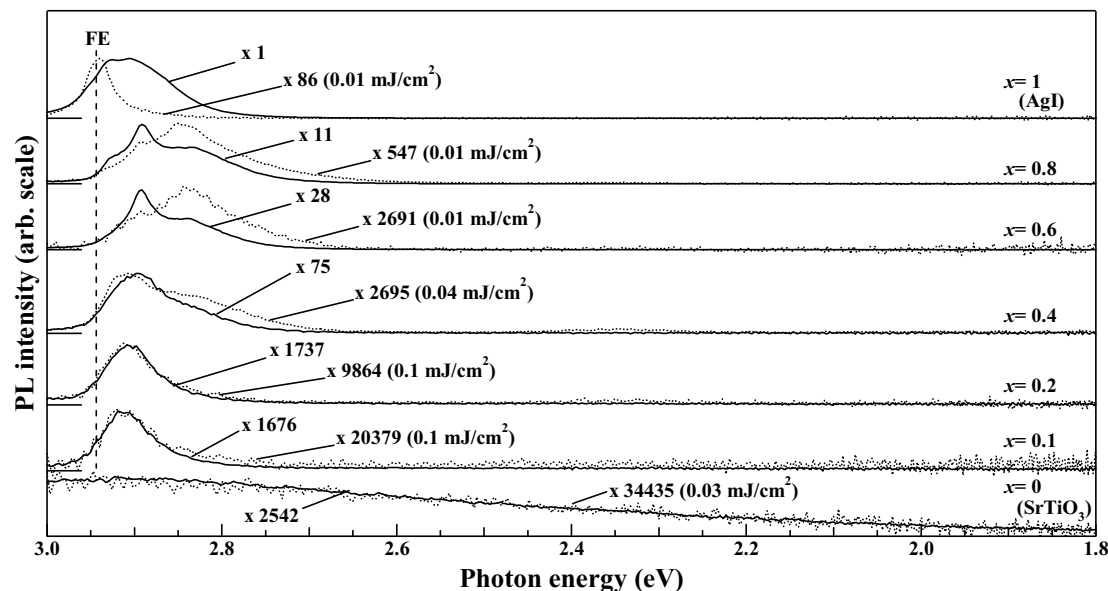


**Fig. 5** Photoluminescence spectra for different  $(x)\text{AgI}-(1-x)\text{SrTiO}_3$  composites at 10 K.

As shown in this figure, the FE luminescence (dotted curve) of pristine AgI is considerably broadened and redshifted to 2.92 eV, with increasing laser intensity. The energy spacing between the FE luminescence peak energy (2.94 eV) and the broad luminescence band peak energy (2.92 eV) is about 20 meV, suggesting the exciton–exciton scattering to higher exciton states or inelastic scattering from the heavy-hole exciton state to light-hole exciton one. Although the detailed exciton structure has not been clarified at the present, a probable energy spacing between  $n = 1$  and  $n = 2$  excitons can be thus estimated 20 meV. On the other hand, all composites specimens (except for pristine AgI and pristine SrTiO<sub>3</sub>) exhibit the luminescence components (which tend to saturate under higher laser intensity) between 2.92 and 2.70 eV. Therefore, it indicates that the luminescence centres responsible for these lower-energy luminescence components are limited in number and they arise from the radiative decay of trapped excitons at the AgI/SrTiO<sub>3</sub> particle interfaces.

We summarize the structural, electrical and PL studies on the AgI–SrTiO<sub>3</sub> composites, as follows. The dispersion of SrTiO<sub>3</sub> fine particles into AgI creates the randomly-stacked γAgI/βAgI heterostructures in the hexagonal βAgI and also the Ag<sup>+</sup> ion adions on SrTiO<sub>3</sub> particle surfaces, enhancing Ag<sup>+</sup> ion conductivity. Incidentally, it is known that an Ag<sup>+</sup> ion-rich AgI solution crystallizes γAgI, while an Ag<sup>+</sup> ion deficient one does so βAgI. Therefore, the randomly-stacked γAgI/βAgI heterostructures and other amorphous-like structures may be created at the interfacial region, providing the Ag<sup>+</sup> ion conduction pathway. It is generally known that the ionic conductivity of an amorphous phase is higher than that of a crystalline phase, because of the large free volume for the ionic migration. Hence, the AgI–SrTiO<sub>3</sub> composites showing a higher ionic conductivity may contain a larger amount of the randomly-stacked γAgI/βAgI heterostructures and amorphous-like structures which act as the non-radiative traps for AgI free exciton. This is a reason why (0.6)AgI–(0.4)SrTiO<sub>3</sub> (which has the maximum conductivity) hardly shows FE luminescence.

**Acknowledgements** This work was partially supported by a Grant-in-Aid for Scientific Research from the Ministry of Education, Science, Sport Culture and Technology, Japan. This work is supported by an Interdisciplinary General Joint Research Grand (Nihon University). This work is also partially supported by a Research Grand from the College of Humanities and Sciences (Nihon University).

## References

- [1] J. Maier, *J. Phys. Chem. Solids* **46**, 309 (1985).
- [2] J.-S. Lee, S. Adams, and J. Maier, *J. Electrochem. Soc.* **147**, 2407 (2000).
- [3] M. Cardona, *Phys. Rev.* **129**, 69 (1963).
- [4] S. Mochizuki and K. Umezawa, *Phys. Lett. A* **228**, 111 (1997).
- [5] S. Mochizuki and Y. Ohta, *J. Lumin.* **87–89**, 299 (2000).
- [6] S. Mochizuki and F. Fujishiro, *J. Phys.: Condens. Matter* **15**, 5057 (2003).
- [7] K. A. Müller and H. Burkard, *Phys. Rev. B* **19**, 3593 (1979).
- [8] F. Fujishiro and S. Mochizuki, Solid State Ionics (in preparation).
- [9] J. -S. Lee, S. Adams, and J. Maier, *J. Phys. Chem. Solids* **61**, 1607 (2000).
- [10] B. L. Davis and L. R. Johnson, *Crystal Lattice Defects* **5**, 235 (1974).
- [11] S. Mochizuki and F. Fujishiro, *phys. stat. sol. (c)* **3**(10), 3586 (2006); this conference.

# Defect-induced optical absorption and photoluminescence of Verneuil-grown SrTiO<sub>3</sub> crystal

Shosuke Mochizuki\*, Fumito Fujishiro, Ken'ichiro Ishiwata, Kohei Shibata

Department of Physics, College of Humanities and Sciences, Nihon University, 3-25-40 Sakurajosui, Setagaya-ku, Tokyo 156-8550, Japan

## Abstract

In order to clarify the mechanism of the photoluminescence (PL) and other photo-induced effects observed for Verneuil-grown SrTiO<sub>3</sub> crystal, a nominally pure dark-blue as-grown crystal, which has high DC conductivity ( $\sigma \simeq 10^{-3} \Omega^{-1} \text{cm}^{-1}$ ) and high dielectric constant ( $\epsilon > 10^6$  at 1 kHz) at room temperature, was prepared and annealed at 973 K in a 90% Ar–10% H<sub>2</sub> mixture gas stream. The optical density (OD) and PL spectra were studied at the different stages of the annealing. In addition to the band gap absorption, at least eight intense optical absorptions due to crystal defects are observed around about 2.9, 2.4, 2.2, 2.1, 1.7, 0.82 and 0.27 eV for the as-grown crystal. With progressing annealing, these absorptions became weak and the crystal became a colorless-transparent insulator. We have found a reasonable connection between the OD spectra and the PL ones.

© 2006 Elsevier B.V. All rights reserved.

PACS: 78.55.–m; 78.40.–q; 61.72.–y

Keywords: Optical absorption; Photoluminescence; Raman scattering; Crystal defects

The optical properties of strontium titanate (SrTiO<sub>3</sub>) crystal have gained a lot of interest in recent years in relation to photo-induced phenomena, for example, photo-enhanced giant dielectric constant [1] and photoluminescence (PL). Up to present, most of the workers use the single crystal grown by the Verneuil method, so-called ‘Verneuil-grown crystal’. The as-grown crystal (which is dark blue) is usually annealed at high temperature in reducing atmosphere. The fully annealed crystals are cut into parallel plate, polished and supplied to workers as a stoichiometric crystal (which is colorless transparent) from different crystal manufacturing company. However, it is well known that the Verneuil-grown crystal contains chemical heterogeneity, different oxygen defects and many dislocations with a density of approximately  $10^9 \text{ cm}^{-2}$  [2,3]. One has to notice also about the purity of the starting material SrTiO<sub>3</sub> powder being at most 99.99%. Main optical- and electrical-active impurity is known to be iron. Although the greenish white PL band centered at 2.4 eV is

well-known for low-temperature SrTiO<sub>3</sub> crystal and it is discussed in connection with the suppression of ferroelectric instability by quantum fluctuation [1]. However, an intense white luminescence has been observed even at room temperature for amorphous SrTiO<sub>3</sub> [4] and nanocrystal SrTiO<sub>3</sub> [5]. Incidentally, the PL intensity of the Verneuil-grown crystal is specimen-dependent. Recently, we have studied the PL properties of the dark-blue as-grown and colorless transparent SrTiO<sub>3</sub> crystals [6]. In addition to the white luminescence band around 2.4 eV, we found a broad band around 2.9 eV, which displays a faint-blue luminescence, and a near-band-edge (NBE) emission at 3.2 eV at low temperatures under intense photoexcitation, which are considerably enhanced for the as-grown crystal. It is an important problem whether the luminescence bands at 2.4, 2.9 and 3.2 eV arise from intrinsic nature or not? In order to clarify it, we have systematically studied both the optical density (OD) and PL spectra at different stages of annealing as-grown crystal.

A dark-blue Verneuil-grown SrTiO<sub>3</sub> single-crystal boule was cut into parallel plates with a size of 10 mm × 10 mm × 0.5 mm in thickness. After polishing

\*Corresponding author. Tel./fax: +81 3 5317 9771.

E-mail address: [motizuki@physics.chs.nihon-u.ac.jp](mailto:motizuki@physics.chs.nihon-u.ac.jp) (S. Mochizuki).

their surfaces to optical flat ones, the as-grown plate was annealed at 973 K in a 10% H<sub>2</sub>–90% Ar mixture gas during desired time. The as-grown crystal has high DC conductivity ( $\sigma \simeq 10^{-3} \Omega^{-1} \text{cm}^{-1}$ ) and high dielectric constant ( $\epsilon > 10^6$  at 1 kHz) at room temperature. With progressive annealing, the crystal becomes colorless transparent insulator ( $\sigma > 10^{-8} \Omega^{-1} \text{cm}^{-1}$  and  $\epsilon \simeq 300$ ). The OD spectrum measurements were first performed at room temperature on the crystal recovered from different stages of annealing. The results are shown in Fig. 1. The annealing time ( $t_{\text{an}}$ ) is given by each curve. As seen in this figure, the as-grown crystal shows an intense background absorption which increases gradually toward infrared (IR) region. As superposing on the background absorption, there appear several absorption peaks around about 2.9, 2.4, 2.2, 2.1, 1.7, 0.82 eV and un-resolved absorptions in the energy regions between 3.1 and 2.6 eV, and between 1.9 and 1.2 eV. The sharp OD increase at photon energies larger than 3.1 eV is due to the band-gap absorption onset (3.2 eV) of cubic SrTiO<sub>3</sub>. With progressive annealing, the absorption around 0.82 eV disappears rapidly and the absorptions around 2.15 and 2.08 eV were merged in the broad absorption band around about 1.7 eV, decreasing the background absorption in intensity. It is noted that the OD spectral change observed under annealing in a reducing H<sub>2</sub>–Ar atmosphere progresses for the reverse of that observed under annealing transparent crystal in a vacuum [7]. As pointed out by Szot et al. [2,3], the thermal reduction creates not only homogeneous crystal defects (oxygen vacancies) but also non-Perovskite phases with the Ruddlesden–Popper phases [(SrO)<sup>n</sup>(SrTiO<sub>3</sub>)<sub>n</sub>]. We have

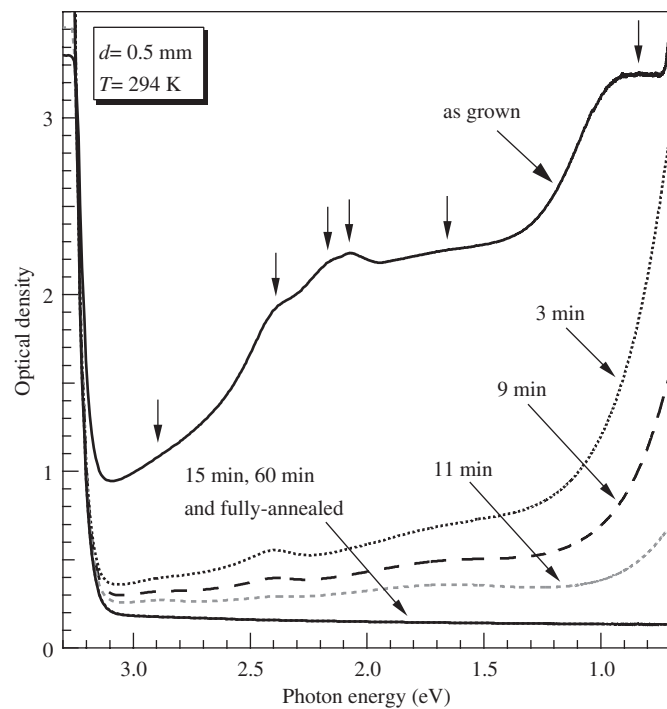


Fig. 1. Room temperature OD spectra of the as-grown and annealed SrTiO<sub>3</sub> crystals.

measured also the OD spectra in the IR region, excepting the as-grown crystal of which IR transmittance is too low to measure the OD. Combining the IR spectra with the UV–NIR spectra, the UV–IR OD spectra were obtained. As a typical example, the OD spectra of the crystal annealed for 11 min and fully annealed (commercially available) crystal are shown in Fig. 2. The spectrum for the annealed crystal ( $t_{\text{an}} = 11$  min) is expanded as shown in the inset. We can see clearly five absorption bands at photon energies, 2.88, 2.36, 1.65, 0.27 eV, and weak phonon absorptions below 0.27 eV. We have also measured the OD spectra and electrical conductivity ( $\sigma$ ) of all the specimens at different temperatures. With decreasing temperature from room temperature to 6 K, both the background absorption intensity and  $\sigma$  decrease, and other absorptions become sharpen. This indicates that the background absorption is closely related to free carriers. However, it is not explained by conventional free carrier absorption, since the absorption has peaked at 0.27 eV. Similar absorption was also observed by heating the transparent crystal in vacuum and it can be assigned to the LO-phonon- or disorder-assisted intervalley scattering between the two minima at the  $\Gamma$  and X points [8]. This interpretation is compatible with the present results. With decreasing temperature, the fundamental absorption edge shifts to higher energy side, and the 2.9, 2.4 and 1.6 eV absorption band shift also to their higher energy sides. The similar absorptions were also observed between 2.8 and 1.8 eV for a stoichiometric SrTiO<sub>3</sub> crystal by Szot et al. [3]. It is also noted that several PL bands were observed for the transparent SrTiO<sub>3</sub> crystal in this photon energy region [6]. Wild et al. [9] studied pure and iron-doped SrTiO<sub>3</sub> crystals and found the optical absorptions at 2.92, 2.4, 2.1 and 1.6 eV, and NIR absorptions in these crystals. They assigned the 2.92 eV absorption and 2.1 eV one to the optical transition from the Fe<sup>4+</sup> donor to the conduction band and the Fe<sup>3+</sup>–oxygen vacancy complex state to the conduction band, respectively. They also assigned the 2.4 and 1.6 eV absorptions to crystal defects proper to SrTiO<sub>3</sub>. Faughnan [10] identified the 2.9 eV peak as an absorption

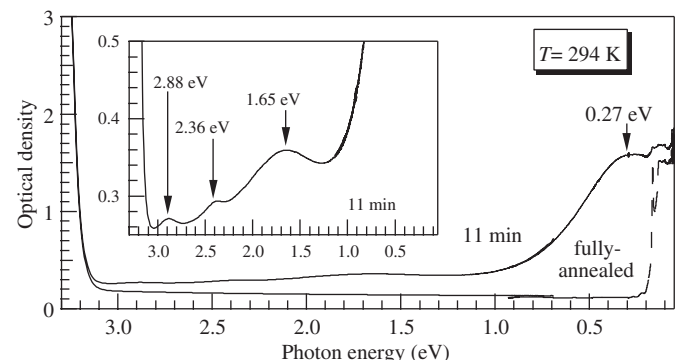


Fig. 2. Room temperature UV–IR OD spectra of SrTiO<sub>3</sub> crystal annealed for 11 min and fully annealed crystal. The spectrum of the annealed crystal for 11 min is expanded in the inset. The specimen thickness is 0.5 mm.

by a  $\text{Fe}^{4+}$  ion in a cubic site, using the electron paramagnetic resonance technique.

We have measured the PL spectra, PL excitation spectra and time-resolved PL spectra of the crystal as functions of  $t_{\text{ir}}$ , excitation laser fluence ( $I_{\text{ex}}$ ) and temperature. With progressing  $t_{\text{ir}}$ , the PL intensity and the luminescence decay time ( $\tau_d$ ) increase. The spectral shape observed for the as-grown and annealed crystals is similar to that observed for the fully annealed crystal which is commercially available [6]. As a typical result, the PL spectra are shown in Fig. 3. The measurements were carried out at 10 K with  $I_{\text{ex}} \approx 1 \text{ mJ cm}^{-2}$ . To see the spectral change clearly, each spectrum is appropriately rescaled in this figure. Each rescaling factor is given by each curve. As seen in this figure, the as-grown crystal shows at least three PL bands. The first one is a sharp band around 3.22 eV which is close to the band edge energy (3.27 eV) of  $\text{SrTiO}_3$ . We call this band ‘NBE luminescence band’. The second one is a broad-and weak-background band extending from 3.2 to 2 eV. A faint peak is seen at 3.11 eV in the weak broad band. Although there are some structures in this band, we call tentatively this band ‘A luminescence band’. The third one is an intense broad band around 2.45 eV. We call this band ‘B luminescence band’. The A and B luminescence peak energies correspond well to the OD peak ones shown in Fig. 1. This suggests that the luminescence centers responsible for the A and B luminescence bands originate from crystal defects. Since any luminescence is not observed below 1.8 eV, the defects giving the OD peaks at 1.67, 0.82 and 0.27 eV do not act directly as luminescence center. With progressive annealing, all the lumines-

cence bands increase in intensity. In particular, the B luminescence increase is prominent, while the NBE luminescence intensity is almost independent of annealing. This indicates that non-radiative trap for the B luminescence decreases in number with increasing  $t_{\text{ir}}$ . The spectrum of the crystal annealed for 3 min is somewhat different from others. The spectrum is dominated by the A luminescence (which may be seen as faint blue luminescence), merging the NBE and B luminescence bands into this band.

We have measured also the PL spectra of the as-grown and different annealed crystals, at about 10 K under different  $I_{\text{ex}}$ . As typical examples, the results for the as-grown crystal and the crystal annealed for 11 min are shown in Fig. 4. With increasing  $I_{\text{ex}}$ , the PL intensity of the B luminescence increases for all the specimens. The B luminescence intensity of the as-grown crystal attains a maximum at about  $1 \text{ mJ cm}^{-2}$ , while all of the annealed crystals show their PL intensity maxima at about  $4 \text{ mJ cm}^{-2}$ , like the case for the colorless transparent crystal [6]. On  $I_{\text{ex}}$  further increasing, the B luminescence intensity decreases monotonically, while both the NBE luminescence band and the A luminescence one continue to grow, without any saturation. This indicates that the NBE luminescence and the A one arise from a great number of crystal defects. Different types of crystal imperfections should be considered for real  $\text{SrTiO}_3$  crystal: for example, surface textures, chemical heterogeneity (for example, Ruddlesden–Popper phases), dislocations,  $\text{Ti}^{3+}$ –oxygen vacancy complexes and oxygen point defects. In the  $\text{Ti}^{3+}$ –oxygen vacancy complex,  $\text{Ti}^{3+}$  ion is one of the

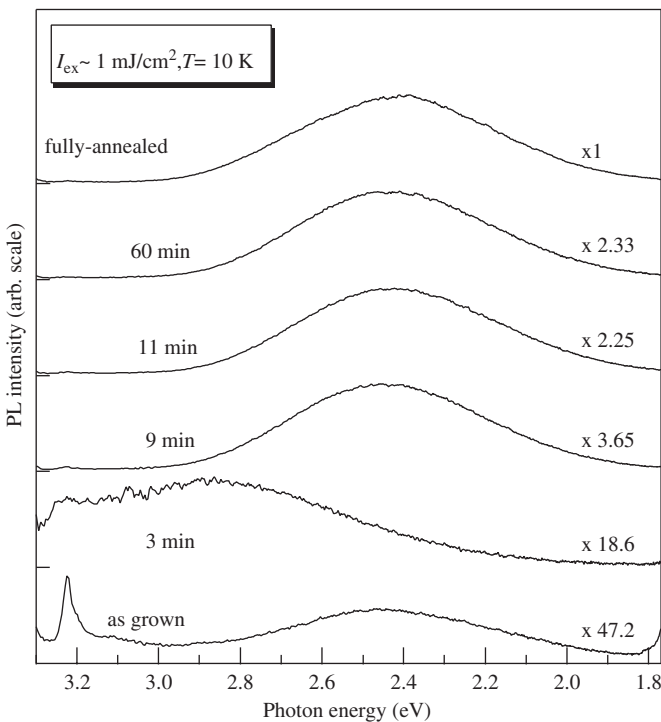


Fig. 3. PL Spectra of the as-grown and different annealed  $\text{SrTiO}_3$  crystals.

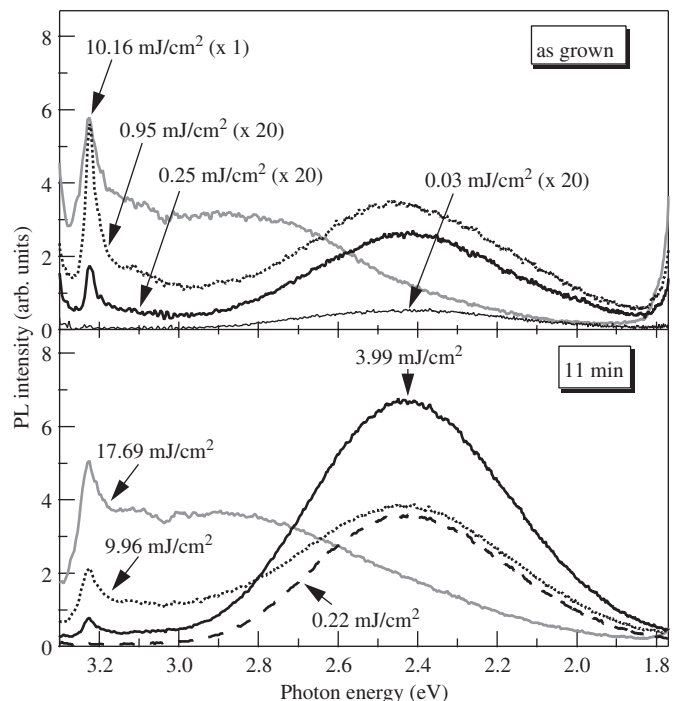


Fig. 4. Excitation-intensity dependence of the PL of the as-grown and annealed  $\text{SrTiO}_3$  crystals for different times.

candidate hole trap centers and the oxygen vacancy is one of the candidate electron trap centers. When excitation laser fluence is low, photo-generated electrons and holes at a crystal surface drift inside the crystal, repeating trapping at some shallow levels and releasing from them, while holes may be rapidly trapped at crystal defects. Incidentally, no phenomena related to free holes has been not observed. Accidental electron–hole recombination at the crystal defects may create the B luminescence. When  $I_{\text{ex}}$  increases, photo-generated electrons become energetic and, therefore, most of the electrons diffuse rapidly inside the crystal (bulk), without recombining at surface. Therefore, the luminescence from the surface region begins decreasing in intensity at a given laser fluence. This may be a reason why the 2.4 eV luminescence intensity maximum is observed on the laser fluence increasing. Generally, such crystal-defect concentration at surface is higher than that inside the crystal. The B luminescence from the inside of the crystal may saturate in intensity with further increasing  $I_{\text{ex}}$ . Further information on the crystal defects inside the crystal (bulk) may be deduced from the two-photon-excitation PL measurement in the transparent photon energy region. Since the annealing enhanced the B luminescence, some kinds of crystal defects acted as non-radiative traps. The defect structure of  $\text{SrTiO}_3$  is hard to be optically determined and, therefore, it is not clear which type of defect structure acts as such traps. On the other hand, since the NBE and the A luminescence never show any saturation at intense photoexcitation ( $>10 \text{ mJ cm}^{-2}$ ), they are hard to connect with the mechanism participating a small number of iron impurity.

Finally, the room-temperature Raman-scattering spectra at different stages of annealing are shown in Fig. 5. The intensity increase with progressing annealing is due to the decolorization. In the inset, the spectra of the as-grown and fully annealed crystal are compared after rescaling. As seen below  $40 \text{ cm}^{-1}$ , the defect-induced mode appears clearly as a Rayleigh-scattering tail in the as-grown crystal.

This work was supported by a Grant-in-Aid for Scientific Research from Ministry of Education, Science, Culture, Sport and Technology, Japan. This work was supported by an Interdisciplinary General Joint Research

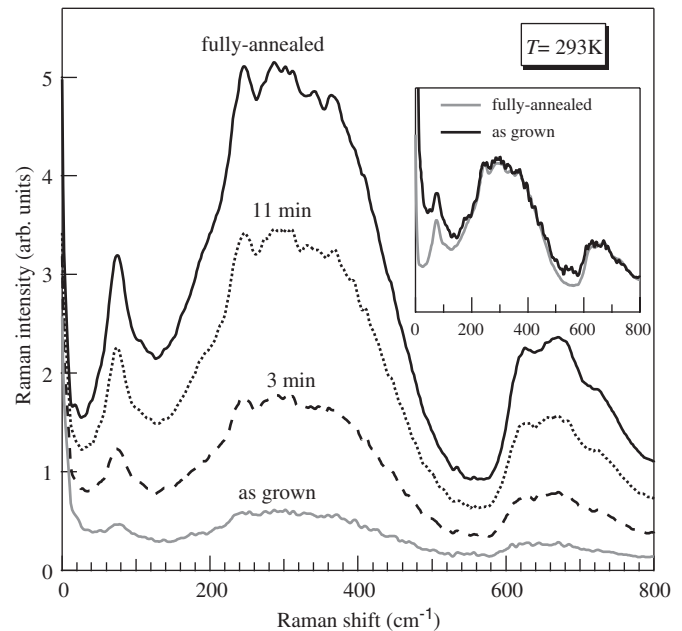


Fig. 5. Room-temperature Raman scattering spectra of  $\text{SrTiO}_3$  crystal at the different stages of annealing.

Grant (Nihon University). This work was also supported by a Research Grant for Science, College of Humanities and Sciences (Nihon University).

## References

- [1] K. Nasu, Rep. Prog. Phys. 67 (2004) 1607.
- [2] K. Szot, W. Speier, Phys. Rev. B 60 (1999) 5909.
- [3] K. Szot, W. Speier, R. Carius, U. Zastrow, W. Beyer, Phys. Rev. Lett. 88 (2002) 075508.
- [4] F.M. Pontes, E. Longo, E.R. Leite, E.J.H. Lee, J.A. Varela, P.S. Pizani, C.E.M. Campos, F. Lanciotti, V. Mastellaro, C.D. Pinheiro, Mater. Chem. Phys. 77 (2002) 598.
- [5] S. Mochizuki, F. Fujishiro, Nanaotechnology, submitted.
- [6] S. Mochizuki, F. Fujishiro, S. Minami, J. Phys.: Condens. Matter 17 (2005) 923.
- [7] H.W. Gandy, Phys. Rev. 113 (1959) 795.
- [8] P. Calvani, M. Capizzi, F. Donato, S. Lupi, P. Maselli, D. Peschiaroli, Phys. Rev. B 47 (1993) 8917.
- [9] R.L. Wild, E.M. Rockar, J.C. Smith, Phys. Rev. B 8 (1973) 3828.
- [10] B.W. Faughnan, Phys. Rev. B 4 (1971) 3623.

# Photo-induced reversible spectral change in several AgI–oxide particle composites

Fumito Fujishiro\*, Shosuke Mochizuki

Department of Physics, College of Humanities and Sciences, Nihon University, 3-25-40 Sakurajosui, Setagaya-ku, Tokyo 156-8550, Japan

---

## Abstract

Different kinds of metal oxide (anatase, ZnO and SrTiO<sub>3</sub>) fine particles were dispersed in silver iodide (AgI). These composites exhibit considerable electrical conductivity enhancement. When these composites are irradiated with a 325 nm laser light in vacuum, their photoluminescence spectra are changed. By irradiating with same laser light at room temperature in O<sub>2</sub> gas, the original spectral structure reappears. The observed reversible phenomena are explained by some excitation energy transfer and traps at the interfaces between AgI and oxide particles. Such reversible phenomena may yield materials for optical oxygen-partial-pressure sensors.

© 2006 Elsevier B.V. All rights reserved.

PACS: 61.72. Jj; 71.35.-y; 78.55.-m

Keywords: AgI-based composite; Photoluminescence; Oxygen defects

---

## 1. Introduction

Recently, considerable attention has been devoted to research for new materials to be used for optical sensor [1] and photomemory. The interest in photoluminescent materials showing photo-induced photoluminescence (PL) spectral change at room temperature has significantly grown. Hitherto, we have observed the photo-induced PL spectral change on several metal oxides [2,3]. When metal oxide is irradiated at room temperature with a continuous wave (CW) 325 nm laser light in a vacuum, a white luminescence band appears and then it increases in intensity with increasing irradiation time ( $t_{ir}$ ). After removing the laser light, the white PL state is recorded for more than several years at room temperature under room light, regardless of any changes of atmosphere. By irradiating with the same laser light at room temperature in O<sub>2</sub> gas, the original PL property reappears. The observed spectral changes are explained by the photooxidation and photoreduction on the oxide surfaces, which induce the valence-number change, and annihilation or creation of oxygen defects.

Till today, we have been studying the reversible photo-induced PL spectral change in different oxides and different composites, in order to find the material having much superior photofunction. In the study, we have observed, for the first time, the reversible photo-induced PL spectral changes in several composites which consist of silver iodide (AgI) and metal oxide fine particles. The spectral change arises from some excitation energy transfer from AgI to photo-generated crystal defect, at the interfaces between AgI and oxide particle. In the present paper, we summarize the recent results obtained in our laboratory.

## 2. Experimental procedure

The AgI–oxide fine particle composites were prepared by fully mixing AgI powder (purity > 99.999%, Alfa Aesar) and different kinds of metal oxide powder, SrTiO<sub>3</sub> nano-sized powder (purity > 99.5%, Aldrich), anatase powder (an averaged diameter of 50 nm, purity > 99.9%, Wako) and ZnO powder (averaged diameter 20 nm, purity > 95.0%, Wako), by compressing under 0.2 GPa for 30 min to fabricate the pellets, and then the pellets were heated at 673 K for 12 h in air. The photo-induced PL

\*Corresponding author. Tel./fax: +81 3 5317 9771.

E-mail address: [fumito@phys.chs.nihon-u.ac.jp](mailto:fumito@phys.chs.nihon-u.ac.jp) (F. Fujishiro).

spectral change was measured by means of a CW He–Cd laser (wavelength = 325 nm) and an optical multichannel analyzer. The specimens were set in a chamber connected with an oil-free vacuum system, which is able to exchange the atmosphere around the specimens at room temperature.

### 3. Results and discussion

Before the measurements on the photo-induced PL spectral change, we studied the electrical conductivities and the PL, PL excitation and time-resolved PL spectra at different temperatures for some composites [4,5]. It is found that  $(x)\text{AgI}-(1-x)\text{anatase}$ ,  $(x)\text{AgI}-(1-x)\text{ZnO}$  and  $(x)\text{AgI}-(1-x)\text{SrTiO}_3$  composites display the electrical conductivity ( $\sigma$ ) maximum against the AgI contents, 0.4, 0.5 and 0.6, respectively. It is also found that  $\sigma$  of  $(0.4)\text{AgI}-(0.6)\text{anatase}$ ,  $(0.5)\text{AgI}-(0.5)\text{ZnO}$  and  $(0.6)\text{AgI}-(0.4)\text{SrTiO}_3$  are enhanced by about three orders, one order and two orders of magnitude in comparison with that of pristine AgI, respectively. Possible causes of such conductivity enhancement are thought to be the silver vacancies and other crystal defects produced at the AgI–oxide particle interfaces [6]. After fully irradiating these composites with 325 nm laser light in  $\text{O}_2$  gas and in vacuum, the photo-induced experiments were performed. The same experiments were carried out for pristine AgI, pristine anatase, pristine ZnO and pristine  $\text{SrTiO}_3$  as the reference specimens. All of the measurements were carried out at room temperature. Regardless of the sensitization of AgI, the photo-induced PL spectral changes are clearly observed for AgI-based composites. As typical results for each composite, the spectral change of  $(0.4)\text{AgI}-(0.6)\text{anatase}$ ,  $(0.5)\text{AgI}-(0.5)\text{ZnO}$  and  $(0.4)\text{AgI}-(0.6)\text{SrTiO}_3$  composites are shown in the present paper, as follows.

Figs. 1(a) and (b) show the photo-induced PL spectral changes of  $(0.4)\text{AgI}-(0.6)\text{anatase}$  composite and pristine anatase, respectively. Curves 1 and 2 are obtained after irradiating for 30 min in  $\text{O}_2$  gas and in vacuum, respectively. In  $\text{O}_2$  gas, the composite shows a maximum at 2.91 eV, which is close to the free exciton energy,  $E_{\text{FE}}^{\text{AgI}}$ , of pristine AgI [7]. The broad background emission band centered at about 1.9 eV is due to oxygen defects in anatase particles. The PL intensity peak energy of this band is smaller than that (2.2 eV) of pristine anatase (curve 3). Generally, the energy of oxygen defect,  $E_{\text{defect}}$ , depends on the site and local symmetry. Surely, the result indicates that  $E_{\text{defect}}$  is affected by adding AgI. When the specimen chamber is evacuated, the AgI free exciton luminescence disappears with increasing  $t_{\text{ir}}$ , while a new anatase-related emission grows at about 2.2 eV with increasing  $t_{\text{ir}}$ . Through many successive experiments, it is found that the spectral changes (1  $\leftrightarrow$  2 and 3  $\leftrightarrow$  4) appear repeatedly. Since the PL intensity peak energy of difference spectra, curve 2–curve 1 and curve 4–curve 3, differ from curves 1 and 3, the energy of photo-induced crystal defects (PID) in both the AgI–anatase composite and pristine anatase is different

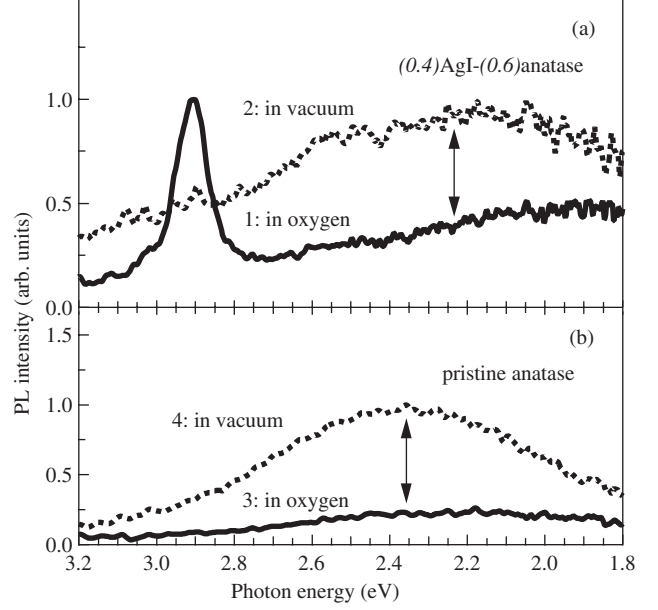
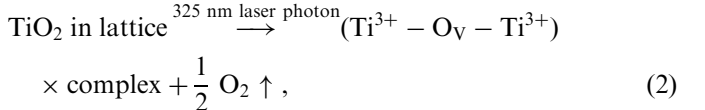
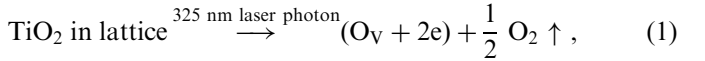


Fig. 1. The photo-induced spectral change AgI–anatase composite: (a)  $(0.4)\text{AgI}-(0.6)\text{anatase}$  composite and (b) pristine anatase.

from that of the original oxygen defect. Such photo-induced defect formation at anatase particle surfaces in vacuum may be given by the following expressions



where  $\text{O}_v$  denotes the oxygen vacancy. In reduced anatase, it is known for the near-band edge absorption due to oxygen defects, see, for example, Sekiya et al. [8]. The small difference of PL intensity peak energy between curve 2 and curve 4 indicates that the PID energy structure is almost unchanged by adding AgI.

Figs. 2(a) and (b) show the photo-induced PL spectral change for  $(0.5)\text{AgI}-(0.5)\text{ZnO}$  composite and pristine ZnO, respectively. The spectra in the figures are obtained in vacuum (dotted curve) and in  $\text{O}_2$  gas (solid curve), after irradiating for 30 min in each atmosphere. In  $\text{O}_2$  gas, this composite shows a maximum at 2.91 eV which is close to  $E_{\text{FE}}^{\text{AgI}}$ . The broad background emission band centered at about 2.2 eV is due to oxygen defects in ZnO particles. This energy is smaller than (2.52 eV) of pristine ZnO particles. It indicates that  $E_{\text{defect}}$  is affected by adding AgI. When the specimen chamber is evacuated, the AgI free exciton luminescence disappears with increasing  $t_{\text{ir}}$ , while the emission due to oxygen defects increases in intensity with increasing  $t_{\text{ir}}$ . However, the magnitude of the spectral change is smaller than that for  $(0.4)\text{AgI}-(0.6)\text{anatase}$  composite. The photo-induced defect formation at ZnO particle surfaces in vacuum may be given by the following

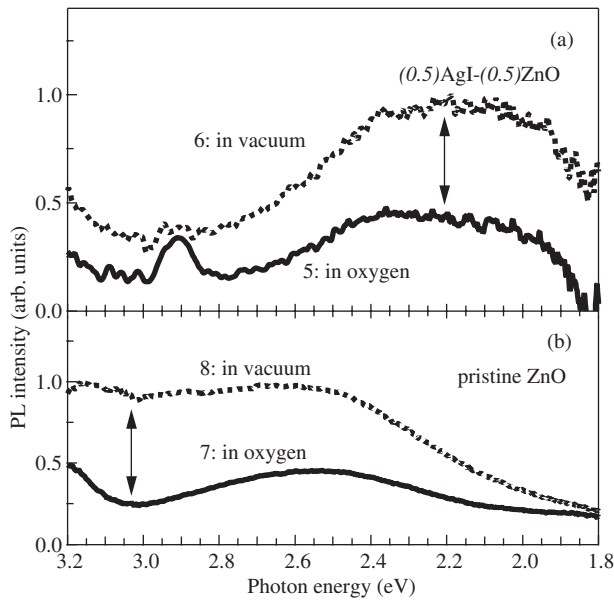
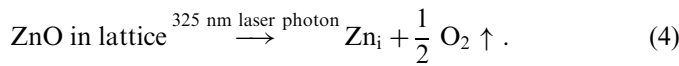
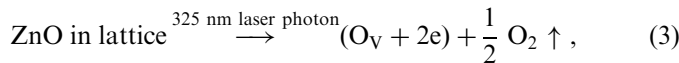


Fig. 2. The photo-induced spectral change AgI-ZnO composite: (a) (0.5)AgI-(0.5)ZnO composite and (b) pristine ZnO.

expressions



It is well-known that the Zn interstitial ( $\text{Zn}_i$ ) and  $\text{O}_v$  create shallow donor levels [9]. Through many successive experiments, it is found that the spectral changes ( $5 \leftrightarrow 6$  and  $7 \leftrightarrow 8$ ) appear repeatedly. Small energy difference of oxygen-defect-related PL intensity peak between curve 5 and curve 6 indicates that  $E_{\text{defect}}$  of (0.5)AgI-(0.5)ZnO composite is almost unchanged by photo-irradiation.

Figs. 3(a) and (b) show the photo-induced PL spectral change of (0.4)AgI-(0.6)SrTiO<sub>3</sub> and pristine SrTiO<sub>3</sub>, respectively. The spectra in the figures are obtained in vacuum (dotted curve) and in oxygen (solid curve), after irradiating for 30 min in each atmosphere. By evacuating O<sub>2</sub> gas from the specimen chamber, the broad emission band grows at about 2.3 eV, which arises from oxygen defects in SrTiO<sub>3</sub> particles. Unlike the case of (0.4)AgI-(0.6)anatase and (0.5)AgI-(0.5)ZnO, AgI exciton emission increases in intensity in vacuum with increasing  $t_{\text{ir}}$ . Through many successive experiments, it is found that the spectral changes ( $9 \leftrightarrow 10$  and  $11 \leftrightarrow 12$ ) appear repeatedly. As seen in curve 11, there are at least four luminescence components at about 3.0, 2.93, 2.85, 2.67 and below 2.6 eV in pristine SrTiO<sub>3</sub> particle. Rescaling and then comparing curve 9 and curve 11, the following are obtained. The PL component higher than 3 eV is suppressed by adding AgI, which is due to the optical absorption by AgI domain. The broad PL component below 2.6 eV, which is centered at 2.35 eV, is considerably enhanced by adding AgI. The luminescence observed

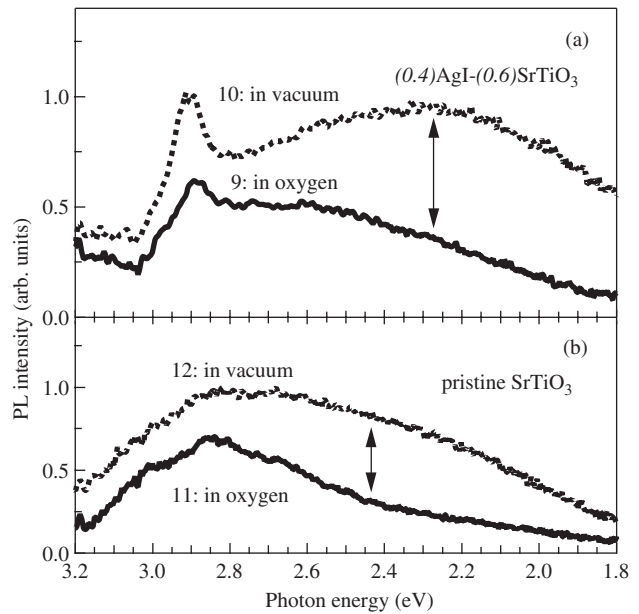
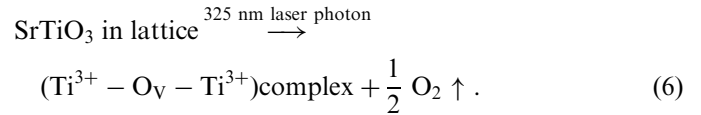
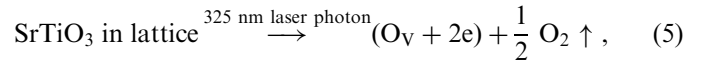


Fig. 3. The photo-induced spectral change AgI-SrTiO<sub>3</sub> composite: (a) (0.4)AgI-(0.6) SrTiO<sub>3</sub> composite and (b) pristine SrTiO<sub>3</sub>.

around 2.4 eV is known to arise from oxygen defects [3]. The process of the photo-induced defect formation at SrTiO<sub>3</sub> particle surfaces in vacuum may be expressed as follows



Before discussing the experimental results, we mention briefly about the structure of these composites. The X-ray diffractograms, SEM observations and EDX measurements show that oxide particles are packed, without alloying, in each large AgI particle domain whose size is approximately several micrometers. The 325 nm (3.8 eV) laser light excites not only AgI ( $E_{\text{FE}}^{\text{AgI}} = 2.9$  eV) but also anatase (whose energy gap  $E_g$  is 3.2 eV), ZnO ( $E_g = 3.2$  eV) and SrTiO<sub>3</sub> ( $E_g = 3.2$  eV), at room temperature. In addition to the interfacial oxygen defects created by adding oxide fine particles to AgI, the irradiation of 325 nm laser light in vacuum creates extra oxygen defects at the surfaces of oxide fine particles. If  $E_{\text{FE}}^{\text{AgI}}$  is close to  $E_{\text{defect}}$ , the excitation energy of AgI is transferred to oxygen defect in adjacent oxide particle, exciting oxygen defect and then displaying luminescence, suppressing the AgI free exciton luminescence. Since the number of photo-induced oxygen defect decreases under 325 nm laser light irradiation in O<sub>2</sub> gas, the deexcitation of photo-excited AgI gives luminescence without exciting oxygen defect. This is the reason why the AgI free exciton luminescence reappears under 325 nm laser light irradiation in O<sub>2</sub> gas for (0.4)AgI-(0.6)anatase and (0.5)AgI-(0.5)ZnO composites.

However, in the case of (0.4)AgI–(0.6)SrTiO<sub>3</sub> composite, the AgI free exciton luminescence in O<sub>2</sub> gas is considerably decreased by adding SrTiO<sub>3</sub>. This suggests that the oxygen defects generated by adding AgI act as nonradiative traps for AgI free exciton. Many optical absorption bands due to oxygen deficiency are also known for SrTiO<sub>3</sub>. Because of large dielectric constant (approximately 300) of SrTiO<sub>3</sub>, photo-generated electrons and holes do not form excitons but they move independently throughout AgI/oxide interfaces. It is also known that, in SrTiO<sub>3</sub> crystal, electrons move freely, while holes are self-trapped. In the (Ti<sup>3+</sup>–O<sub>V</sub>–Ti<sup>3+</sup>) complex, the Ti<sup>3+</sup> ions act as hole traps, while the O<sub>V</sub> act as electron traps. Accidental recombination of electron and hole at photo-generated (Ti<sup>3+</sup>–O<sub>V</sub>–Ti<sup>3+</sup>) complex induces the 2.4 eV luminescence. On the other hand, another portion of photocarriers may compensate the traps, enhancing the AgI free exciton luminescence. This may be the reason why the AgI free exciton luminescence is enhanced under 325 nm laser light irradiation in vacuum for (0.4)AgI–(0.6)SrTiO<sub>3</sub> composite. Since the defect structure is hard to be optically determined, it is not clear which type of defect acts as such traps.

Finally, we are now studying the reversible photo-induced PL spectral change as a function of oxygen

pressure, for applying the phenomena to the optical oxygen-partial-pressure sensor.

### Acknowledgements

This work was supported by a Grant-in-Aid for Scientific Research from Ministry of Education, Science, Culture, Sport and Technology, Japan, Interdisciplinary General Joint Research Grant (Nihon University) and Research Grant for Science, College of Humanities and Sciences (Nihon University).

### References

- [1] Y. Amao, K. Asai, I. Okura, Anal. Commun. 36 (1999) 179.
- [2] S. Mochizuki, T. Nakanishi, Y. Suzuki, Appli. Phys. Lett. 79 (2001) 3785.
- [3] S. Mochizuki, F. Fujishiro, S. Minami, J. Phys.: Condens. Matter 17 (2005) 923.
- [4] S. Mochizuki, F. Fujishiro, J. Phys.: Condens. Matter 15 (2003) 5057.
- [5] F. Fujishiro, S. Mochizuki, Physica B 340–342 (2003) 216.
- [6] T. Jow, J.B. Wagner Jr., J. Electrochem. Soc. 126 (1979) 1963.
- [7] S. Mochizuki, Physica B 308–310 (2001) 1042.
- [8] T. Sekiya, K. Ichimura, M. Igarashi, S. Kurita, J. Phys. Chem. Solids 61 (2000) 1237.
- [9] S.B. Zhang, S.-H. Wei, A. Zunger, Phys. Rev. B 63 (2001) 075205-1.

# Photo-induced phenomena in SrTiO<sub>3</sub>

Fumito FUJISHIRO, Shosuke MOCHIZUKI

Department of Physics, College of Humanities and Sciences, Nihon University, 3-25-40 Sakurajosui, Setagaya-ku, Tokyo 156-8550, Japan

E-mail: fumito@phys.chs.nihon-u.ac.jp

**Abstract.** When different SrTiO<sub>3</sub> single crystals are irradiated at room temperature with a continuous wave 325 nm laser light in an evacuated specimen chamber, their luminescence increase in intensity, creating a broad visible luminescence band centred at about 2.4 eV. Then, introducing oxygen gas into the specimen chamber, the photoluminescence spectra return reversibly to the original weak luminescence with the same laser light irradiation. After removing the laser light irradiation, each photoluminescent state is stored for a long time at room temperature under room light, regardless of any changes of atmosphere. Such photo-induced spectral change has been also observed at different temperatures from 6 K to room temperature. The observed phenomenon is explained by the photo-induced oxygen defect at the surfaces of SrTiO<sub>3</sub> crystal. The observed photo-induced optical phenomena are discussed in the light of both the crystal defect chemistry of SrTiO<sub>3</sub> and the exciton theory.

## 1. Introduction

In recent years, considerable attention has been devoted to the search for new photo-induced phenomena to be used as erasable photomemory materials [1]. We have observed the reversible photo-induced spectral transitions in the photoluminescence of Eu<sub>2</sub>O<sub>3</sub> [2], Sm<sub>2</sub>O<sub>3</sub> [3], anatase TiO<sub>2</sub> [4], vitreous SiO<sub>2</sub> [5] and other materials [6]. When these materials are irradiated at room temperature with a continuous wave (CW) 325 nm laser light in an evacuated specimen chamber, their luminescence change in intensity, creating a broad visible luminescence band. Then, introducing oxygen gas into the specimen chamber, the photoluminescence (PL) spectra return reversibly to the original luminescence with the same laser light irradiation. After removing the laser light irradiation, each PL state is stored for a long time at room temperature under room light, regardless of any changes of atmosphere. Such photo-induced spectral change has been also observed at different temperatures from 6 K to room temperature. Such reversible phenomena may well yield materials for erasable optical storage and white-light-emitting devices. Very recently, we have also observed quite similar photo-induced PL spectral change in strontium titanate SrTiO<sub>3</sub> single crystal. Grabner [7] measured the PL properties of doped and undoped SrTiO<sub>3</sub> crystals, and observed a near-infrared luminescence band around about 1.6 eV and a visible luminescence band around 2.4 eV. In addition to these PL bands, we have found a near-band-edge emission at 3.2 eV, accompanied by a broad PL band around 2.9 eV [8, 9]. In particular, the 2.4 eV luminescence shows clear spectral change.

In the present paper, we summarize our recent studies on the photo-induced PL spectral change observed for different SrTiO<sub>3</sub> crystals and discuss them in the light of both the crystal defect chemistry of SrTiO<sub>3</sub> and the exciton theory.

## 2. Experimental

The  $\text{SrTiO}_3$  crystal was grown by the Verneuil method and the as-grown crystal is dark blue. The as-grown crystal became perfectly colourless and transparent by annealing in reducing  $\text{Ar}-\text{H}_2$  mixture gas atmosphere at high temperature. We have measured the optical density (OD), PL, PL excitation and time-resolved PL spectra for the as-grown and annealed crystals at different temperature between 6 K to room temperature. The details of experimental procedure are described in our previous papers [8, 9]. The reversible photo-induced PL spectral changes were measured by means of a CW He-Cd laser (wavelength= 325 nm) as the excitation source and an optical multichannel analyzer. The specimens were set in a chamber connected with an oil-free vacuum system, which is able to exchange the atmosphere around the specimens at room temperature. The experimental setup is shown in figure 1.

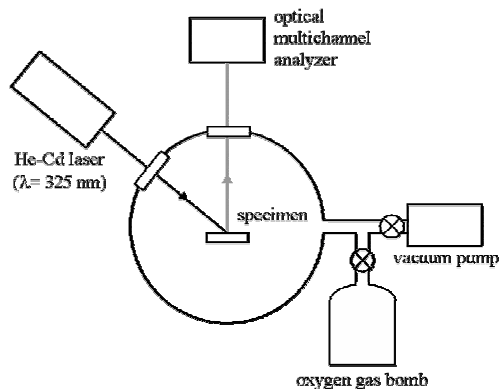


**Figure 1.** The experimental setup.

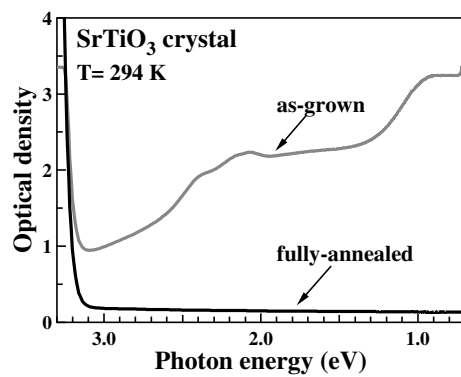


**Figure 2.** Optical density spectra of the as-grown and fully-annealed  $\text{SrTiO}_3$  crystals at 294 K.

## 3. Results and discussion

Figure 2 shows the OD spectra of the as-grown and fully-annealed  $\text{SrTiO}_3$  crystals at room temperature. As seen in this figure, the as-grown crystal shows an intense background absorption which increases gradually toward IR region. We name tentatively this background NIR absorption. As superposing on the NIR absorption, there appear several absorption peaks around 2.4, 2.15, 2.08 and 0.82 eV and un-resolved absorptions in the energy ranges between 3.1 and 2.6 eV, and between 1.9 and 1.2 eV. The OD spectra increased steeply at photon energies larger than 3.1 eV is ascribed to the fundamental electronic absorption onset (3.2 eV) of cubic  $\text{SrTiO}_3$  [8]. With progressing annealing, the absorption around 0.82 eV disappears rapidly and the absorptions around 2.15 and 2.08 eV merge into the broad absorption band around 1.65 eV, decreasing the NIR absorption in intensity. As seen above, many absorptions appear at energies lower than the bandgap energy (3.2 eV), which indicates that there are many crystal-defect-induced levels in the energy gap. The midgap absorptions below 3.1 eV may arise not from homogeneously crystal defects (oxygen vacancies) but from non-Perovskite phases with the Ruddlesden-Popper phases  $[(\text{SrO})^n(\text{SrTiO}_3)_n]$  [10] and  $(\text{Ti}^{3+}\text{-oxygen vacancy-Ti}^{3+})$  complex [11,12].

During a CW 325 nm laser light irradiation in vacuum (or in oxygen) at room temperature, we have measured the PL spectral change of the as-grown and fully-annealed crystals as a function of the irradiation time. The result for the as-grown crystal at room temperature in vacuum is shown in figure 3(a). The irradiation time is shown by each curve. As seen in figure 3 (a), the initial PL spectrum is very broad, and it has an intensity peak at about 2.8 eV and two faint kinks at about 2.4 and 2.15 eV. With increasing irradiation time, the intensity increases, growing the PL component below 2.8 eV and the speed of the spectral change becomes deduced. A difference spectrum between the spectrum obtained at 60 min and rescaled spectrum obtained at 0 min is calculated, which is shown in figure 3

(b). This figure shows clearly that a broad PL band has grown at 2.4 eV under CW 325nm laser light irradiation in vacuum.

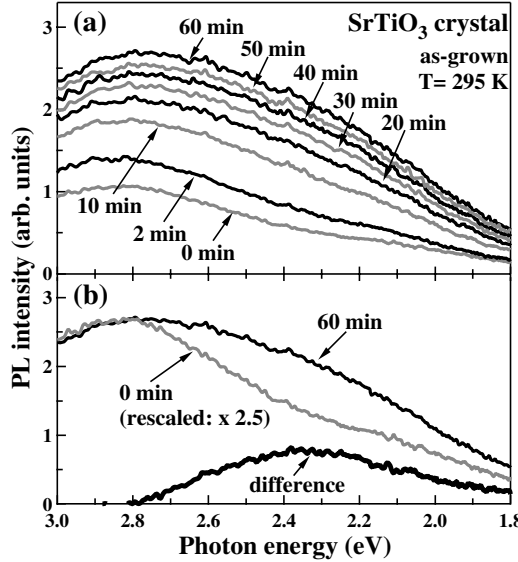


**Figure 3.** Photo-induced PL spectral change of the as-grown  $\text{SrTiO}_3$  crystal at 295 K. (a) Spectral change in vacuum. (b) Extraction of photo-induced component.

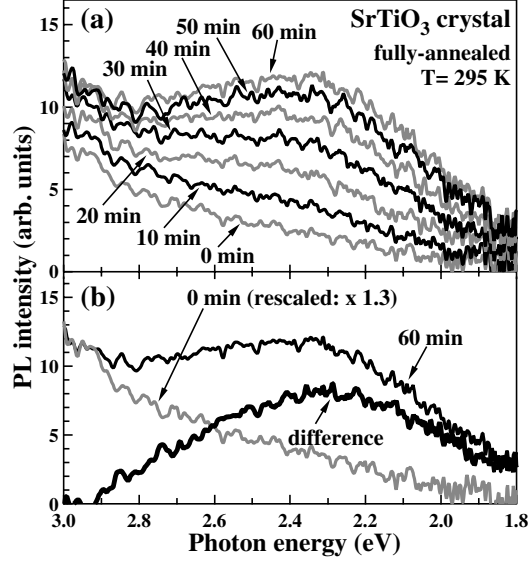


**Figure 4.** Photo-induced PL spectral change of the fully-annealed  $\text{SrTiO}_3$  crystal at 295 K. (a) Spectral change in vacuum. (b) Extraction of photo-induced component.

Figure 4 (a) shows the photo-induced PL spectral change of the fully-annealed crystal at room temperature in vacuum. The PL component below 2.8 eV grows with increasing irradiation time. With further increasing irradiation time, the rate of the change becomes small. As done for the results of the as-grown crystal, the difference spectrum is also calculated, which is given in figure 4 (b). It clearly indicates that a broad PL band has grown at 2.4 eV under 325nm laser light irradiation in vacuum. Then we have introduced the oxygen gas to the specimen chamber and irradiated the same laser light. The 2.4 eV band decreases in intensity for both the as-grown and fully-annealed crystals, returning to the original weak PL state. The spectral changes observed for the  $\text{SrTiO}_3$  single crystals are mainly characterized by an intensity change of the 2.4 eV luminescence. Since the 325nm laser light never dissociates directly free  $\text{O}_2$  molecule, the observed spectral changes arise from the photo-induced associative detachment and photo-induced dissociative adsorption of  $\text{O}_2$  molecules near the  $\text{SrTiO}_3$  surfaces. In the other word, these phenomena correspond to the photo-reduction and the photo-oxidation, respectively. It has also found that the speed of the spectral change accelerates on increasing the intensity of the activating light. The same experiments were carried out by changing the wavelength of the irradiating laser light. As results, it has been found that no spectral change was observed except for the CW 325 nm laser light.

The PL spectra of the as-grown and different annealed  $\text{SrTiO}_3$  crystals were measured at different temperatures between 295 and 6 K under a CW 325 nm and a pulsed 355 nm laser light of different laser fluences. With decreasing temperature, the 2.4 eV band merged in the broad band at room temperature becomes prominent and then the PL spectra of these crystals below 30 K are characterized by the 2.4 eV band for weak excitation. As typical results, the PL spectra of the as-grown and fully annealed crystals are shown in figure 5. It has also found that the photo-induced PL spectral change has been more clearly observed at 13 K. The result for the fully-annealed  $\text{SrTiO}_3$  single crystal is shown in figure 6 (a), as a typical result. The irradiation time is given by each curve. The peak intensity of the 2.4 eV luminescence is plotted against irradiation time in figure 6 (b). The PL increases in intensity and then tends to saturate at 90 min without any change of the spectral shape. It

has been found that the magnitude of the spectral change at 2.4 eV for 60 min is nearly independent of temperature.

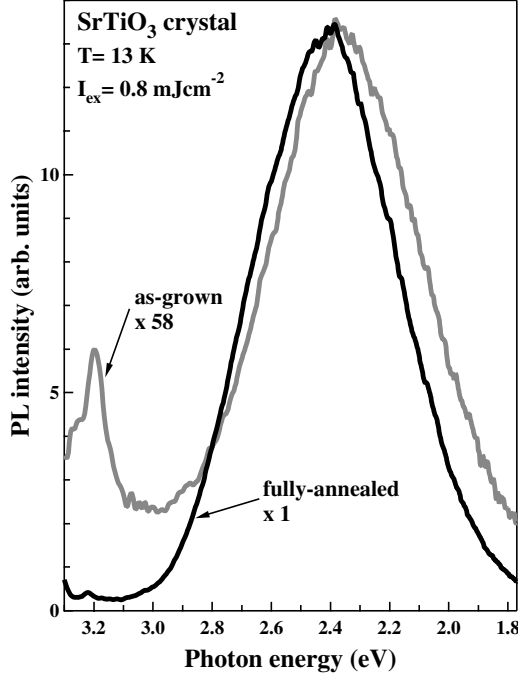


**Figure 5.** PL spectra of the as-grown and fully-annealed  $\text{SrTiO}_3$  crystals at 13 K. The excitation laser wavelength is 355 nm and laser fluence is  $0.8 \text{ mJcm}^{-2}$ .

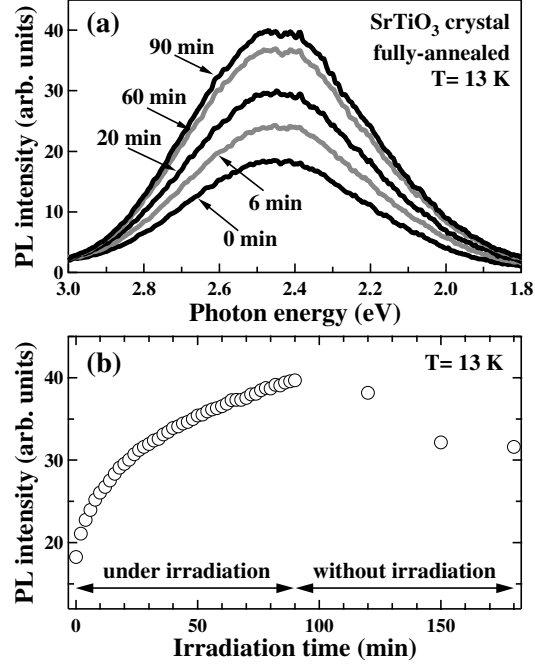


**Figure 6.** Photo-induced PL spectral change of the fully-annealed  $\text{SrTiO}_3$  crystal at 13 K. (a) Spectral change in vacuum. (b) Irradiation time vs the peak PL intensity.

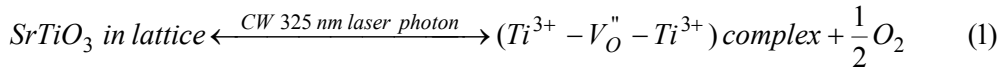
#### 4. Mechanism of the photo-induced photoluminescence spectral change in $\text{SrTiO}_3$

Through our many optical experiments [8, 9, 13] on the as-grown  $\text{SrTiO}_3$  crystal and the  $\text{SrTiO}_3$  crystals recovered from different annealing stages, it has found that the PL of real  $\text{SrTiO}_3$  crystals is considerably affected by crystal defects. All of the results on the reversible photo-induced PL spectral change of the as-grown and different annealed  $\text{SrTiO}_3$  single crystals may be summarized as follows.

- (1) The reversible photo-induced PL spectral change can be observed at different temperatures, from 6 K to room temperature. The spectral change takes time and the speed of change is nearly independent of temperature, but it increases with increasing light intensity.
- (2) The spectral change tends to saturate at long light irradiation time (more than 90 min).
- (3) The spectral change is induced by changing the specimen atmosphere between oxygen gas and vacuum only under a CW 325 nm laser light.
- (4) After removing the light irradiation, each PL property persists for a long time even at room temperature under room light, regardless of any changes of atmosphere.

The result (1) indicates that the observed spectral changes are not phonon-assisted phenomena but purely electronic ones and that the PL band at 2.4 eV is an extrinsic luminescence due to the luminescence centres introduced by a CW 325 nm laser light. Since the 325 nm ( $= 3.81 \text{ eV}$ ) laser light never dissociates directly free  $\text{O}_2$  molecule, the result (3) indicates that the phenomena arise from the photo-induced associative detachment and the photo-induced dissociative adsorption of  $\text{O}_2$  molecules near the  $\text{SrTiO}_3$  surface. In this case, photo-excited  $\text{SrTiO}_3$  crystal acts as a photocatalyst for decomposing  $\text{O}_2$  molecule and also as an oxygen reservoir. The results also summarize how spectral change arises naturally from the photo-activated oxidation and reduction. The reduction of  $\text{SrTiO}_3$

surface under a CW 325 nm laser light in vacuum may be accompanied by creation of electron-captured oxygen vacancy  $V_O^{''}$ . Using a local spin density approximation plane-wave pseudo potential method, Astala and Bristowe [14] have shown that the doubly positively charged state is most stable. It is well in agreement with the experimental result that oxygen deficiency in  $\text{SrTiO}_3$  enhances the electrical conductivity even at low temperatures [15]. This means that most of the electrons around oxygen vacancies are released and, therefore, such oxygen vacancy sites are relatively positively charged. Therefore, the oxygen vacancies tend to trap photo-generated electrons. Several authors [11, 12, 16] proposed another type of defect,  $(\text{Ti}^{3+}-V_O^{''}-\text{Ti}^{3+})$  complex, at  $\text{SrTiO}_3$  surface. Taking account of this complex, the photo-induced oxygen desorption can be explained as follows.



In the complex, the  $\text{Ti}^{3+}$  ions act as hole traps ( $S_h$ ), while the vacancy  $V_O^{''}$  do as electron traps ( $S_e$ ). In  $\text{SrTiO}_3$  crystal, it has been known that electrons determine well the transport properties, for example, electrical conductivity and photoconduction, while any phenomena related to holes have been not observed. This indicates that holes are almost trapped around crystal defects. Toyozawa [17] proposed three types of symmetry-breaking instabilities of excitons in the phonon field and when the electron and the hole have deformation potentials of opposite sign, the decomposition into a pair of self-trapped particles occurs. This instability of an exciton leads to lattice decomposition into an electron centre (an anion vacancy)  $S_e$  and a hole centre (an anion interstitial)  $S_h$ , if exciton is formed in the bulk. On surfaces, the hole center is emitted out of the surface, thus leaving only the electron center. Therefore, such exciton instability may result in oxygen desorption at  $\text{SrTiO}_3$  surface in vacuum and thus the oxygen vacancies produced give rise to the 2.4 eV luminescence. It is noted that the CW 325 nm laser light is indispensable for the spectral change due to the photo-induced oxidation and -reduction in  $\text{SrTiO}_3$ . The CW 325 nm laser fluence in our experiments was at most  $0.8 \text{ Wcm}^{-2}$ , and therefore any bond breaking mechanism based on the instability under high-density excitation may be rejected from the present discussion. Unlike alkali halides, a single interband excitation never induces the desorption of surface atom in semiconductors, since the binding energy of atoms is larger than the energy gap. In the case of photo-excitation of such semiconductor, only atom around crystal defect at the surfaces can be released [18, 19, 20, 21]. Astala and Bristowe[14]calculated the oxygen vacancy formation energy of about 7 eV, which are approximately twice of the bulk energy gap and are slightly smaller than twice of the CW 325 nm laser photon energy, at the  $\text{TiO}_2$ -terminated (100) surface of  $\text{SrTiO}_3$ . Both the oxygen defects (for example,  $\text{Ti}^{3+}-\text{O}^{''}_v-\text{Ti}^{3+}$  and  $\text{O}^{''}_v$ ) inherent to  $\text{SrTiO}_3$  surfaces and the infinite continuity of the laser light may enable the 325 nm laser photon to release  $O_2$  molecule from the surface. Incidentally, the pulsed 355 nm laser light (the pulse width = 4~5 ns), though the photon energy is close to the CW 325 nm laser light, never induced the spectral change even at  $14 \text{ mJcm}^{-2}$  [8]. The oxygen desorption via such excited state may occur immediately after a laser pulse incidence. However, it is found that relatively long time is taken to complete the spectral change in  $\text{SrTiO}_3$ , as the result (2). This indicates that the photo-induced oxygen desorption probability is very low at  $\text{SrTiO}_3$ surface. The observed saturation tendency with further increasing irradiation time suggests that the photo-induced oxygen defect increases the potential energy of the surface irradiated by light. In such case, equilibrium may be realized in a system composed of a matter ( $\text{SrTiO}_3$  crystal) and a radiation field (325 nm laser photon field). It can be assumed that the intensity, coherency and continuity of laser light determine the degree of fluctuation in the system and the dynamics of the photo-induced PL spectral change.

Recently, there are several reports on the photo-induced change of dielectric and transport properties of  $\text{SrTiO}_3$  crystal under ultraviolet irradiation and the change is frequently explained as the intrinsic property of  $\text{SrTiO}_3$  crystal. However, if some of photo-generated carriers are trapped at the oxygen defects, large enhancement of the dielectric constant may be observed as an extrinsic effect. In the past, Uwe [22] pointed out the importance of the ferroelectric microregion [23] in the photo-

excited  $\text{SrTiO}_3$  crystal, as follows. Photo-generated electrons create  $\text{Ti}^{3+}$  ions and then these ions produce electric dipoles with oxygen defects. The dipoles may produce ferroelectric microregions which give large enhancement of the dielectric constant.

Finally, since some chemical heterogeneity on the surface has been pointed out for the surfaces of  $\text{SrTiO}_3$  crystal reduced and oxidized at high temperatures [10] and small amount of  $\text{OH}$  ions are introduced inevitably during crystal growth by the Verneuil method, these effects must be considered for more detailed discussion.

### Acknowledgments

This work was supported by a Grant-in-Aid for Scientific Research from the Ministry of Education, Science, Sports, Culture and Technology, Japan. This work was also supported by an Interdisciplinary General Joint Research Grant for Nihon University.

### References

- [1] Nagaosa N, Ogawa T 1989 Theory of photoinduced structure change *Phys. Rev. B* **39** 4472–4483.
- [2] Mochizuki S, Nakanishi T, Suzuki Y and Ishi K 2001 Reversible photoinduced spectral change in  $\text{Eu}_2\text{O}_3$  at room temperature *Appl. Phys. Lett.* **79** 3785–3787
- [3] Mochizuki S 2003 Intense white luminescence of  $\text{Sm}_2\text{O}_3$  irradiated with ultraviolet laser light under vacuum *Physica B* **340–342** 944–948
- [4] Mochizuki S, Shimizu T and Fujishiro F 2003 Photoluminescence study on defects in pristine anatase and anatase-based composites *Physica B* **340–342** 956–959
- [5] Mochizuki S and Araki H 2003 UV-laser-light-produced defects and reversible blue–white photoluminescence change in silica *Physica B* **340–342** 969–973
- [6] Mochizuki S and Fujishiro F 2003 Structural, electrical and optical studies on  $\text{AgI}$ -anatase composites *J. Phys.:Condens. Matter* **15** 5057–5072
- [7] Grabner L 1969 Photoluminescence in  $\text{SrTiO}_3$  *Phys. Rev.* **177** 1315–1323
- [8] Mochizuki S, Fujishiro F and Minami S 2005 Photoluminescence and reversible photo-induced spectral change of  $\text{SrTiO}_3$  *J. Phys.:Condens. Matter* **17** 923–948
- [9] Mochizuki S, Minami S and Fujishiro F 2005 The reversible UV-laser-light-induced spectral change and origin of the 2.4 eV luminescence band in  $\text{SrTiO}_3$  *J. Lumin.* **112** 267–270
- [10] Szot K and Speier W 1999 Surfaces of reduced and oxidized  $\text{SrTiO}_3$  from atomic force microscopy *Phys. Rev. B* **60** 5909–5926
- [11] Henrich V E, Dresselhaus G and Zeiger H J 1978 Surface defects and the electronic structure of  $\text{SrTiO}_3$  surfaces *Phys. Rev. B* **17** 4908–4921
- [12] Kimura S, Yamauchi J, Tsukada M and Watanabe S 1995 First-principles study on electronic structure of the (001) surface of  $\text{SrTiO}_3$  *Phys. Rev. B* **51** 11049–11054
- [13] Fujishiro F and Mochizuki S 2005 Optical spectra change of Verneuil-grown  $\text{SrTiO}_3$  single crystal during decolorization process *submitted*.
- [14] Astala R and Bristowe P D 2001 Ab initio study of the oxygen vacancy in  $\text{SrTiO}_3$  *Modelling Simul. Mater. Sci. Eng.* **9** 415–422
- [15] Jourdan M and Adrian H 2003 Possibility of unconventional superconductivity of  $\text{SrTiO}_{3-\delta}$  *Physica C* **388/389** 509–510
- [16] Cord B and Courths R 1985 Electronic study of  $\text{SrTiO}_3(001)$  surfaces by photoemission *Surf. Sci.* **162** 34–38
- [17] Toyozawa Y 1983 Symmetry breaking excitonic instabilities in deformable lattice *Physica B+C* **117–118** 23–29
- [18] Puchin V E, Shluger A L and Itoh N 1993 Theoretical studies of atomic emission and defect formation by electronic excitation at the (100) surface of  $\text{NaCl}$  *Phys. Rev. B* **47** 10760–10768
- [19] Itoh N, Kansaki J, Okano A and Nakai Y 1995 Laser-Beam Interaction with Defects on Semiconductor Surfaces: An Approach to Generation of Defect-Free Surfaces *Annu. Rev.*

*Mater. Sci.* **25** 97–127

- [20] Itoh N and Stonham A M 2000 *Material Modification by Electronic Excitation* (Cambridge: Cambridge University Press)
- [21] Song K S and Williams R T 1993 *Self-Trapped Excitons* (Berlin: Springer)
- [22] Uwe H 2003 Impurity effect in quantum paraelectrics *Meeting Abstract of the Physical Society of Japan* **58** 640
- [23] Abe H, Harada K, Matsuo R J, Uwe H and Ohshima K 2002 X-ray diffuse scattering associated with ferroelectric microregions in  $\text{KTa}_{1-x}\text{Nb}_x\text{O}_3$  *J. Phys.: Condens. Matter* **13** 3257

# Photo-induced valence-number changes and defects in Eu<sub>2</sub>O<sub>3</sub> fine particle films

**Shosuke Mochizuki<sup>1</sup>, Fumito Fujishiro, Ken'ichiro Ishiwata**

Department of Physics, College of Humanities and Sciences, Nihon University, Tokyo 156-8550, Japan

E-mail: motizuki@physics.chs.nihon-u.ac.jp

**Abstract.** Different Eu<sub>2</sub>O<sub>3</sub> fine particle films were prepared by the laser ablation method. Under a continuous wave (CW) 325 nm laser light irradiation, their photoluminescence spectra are measured both in vacuum and in O<sub>2</sub> gas atmosphere. All the specimens display reversible spectral change and clear luminescence colour changes (red luminescence ↔ white luminescence) for changing specimen atmosphere. Moreover, the white-luminescent state is stored for more than several years at room temperature in air under room light. The obtained results suggest that the spectral changes arise from both the photo-induced valence (Eu<sup>3+</sup> → Eu<sup>2+</sup>) change of europium ions and the photo-generated oxygen defect structure at Eu<sub>2</sub>O<sub>3</sub> particle surfaces in vacuum, which is expressed by the following reaction, Eu<sub>2</sub>O<sub>3</sub> in lattice + CW 325 nm photon → (Eu<sup>2+</sup>-oxygen vacancy-Eu<sup>2+</sup>) complex + ½O<sub>2</sub>. The obtained results are discussed in the light of the exciton theory.

## 1. Introduction

Europium sesquioxide Eu<sub>2</sub>O<sub>3</sub> exhibits five crystal phases designated by X, H, A, B and C at normal pressure in the order of decreasing temperature [1]. Cubic X form transforms into hexagonal H form at about 2553 K, to hexagonal A form at about 2413 K, to monoclinic B form at about 2313 K, to cubic C form at about 1373 K. The B form contains six formulae per unit cell of which space group is C2/m. The body-centered cubic C form contains 32 europium ions and 48 oxygen ions per unit cell of which space group is Ia3. Several years ago, we found reversible photo-induced spectral change in Eu<sub>2</sub>O<sub>3</sub> at room temperature [2, 3]. When Eu<sub>2</sub>O<sub>3</sub> powder compacts, films and particles are irradiated with a 325 nm laser light in vacuum, their photoluminescence (PL) spectra change from a red sharp-line structure to a white broad band, which can be clearly seen with the naked eye. After removing the UV laser light, the white PL state is stored for more than several years at room temperature under room light, regardless of any changes of atmosphere. By irradiating with the same UV laser light at room temperature under oxygen gas atmosphere, the original red PL state reappears. Such reversible phenomenon may well yield materials for white-light-emitting devices and erasable optical storage. Especially, Eu<sub>2</sub>O<sub>3</sub> fine particles are thought to have potential application for high-density luminescent device and they lead to important modifications of some of the bulk properties. For example, particle-size reduction may give rise to the confinement of Eu<sup>3+</sup> excitation and long-wavelength phonon modes

<sup>1</sup> To whom any correspondence should be addressed.

in the particle [4, 5]. In the present paper, we report upon the structural and optical studies on Eu<sub>2</sub>O<sub>3</sub> fine particle films and we arrive at a view on the photo-induced spectral change.

## 2. Specimen preparation and characterization

The laser ablation target was prepared by compressing Eu<sub>2</sub>O<sub>3</sub> powder 99.98 % in purity under a pressure of 0.2 GPa for 1 h at room temperature and then by sintering at 1273 K for 24 h in air. Eu<sub>2</sub>O<sub>3</sub> fine particle production and deposition were carried out in oxygen atmosphere of different pressures with a pulsed Nd<sup>3+</sup>-YAG laser light (wavelength  $\lambda=355$  nm, pulse width=3 ns, repetition =10 Hz). The temperature of the silica glass substrate was room temperature. After deposition, the half of the as-deposited film specimens was annealed at 873 K in air for 24 h. The conditions of the specimen preparation are listed in table 1.

**Table 1.** Summary of Eu<sub>2</sub>O<sub>3</sub> films investigated.

Specimen	Laser ablation atmosphere	Comments
Oxygen pressure (Pa)		
#1 $\alpha$	0.00	as deposited
#1 $\beta$	0.00	annealed at 873 K in air
#2 $\alpha$	1.26	as deposited
#2 $\beta$	1.26	annealed at 873 K in air
#3 $\alpha$	2.54	as deposited
#3 $\beta$	2.54	annealed at 873 K in air
#4 $\alpha$	5.10	as deposited
#4 $\beta$	5.10	annealed at 873 K in air

As standard specimens, the B-form and C-form specimens were also prepared by sintering Eu<sub>2</sub>O<sub>3</sub> powder compacts at 1823 K and 1273 K in air, respectively. The films were characterized by the x-ray diffraction (XRD) analysis with Cu K $\alpha_1$  radiation at 300 K. Distribution maps of europium and oxygen atoms in the films were obtained by using a scanning electron microscope (SEM) with an energy dispersive x-ray (EDX) fluorescence spectrophotometer (Shimadzu SSX-550). Figures 1(a), (b), (c) and (d) show the room-temperature XRD patterns of Eu<sub>2</sub>O<sub>3</sub> specimens listed in table 1. Gray bold and black solid curves correspond to as-deposited film and annealed one, respectively. The XRD lines of the B-form and C-form Eu<sub>2</sub>O<sub>3</sub> crystals [6] are given as histograms in figures 1(e) and (f), respectively. As seen in these figures, the as-deposited films display halo XRD pattern. The halo XRD pattern is reproduced by rescaling and broadening these B-form- and C-form XRD lines and then by superposing them. This suggests that the as-deposited films consist of very small crystallites or that the as-deposited films are amorphous. As-deposited films were fully transformed to crystalline Eu<sub>2</sub>O<sub>3</sub> ones by heating at 873 K in air for 24 h. The crystalline Eu<sub>2</sub>O<sub>3</sub> films are mixtures of a lot of C-form crystallites and few B forms. The EDX fluorescence map of europium atoms coincides well with that of oxygen atoms. Both the XRD patterns and the EDX fluorescence maps indicate that the produced films are chemically uniform Eu<sub>2</sub>O<sub>3</sub>. The film morphology was analyzed by the SEM and an optical microscope with a charge-coupled device camera system. As typical results, the SEM images of the as-deposited Eu<sub>2</sub>O<sub>3</sub> film (#4 $\alpha$ ) and annealed film (#4 $\beta$ ) are shown in figures 2(a) and (b), respectively. The uniform particle layer consists of particles smaller than several ten nanometers. Few particles with size larger than several hundred nanometers are seen. These particles may be explosively spouted out

from Eu<sub>2</sub>O<sub>3</sub> target. As seen in figure 2(b), annealing gives rise to many crevices in the uniform layer and divide into large number of domains of several micronmeter sizes.

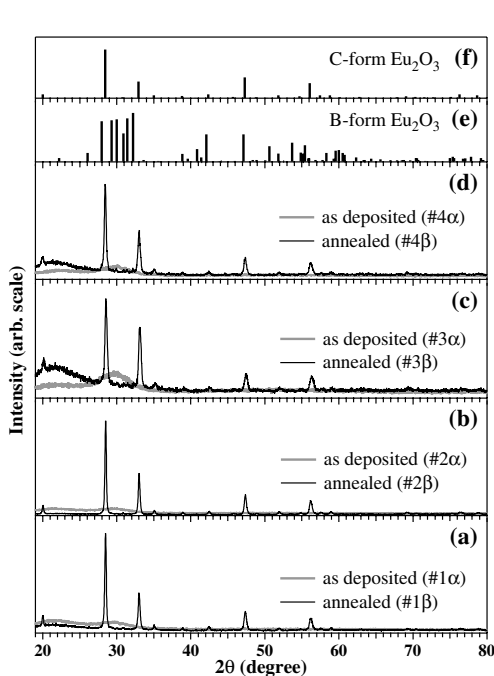


**Figure 1.** Room-temperature x-ray diffractograms of different Eu<sub>2</sub>O<sub>3</sub> films for CuK $\alpha$ 1 radiation.

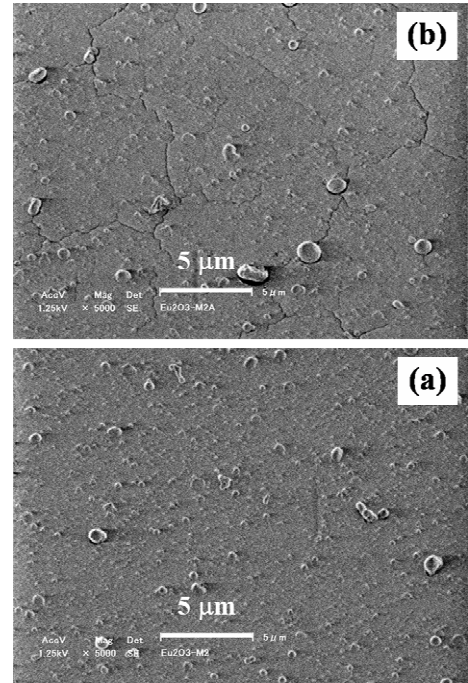


**Figure 2.** SEM images of Eu<sub>2</sub>O<sub>3</sub> films: (a) as-deposited film (#4α), (b) annealed film (#4β).

### 3. Results and discussion

Figures 3(a), (b), (c) and (d) show the PL spectra of the as-deposited and annealed Eu<sub>2</sub>O<sub>3</sub> films. The measurements were carried out at room temperature in air under CW 325 nm photoexcitation. These specimens show the  $^5D_0 \rightarrow ^7F_J$  ( $J=0, 1, 2, 3, 4$ ) emissions at wavelengths between 570 and 720 nm [7]. With increasing oxygen pressure for the pulsed laser ablation, the  $^5D_0 \rightarrow ^7F_0$  emission band becomes sharpen. At wavelengths shorter than 550 nm, these specimens show also broad band emission. The large PL intensity ratio of the broad band emission to the  $^5D_0 \rightarrow ^7F_2$  one is observed for the #1α, #1β, #2α and #2β films which were fabricated in vacuum or extremely low oxygen pressure. Except for the #1 specimen fabricated under vacuum, annealing depresses considerably the PL intensity and makes the spectrum to resolve clearly into several emission bands. Since crystallites grows in size and transform to predominant C-form film by annealing, the selection rule may become rigorously effective to depress PL intensity. In figure 4, the room-temperature PL spectra of different Eu<sub>2</sub>O<sub>3</sub> specimens are compared. Although the spectra are rescaled to each maximum intensity value, the C-form bulk specimen shows more intense emission than the B-form bulk one. These  $^5D_0 \rightarrow ^7F_J$  emission lines appear at almost the same wavelength in every specimen, but the bandwidths in the as-deposited fine particle films are larger than those in annealed films. Such broadening may arise from both random arrangement of crystallites and finite size of crystallites at which surfaces the electronic excitations of Eu<sup>3+</sup> ions are scattered. It is also found that the PL spectra of the as-deposited and annealed fine particle films consist of the emission lines observed at both the B-form and C-form crystals. More high resolution measurements indicate that there are, at least, three distinct  $^5D_0 \rightarrow ^7F_0$  emissions in the annealed films, while there is a very broad  $^5D_0 \rightarrow ^7F_0$  emission in the as-deposited

films. In addition, the presence of the  $^5D_0 \rightarrow ^7F_{0,3}$  emissions and the J-degeneracy of  $^7F_{1,2}$  level suggest that the local site environments of these  $\text{Eu}^{3+}$  ions may be described by different point groups, for example,  $C_{1,2}$ ,  $C_s$  and  $C_{2v}$  [8]. The effects of surface reconstruction of constituent atoms and surface defects have been frequently pointed out for fine particle specimens.

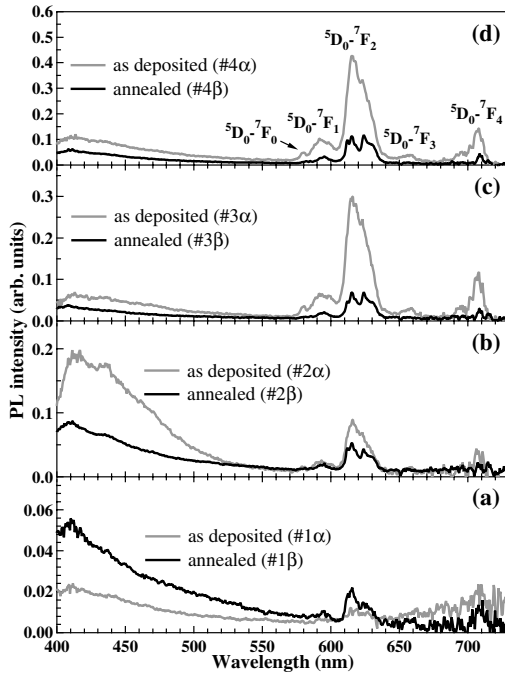


**Figure 3.** Photoluminescence spectra of different  $\text{Eu}_2\text{O}_3$  films before and after annealing.

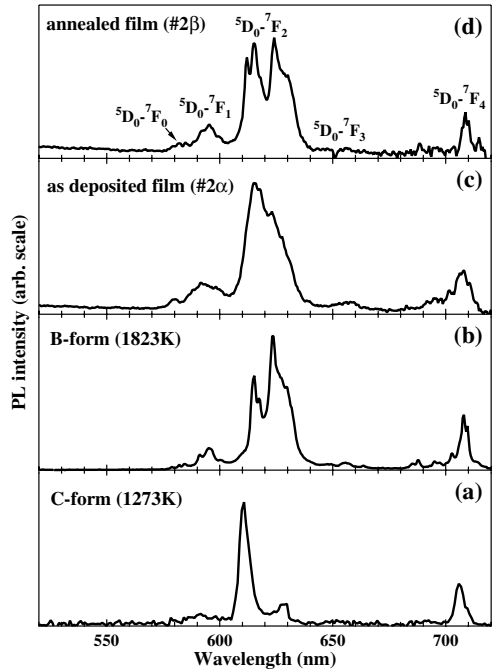


**Figure 4.** Photoluminescence spectra of different  $\text{Eu}_2\text{O}_3$  specimens.

As shown in figure 4(b), the B-form (monoclinic crystalline phase) with  $C_s$  point group can exist at room temperature, as a metastable state. Moreover,  $\text{Eu}_2\text{O}_3$  tends to be structurally degenerated at room temperature. Therefore, some local structural mixture of the B and C forms may occur in  $\text{Eu}_2\text{O}_3$  fine particles, as seen in figure 1. This is compatible with the results obtained for  $\text{Eu}^{3+}$  doped  $\text{Y}_2\text{O}_3$  nanocrystals and  $\text{Eu}_2\text{O}_3$  nanocrystals [9, 10].

The as-deposited and annealed films were irradiated with the 325 nm laser light in oxygen gas of  $1.01 \times 10^5$  Pa or in air, the specimens showed red emission which can be seen with the naked eye. When the specimen chamber was evacuated, the PL colour changes from red to white. The intensity of the white emission increases with increasing irradiation time, which can be clearly seen with the naked eye. Oxygen gas of  $1.01 \times 10^5$  Pa was again introduced in the chamber. The red PL colour appeared again, while the white-colour PL decreased in intensity with increasing irradiation time. Such PL colour change took place repeatedly with sufficient reproducibility, when the kind of atmosphere about specimen was exchanged. After removing the 325 nm laser light irradiation, each PL-state is stored for more than several years at room temperature under room light, regardless of any change of atmospheres ( $1.01 \times 10^5$  Pa  $\text{O}_2$  gas and air). The change to white PL occurs only as a result of the CW 325 nm laser light irradiation in vacuum, while we have not observed the colour change in any other reducing atmosphere; for example, Ar-H<sub>2</sub> mixture gas. The change to white PL can be observed at different temperatures from 7 K to room temperature. This indicates the observed spectral changes are purely electronic phenomena and are not phonon-assisted.

By irradiating with the same 325 nm laser light, we have then measured the PL spectral change of all of the films listed in table 1 at room temperature under both vacuum of  $1.33 \times 10^{-4}$  Pa and

atmospheric O<sub>2</sub> gas, as a function of irradiation time. As typical results, the spectra obtained for the specimens (#1α and #1β) and the specimens (#3α and #3β) are shown figures 5 and 6, respectively. The spectral change for 30 minutes is shown in the figures at intervals of 2 minutes for each specimen. The arrows indicate progress of irradiation time. The kind of atmosphere is given in each figure.

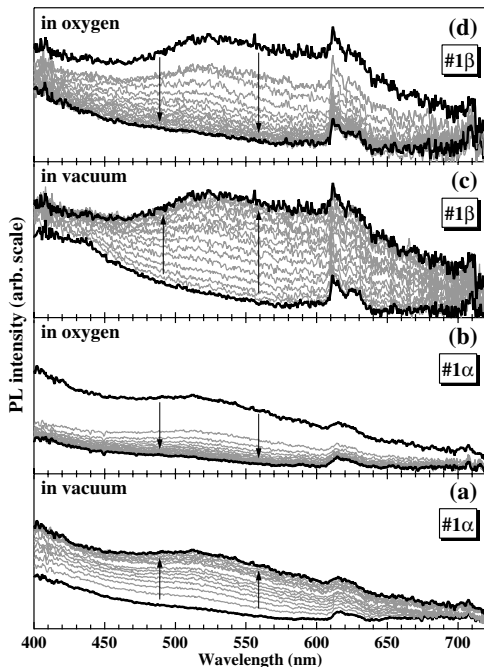


**Figure 5.** Photo-induced spectral change of Eu<sub>2</sub>O<sub>3</sub> films (#1α and #1β).

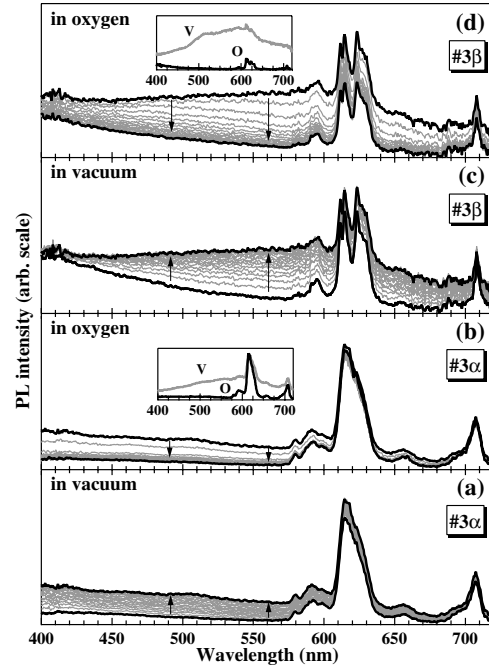


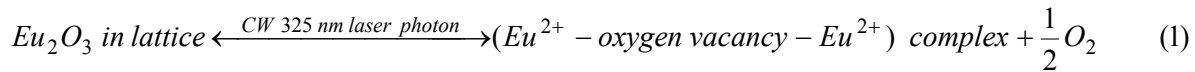
**Figure 6.** Photo-induced spectral change of Eu<sub>2</sub>O<sub>3</sub> films (#3α and #3β).

The speed of the spectral change is increased with increasing laser fluence. The annealed films (#2β, #3β, #4β) show larger PL-intensity change than the as-deposited films (#2α, #3α, #4α). Specimen fabricated under higher oxygen pressure shows more structure-less white luminescence. We also studied the spectral transition in all the specimens for more than four hours. The results for the #3α- and #3β specimens are shown in the insets in figures 6(b) and (d), as typical results. In the insets, V and O indicate vacuum and oxygen atmosphere, respectively. The irradiation time was about 120 minutes for each atmosphere. It is noted that the white PL band increases in intensity with depressing  $^5D_0 \rightarrow ^7F_J$  emissions. Then, the structure of the white band becomes pronounced.

#### 4. Mechanism of the photo-induced spectral transition

The results given in the section 3 suggest that the reversible spectral transition observed in the Eu<sub>2</sub>O<sub>3</sub> fine particle films arises from photo-activated oxidation and reduction near particle surfaces. Since the 325 nm laser light cannot dissociate directly free O<sub>2</sub> molecules as atmospheric gas, the photo-induced oxidation indicates that the photo-dissociation energy of O<sub>2</sub> is considerably decreased at the particle surfaces by the interactions between O<sub>2</sub> and Eu<sub>2</sub>O<sub>3</sub>. The photo-activated reduction of Eu<sub>2</sub>O<sub>3</sub> fine particle is accompanied both by a valence-number change of europium ions (Eu<sup>3+</sup> → Eu<sup>2+</sup>) and by oxygen defect formation. Broad band emission may be connected with Eu<sup>2+</sup> ions and local structural changes arising from oxygen defects. We prepared also a EuO film by reducing Eu<sub>2</sub>O<sub>3</sub> powder compact at 1273 K in vacuum. The EuO film shows a broad PL band centred at about 1.03 μm. This centre wavelength is far away from that of the observed white PL. Therefore, the photo-generated Eu<sup>2+</sup> ions and oxygen defects do not form any structure based on EuO crystal, but they may form (Eu<sup>2+</sup>-

oxygen vacancy-Eu<sup>2+</sup>) complex. Therefore, the observed photo-induced phenomena can be described the following reaction:



In the complex, the Eu<sup>2+</sup> ions act as hole traps (S<sub>h</sub>), while the oxygen vacancy do as electron traps (S<sub>e</sub>). Toyozawa [11] proposed three types of symmetry-breaking instabilities of excitons in the phonon field and when the electron and the hole have deformation potentials of opposite sign, the decomposition into a pair of self-trapped particles occur. In other word, the instability of an exciton leads to lattice decomposition into an electron centre (an anion vacancy) S<sub>e</sub> and a hole centre (an anion interstitial) S<sub>h</sub>, if the exciton is formed in the bulk. On surfaces, the hole centre is emitted from the surface, thus leaving only the electron centre. Therefore, such exciton instability may result in oxygen desorption at Eu<sub>2</sub>O<sub>3</sub> surfaces. Unlike alkali halides, a single interband excitation never induces the desorption of surface atom in semiconductors, since the binding energy of atoms is larger than the energy gap. In such semiconductor case, only atom around crystal defect at the surfaces can be released for single photoexcitation [12]. In the present Eu<sub>2</sub>O<sub>3</sub> specimens, the seeds of the observed photo-induced spectral change may be the defects which had already existed at particle surfaces. It has been said that the desorption via such excited state occurs within 10<sup>-13</sup> s after a laser pulse incidence. However, considerable time is taken to complete the spectral change in Eu<sub>2</sub>O<sub>3</sub>, as seen in figures 5 and 6. This indicates that the photo-induced oxygen desorption probability is very low at the Eu<sub>2</sub>O<sub>3</sub> particle surfaces. The saturation tendency observed at further increasing irradiation time suggests that photo-induced oxygen defect structure increases the lattice potential energy of the light irradiated surface. In such case, equilibrium may be realized in a system composed of a matter (Eu<sub>2</sub>O<sub>3</sub> particles) and a radiation (laser photon) field.

### Acknowledgements

This work was partially supported by a Grant-in-Aid for Scientific Research from the Ministry of Education, Science, Sports, Culture and Technology, Japan. This work was supported by an Interdisciplinary General Joint Research Grant (Nihon University).

### References

- [1] Gschneid K A Jr, Eyring L R 1979 *Handbook on the Physics and Chemistry on Rare Earths*, vol. 3 (Amsterdam: North-Holland).
- [2] Mochizuki S, Suzuki Y, Nakanishi T, Ishi K 2001 *Physica B* **308-310** 1046.
- [3] Mochizuki S, Nakanishi T, Suzuki Y, Ishi K 2001 *Appl. Phys. Lett.* **70** 3785.
- [4] Wakefield G, Keron H A, Dobson P J, Hutchison L H 1999 *J. Colloide Interface Sci.* **215** 179.
- [5] Hong K S, Meltzer R S, Bihari B, Williams D K, Tissue B M 1998 *J. Lumin.* **76&77** 234.
- [6] Powder Diffraction File: Inorganic Phases Sets 1-50, International Center for Diffraction Data, Pennsylvania, 2000
- [7] Dicke G H 1967 *Spectra and Energy Levels of Rare Earth Ions in Crystal* (New York: Interscience, p. vi).
- [8] Caros L D, Videira A L L 1994 *Phys. Rev. B* **49** 11721.
- [9] Williams D K, Yuan H, Tissue B 1999 *J. Lumin.* **83-84** 297.
- [10] Eilers H, Tissue B M 1996 *Chem. Phys. Lett.* **251** 74.
- [11] Toyozawa Y 1983 *Physica B* **112&118** 23.
- [12] Itoh N, Stonerham A M 2000 *Material Modification by Electronic Excitation* (Cambridge: Cambridge University Press).

# Photoluminescence and reversible photo-induced spectral change of SrTiO<sub>3</sub>

Shosuke Mochizuki<sup>1</sup>, Fumito Fujishiro and Seiko Minami

Department of Physics, College of Humanities and Sciences, Nihon University, 3-25-40  
Sakurajosui, Setagaya-ku, Tokyo 156-8550, Japan

E-mail: motizuki@physics.chs.nihon-u.ac.jp

Received 7 June 2004, in final form 4 January 2005

Published 28 January 2005

Online at [stacks.iop.org/JPhysCM/17/923](http://stacks.iop.org/JPhysCM/17/923)

## Abstract

When strontium titanate (SrTiO<sub>3</sub>) single crystal is irradiated at room temperature with a 325 nm laser light in an evacuated specimen chamber, the luminescence intensity increases, creating a broad visible luminescence centred at about 2.4 eV. Then, introducing oxygen gas into the specimen chamber, the photoluminescence spectrum returns reversibly to the original weak luminescence under the same laser light irradiation. After removing the laser light irradiation, each photoluminescent state is stored for a long time at room temperature under room light, regardless of any changes of atmosphere. Such photo-induced spectral change has been observed also at different temperatures from 13 K to room temperature. The observed phenomenon is explained by means of the photo-induced oxygen defect formation at the surfaces of SrTiO<sub>3</sub> crystal. For the same SrTiO<sub>3</sub> single crystal, we have studied the photoluminescence properties. Besides the 2.4 eV luminescence band, we have observed new two luminescence bands centred at about 3.2 eV and about 2.9 eV. The energy, 3.2 eV, is close to both the photoluminescence excitation edge energy and the reported band edge energy of SrTiO<sub>3</sub> crystal. Both the 3.2 eV luminescence and the 2.9 eV luminescence decay rapidly after a pulsed photoexcitation, while the 2.4 eV luminescence lasts for several seconds at 13 K. The excitation light intensity dependence of these luminescence bands has been also measured at 13 K. The 2.4 eV luminescence increases in intensity with increasing excitation intensity up to 4 mJ cm<sup>-2</sup>, and then it becomes decreased with further increase in the excitation intensity. On the other hand, both the 3.2 eV luminescence and the 2.9 eV luminescence increase in intensity with increasing excitation intensity, without any saturation. Although the 2.4 eV luminescence had been assigned to the radiative decay of intrinsic self-trapped excitons in a superparaelectric state by several workers, the present studies have clarified that the luminescence originates mainly from crystal defects (oxygen defects and chemical heterogeneity in the surface region).

<sup>1</sup> Author to whom any correspondence should be addressed.

Both the 3.2 eV luminescence and the 2.9 eV luminescence are discussed qualitatively.

## 1. Introduction

Considerable attention has been given to clarifying the quantum paraelectric state in strontium titanate ( $\text{SrTiO}_3$ ). The lattice of  $\text{SrTiO}_3$  has the cubic perovskite-type structure at room temperature. At 105 K, it transforms into a tetragonal structure. With temperature decreasing from room temperature, the static dielectric constant increases prominently, and it attains several ten thousands at 4 K without any paraelectric–ferroelectric transition (Müller and Burkard 1979). Between 4 and 0.3 K, the dielectric constant was found to be independent of temperature. Recently, a prominent enhancement of the dielectric constant has been observed under ultraviolet light irradiation (Katsu *et al* 2001, Takesada *et al* 2003, Hasegawa *et al* 2003), but it is now under dispute, involving some complicated problems relating to electrode/ $\text{SrTiO}_3$  interfaces. In order to explain the quantum paraelectric state, one may assume first that  $\text{Ti}^{4+}$  ions are fluctuating quantum mechanically in the  $\text{SrTiO}_3$  lattice, as if they are in the critical state just before the paraelectric–ferroelectric transition in usual ferroelectrics. Müller *et al* (1991) proposed that  $\text{SrTiO}_3$  is in a coherent quantum state associated with a rotonic minimum in the transverse acoustic mode. For the photo-enhanced dielectric constant, Nasu (2004) assumed that ultraviolet light broke the crystal inversion symmetry, creating ferroelectric microdomains. He assumed also that such microdomains fluctuated and itinerated quantum mechanically in the  $\text{SrTiO}_3$  crystal.  $\text{SrTiO}_3$  crystal has an indirect gap and a direct gap in an energy range between about 3.2 eV and about 3.5 eV (Cohen and Blunt 1968, Blazey 1971, Capizzi and Frova 1970, Capizzi *et al* 1972, Cardona 1965, Zollner *et al* 2000, Hasegawa *et al* 2000). It is known that the luminescence intensity is specimen dependent (Grabner 1969). Hasegawa *et al* (2000) measured the optical absorption and photoluminescence spectra at temperatures between 10 K and room temperature. They found that the crystal exhibited a broad photoluminescence band around 2.4 eV. Through time-resolved photoluminescence measurements, they assigned the 2.4 eV luminescence to the radiative decay of intrinsic self-trapped excitons. However, many metal oxides display very similar broad photoluminescence between 2 and 3 eV: for example,  $\text{Sm}_2\text{O}_3$  (Mochizuki 2003),  $\text{Eu}_2\text{O}_3$  (Mochizuki *et al* 2001), anatase  $\text{TiO}_2$  (Mochizuki *et al* 2003),  $\text{Al}_2\text{O}_3$  (Mochizuki and Araki 2003a), vitreous  $\text{SiO}_2$  (Mochizuki and Araki 2003b) and  $\text{LaAl}_2\text{O}_3$  (Kawabe *et al* 2000). Moreover, their luminescence intensities are specimen dependent, especially as regards the thermal history and crystal preparation method. Unfortunately, this specimen-dependent nature of the 2.4 eV luminescence has been accorded too little respect in the optical study of  $\text{SrTiO}_3$  and it has led many researchers astray.

Very recently, we have found at room temperature that the 2.4 eV luminescence band of  $\text{SrTiO}_3$  grows under a 325 nm laser light irradiation in vacuum, while it disappears under the same laser light irradiation in oxygen gas. Through many successive experiments involving replacing the specimen atmosphere, it was found that the spectral change occurs reversibly under the 325 nm laser light irradiation. The observed phenomenon relates to the photo-induced oxygen defects at the surfaces of  $\text{SrTiO}_3$ . Now or never is the time to reinvestigate the photoluminescence properties of  $\text{SrTiO}_3$  in detail, taking account of such oxygen defects.

In the present paper, we report the photoluminescence spectrum, its excitation intensity dependence, the decay profile, the photoluminescence excitation spectrum, the time-resolved photoluminescence spectrum and the reversible photo-induced spectral change of  $\text{SrTiO}_3$  single crystal at different temperatures between 12 K and room temperature in detail.

## 2. Experimental detail

The SrTiO<sub>3</sub> crystal was well grown by the Verneuil method and the as-grown crystal is dark blue. The as-grown crystal was then annealed under an appropriate reducing atmosphere. The crystal became perfectly colourless and transparent under the annealing. Several as-grown (dark blue) and annealed (colourless transparent) SrTiO<sub>3</sub> single crystals, 10 × 10 × (0.5–1.0) mm in size, were supplied by Sinkosya Corporation. The broad surfaces of the crystals are optically flat and they are oriented in the [100] direction. It should be noted that such transparent SrTiO<sub>3</sub> crystals grown by the Verneuil method have been widely used by many workers for studying electrical and optical properties. As reference specimens, we have used also several SrTiO<sub>3</sub> powder compact discs which were sintered at 1273 K and annealed at different atmosphere.

The photoluminescence (PL) spectra were measured by using an optical multichannel analyser consisting of a grating monochromator (focal length = 32 cm, grating = 1200 or 150 grooves mm<sup>-1</sup>) and an image-intensified diode-array detector (number of channels = 1024, gate time = 5 ns). An Nd<sup>3+</sup>:YAG laser (wavelength = 355 nm, pulse width = 4–5 ns, repetition = 10 Hz), a continuous wave (CW) He–Cd laser (wavelength = 325 nm) and a monochromatic light source consisting of a 150 W xenon lamp and a grating monochromator (focal length = 20 cm) were used as the excitation source. The excitation light intensity dependence of the PL spectrum was measured by attenuating the incident laser light intensity with glass attenuators calibrated in transmissivity. The PL excitation (PLE) spectra were recorded by varying the excitation light wavelength  $\lambda_{\text{ex}}$  with the same monochromatic light source as described above, and by detecting the luminescence light intensity at a desired wavelength  $\lambda_{\text{ob}}$  as a function of  $\lambda_{\text{ex}}$  with a grating monochromator (focal length = 20 cm) and a synchronous light detection system. The time-resolved PL spectra were taken using the same optical multichannel analyser to which two delay pulse generators were attached. The delay time  $t_d$ , which is the measurement start time after a laser pulse incidence, and the gate time  $t_g$ , which is the time after  $t_d$  of the spectral measurement, were set with these delay pulse generators which were controlled with a personal computer. The actual minimum gate time was 5 ns. The decay curves were measured with an apparatus consisting of a grating monochromator (focal length = 20 cm) equipped with a photodetection system (time constant = about 1  $\mu$ s) and the Nd<sup>3+</sup>:YAG laser oscillating at 355 nm. The optical density (OD) spectrum was measured using another optical multichannel analyser.

An optical cryostat was used for the specimen chamber, in which a closed-cycle helium refrigerator equipped with a temperature controller was used to change the specimen temperature between 12 K and room temperature. Another specimen chamber was also used for the measurement of the reversible spectral change at room temperature. An oil-free vacuum system was used for evacuating these specimen chambers.

## 3. Results

### 3.1. Photoluminescence spectra of SrTiO<sub>3</sub> under weak excitation

Figure 1(a) shows the PL spectra of SrTiO<sub>3</sub> at different temperatures under a pulsed 355 nm laser light excitation (pulse width = 4–5 ns, repetition = 10 Hz, fluence = 0.079 mJ cm<sup>-2</sup>). A broad luminescence band is observed around 2.4 eV at 12 K. The band seems slightly asymmetrical in spectral shape and it consists of two luminescence bands centred at 2.46 and 2.40 eV, which are labelled B' and B'', respectively. This indicates that this photoluminescence comes from at least two kinds of luminescent centres. The spectral shape and intensity differ slightly with the specimens. We measured also the PL spectra of an as-grown crystal as a function of annealing time at 973 K in a reducing atmosphere. It has been found that the PL

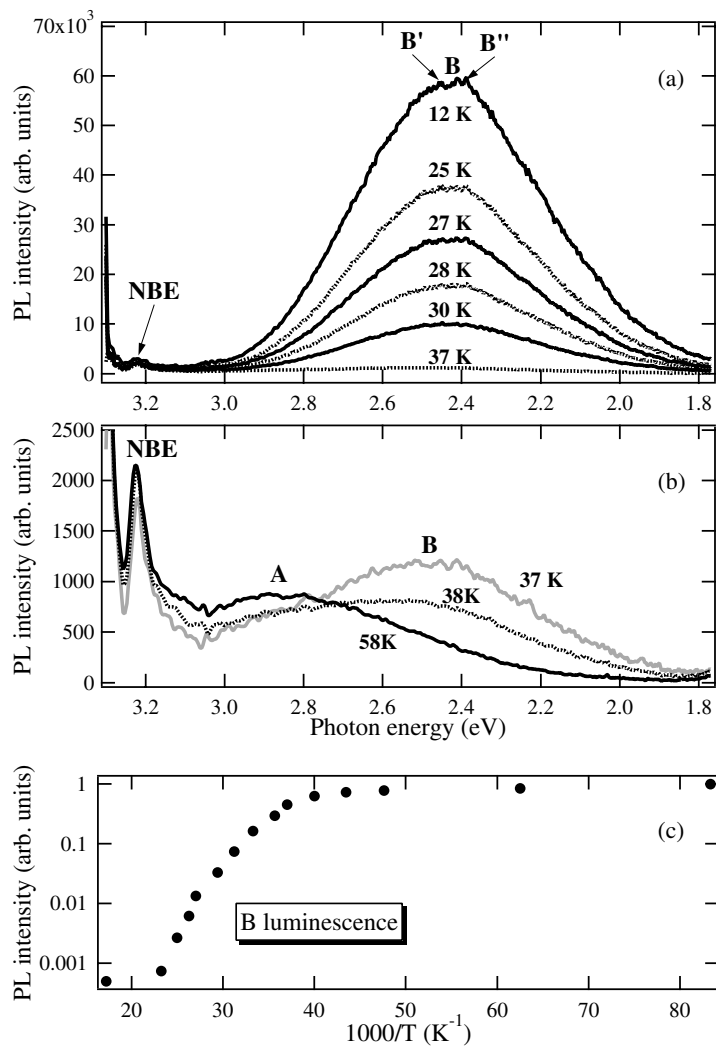


**Figure 1.** The photoluminescence spectra of  $\text{SrTiO}_3$  at different temperatures: (a)  $T \leq 37$  K; (b)  $T \geq 37$  K. (c) The temperature dependence of the integrated intensity. The excitation laser fluence was  $0.079 \text{ mJ cm}^{-2}$ . The spectral integration was performed in a photon energy range between 2.9 and 1.77 eV.

intensity increases with increasing annealing time, while the PL intensity peak energy and spectral width are slightly dependent on the annealing time. With increasing temperature, the 2.46 eV luminescence band grows more and then this band becomes together with the 2.40 eV luminescence band, displaying an asymmetrical band centred at about 2.44 eV above 27 K. We call this luminescence band the ‘B luminescence band’. On further increasing the temperature, the B luminescence intensity continues to decrease, while a new luminescence band appears at 2.89 eV and becomes prominent, as seen in figure 1(b). We tentatively call this luminescence band the ‘A luminescence band’. The A luminescence band seems to extend above 3.2 eV. The A luminescence band grows to the detriment of the B luminescence and it is superior to the B luminescence band above 58 K. The integrated PL intensity of the B luminescence band is plotted against inverse temperature on a semi-logarithmic scale in figure 1(c). The

spectral integration was performed in a photon energy region between 2.9 and 1.77 eV. In this figure, the maximum luminescence intensity is normalized to unity. As seen in this figure, the luminescence intensity decreases gradually with increasing temperature to 25 K and, on further increasing the temperature above 28 K, the intensity decreases exponentially. Approaching 43 K, the intensity becomes constant. Although such temperature dependence approaching a constant has been not reported for SrTiO<sub>3</sub>, a slight sign of such constant intensity appeared in the reported curve (figure 3(b): Hasegawa *et al* 2000), as some deviation from the curve fitting to the data. The constant intensity is due to the A luminescence component which grows gradually at high temperatures. Although the PL band consists of several luminescence components as described above, we subtract the constant intensity from the data and we assume a phonon-assisted non-radiative decay process for the observed B luminescence. Then, we perform a curve fitting by using the well-known expression for the integrated PL intensity  $I(T)$ ,

$$I(T) = \frac{1}{1 + C \exp(-\Delta E/kT)}, \quad (1)$$

where  $C$  is a constant and  $\Delta E$  is the height of an average potential barrier separating a luminescent state from the ground state. In addition to such a phonon-assisted non-radiative process, thermal ionization of luminescence states is also considered to participate in the intensity decrease with increasing temperature. In such a case,  $\Delta E$  may correspond to the ionization energy. In the fitting, the data obtained above 40 K are taken off to avoid the effect of the A luminescence. The best-fitted curve is obtained with a  $\Delta E = 32$  meV. The value is slightly smaller than the value (43 meV) reported by Hasegawa *et al* (2000). At present, it is not clear whether the difference arises from the specimen-dependent nature or from the error in the specimen surface temperature measurements or from the manner of the curve fitting—performed probably ignoring the effect of the A luminescence.

As seen in figures 1(a) and (b), a sharp luminescence band is also observed at 3.23 eV which is close to the observed PLE edge (3.26 eV) and the reported indirect band gap energy  $E_g^{id}$  (3.27 eV) of SrTiO<sub>3</sub>. We tentatively call this luminescence band appearing near the band edge the ‘NBE luminescence band’. The steep rise above 3.26 eV is due to the parasitic luminescence of the optical multichannel analyser used.

### 3.2. Photoluminescence excitation spectra of SrTiO<sub>3</sub>

The photoluminescence excitation (PLE) spectra of the same SrTiO<sub>3</sub> single crystal have also been measured at different temperatures. Some of the spectra are selected and shown in figure 2, in which the PL spectrum observed at 13 K is also shown. The luminescence intensity was monitored at the intensity peak energy of the B luminescence band. The PLE spectrum displays a sharp edge at 3.26 eV and a kink at 3.42 eV, which are close to the reported indirect gap energy  $E_g^{id}$  (3.27 eV) and the direct gap energy  $E_g^d$  (3.46 eV) of SrTiO<sub>3</sub> (Capizzi and Frova 1970), respectively. The PLE spectrum indicates that the B luminescence is caused mainly by the interband excitations. The energy difference of the B luminescence band from the PLE edge is about 0.80 eV. The shape of the PLE spectrum differs in an energy region higher than the PLE edge from the absorption spectra reported by Blazey (1971), Capizzi and Frova (1970), Capizzi *et al* (1972), Cardona (1965) and Zollner *et al* (2000). Generally, there are many crystal defects at the specimen surfaces where photoexcited states tend to decay non-radiatively. Such a luminescence quench effect appears more prominently in an energy region higher than the fundamental absorption edge. The excitation with photons above the band gap energy produces energetic electrons and holes, which are eventually thermalized by emitting phonons. Therefore, the PLE above the band gap is governed not necessarily by the direct

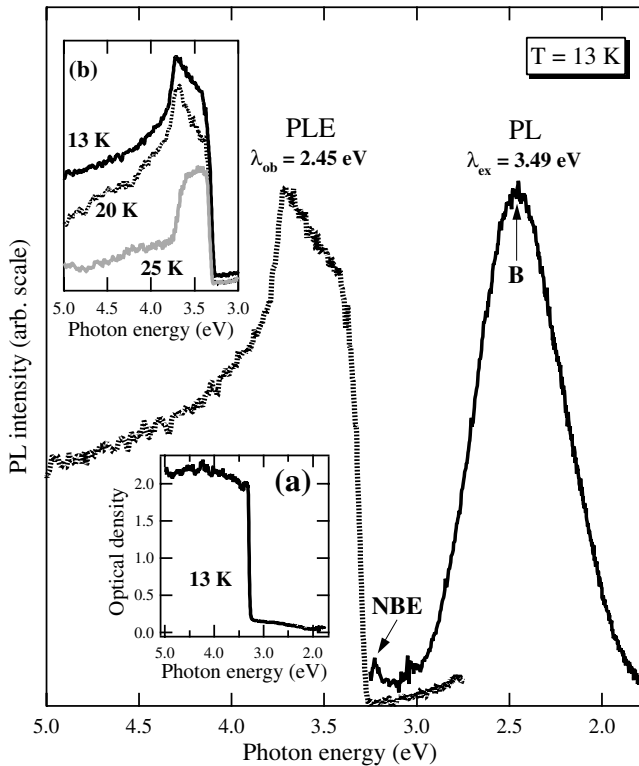


**Figure 2.** The photoluminescence (PL), optical density (OD) and photoluminescence excitation (PLE) spectra of  $\text{SrTiO}_3$  at 13 K. The luminescence is monitored at the peak energy ( $=2.45$  eV) of the B luminescence band. The OD spectrum at 13 K and the PLE spectra at different temperatures are shown in inset (a) and inset (b), respectively.

quenching of highly excited electrons at defect sites but by the change in the probability of the interaction of electron–hole pairs with defects.

As shown in inset (a) of figure 2, the OD spectrum has a faint tail below 3.2 eV. It is found that the OD of the tail decreases with annealing in a reducing atmosphere. Although the B luminescence band is well excited by the interband transition, the PLE spectra indicate that the luminescence can also be excited even by photons having energies lower than indirect gap. Under a 442 nm ( $=2.80$  eV) laser light excitation, we have certainly detected the B luminescence spectrum through a laser light sharp cut filter (HOYA: Y48). The B luminescence can also be ascertained clearly by the naked eye through the same filter. Under the same 442 nm excitation, we have also found more intense luminescence for sintered  $\text{SrTiO}_3$  powder compact specimens (Mochizuki and Fujishiro 2005). These results indicate that there are different defect-related luminescent levels in the energy gap.

As seen in inset (b), the PLE spectral shape changes with increasing temperature, except for the absorption edge profile. The suppression seen at photon energies higher than 3.7 eV becomes prominent with increasing temperature. The suppression may arise from the temperature change in the probability of the interaction of electron–hole pairs with defects.

In the following sections, the observed energy difference (0.8 eV), together with the photo-induced spectral change, will be discussed, and it will be concluded that the B luminescence band comes from the extrinsic luminescent centres around which photo-generated carriers (free electron or free hole, or both) are trapped.

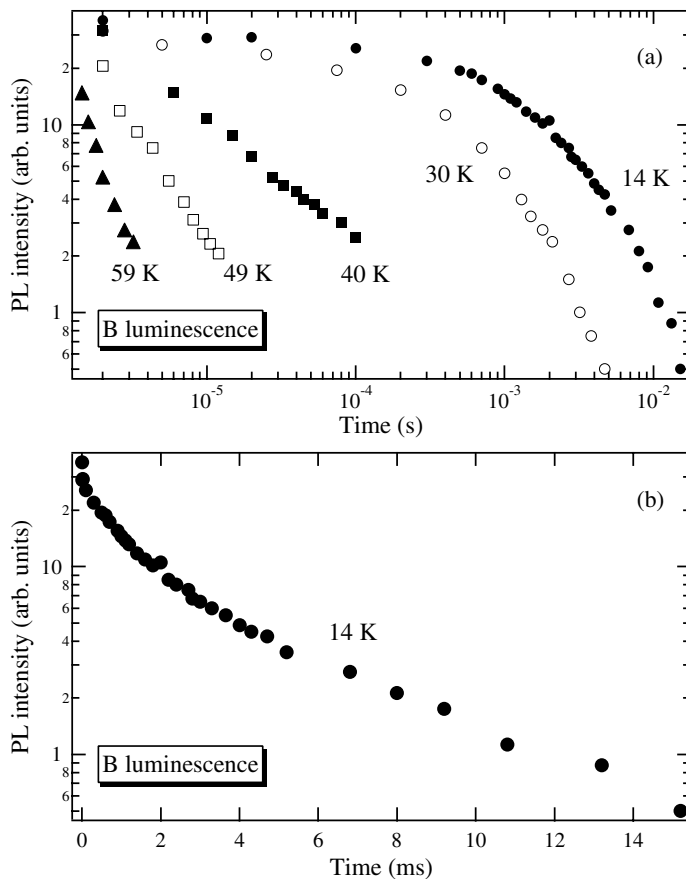


**Figure 3.** The photoluminescence decay profile of the B luminescence band of SrTiO<sub>3</sub>: (a) log (PL intensity)–log  $t$  plots at different temperatures, (b) log (PL intensity)– $t$  plots at 14 K. The photoluminescence was monitored at 2.45 eV. The 355 nm excitation laser fluence was approximately 0.2 mJ cm<sup>-2</sup>.

### 3.3. The photoluminescence decay profile of SrTiO<sub>3</sub>

We have measured the luminescence decay curves of the B luminescence of the same SrTiO<sub>3</sub> single crystal at different temperatures. The luminescence was monitored at an intensity peak wavelength of the B luminescence band. Figure 3(a) shows the PL decay profiles of the B luminescence at different temperatures. The PL intensity is plotted against time on a log–log scale. The decay profile at 14 K is also displayed as a semi-log plot in figure 3(b). It is noted that the crystal displays luminescence for times longer than several tens of milliseconds at 14 K. The profile at 14 K can be well expressed as a three-component exponential decay curve,

$$I(t) = I_1 \exp(-t/\tau_1) + I_2 \exp(-t/\tau_2) + I_3 \exp(-t/\tau_3), \quad (2)$$

with the following parameters:

$$\begin{aligned} I_1 &= 15.408, & \tau_1 &= 2.6533 \times 10^{-6} \text{ s}, & I_2 &= 11.134, & \tau_2 &= 5.4218 \times 10^{-4} \text{ s}, \\ I_3 &= 16.909, & \tau_3 &= 2.8396 \times 10^{-3} \text{ s}. \end{aligned}$$

Since the photodetection system used for decay curve measurements has a long time constant (about 1  $\mu$ s), the shorter lifetime component is not resolved. Therefore, the B luminescence may arise from at least three kinds of luminescence centres.

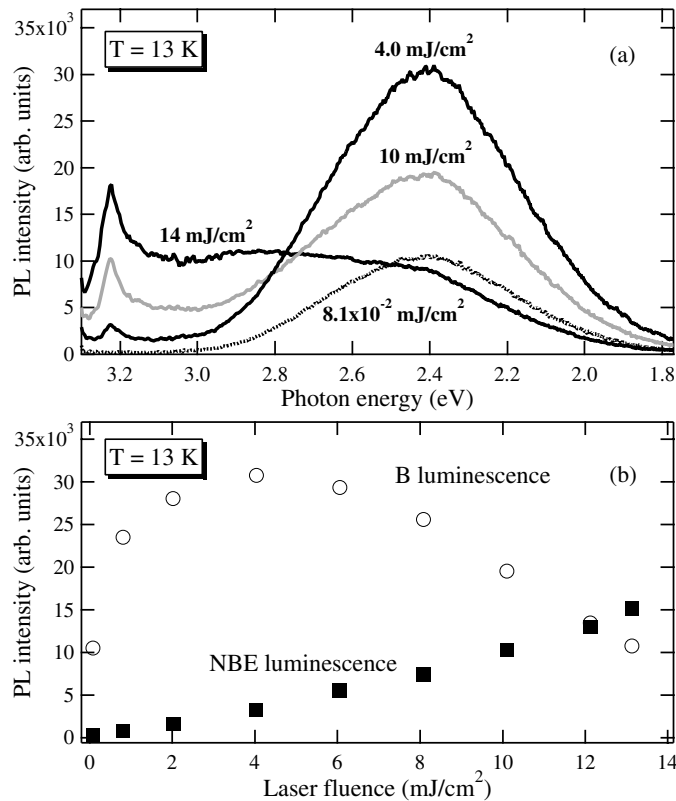


**Figure 4.** The excitation light intensity dependence of the photoluminescence spectrum of  $\text{SrTiO}_3$  at 13 K: (a) spectra under intense, medium and weak excitations; (b) the excitation laser fluence dependence of the peak intensities of the near-band-edge luminescence (NBE) band and the B luminescence band. The NBE luminescence peak energy and the B luminescence peak energy are 3.2 and 2.4 eV, respectively.

Alternatively, the same decay data were examined with a power law ( $t^{-n}$ ). It is found that the curve cannot be uniquely expressed with the  $t^{-2}$  law (Tsang and Street 1979); rather it has a  $t^{-1/2}$  dependence. Hasegawa *et al* (2000) performed also decay curve fitting with the  $t^{-n}$  law, and they inferred suitability of the  $t^{-2}$  law for  $\text{SrTiO}_3$ . However, a caution should be required for result to differ greatly by which data points are selected for the curve fitting with the power law.

At the present stage, the observed decay curve should be regarded obediently as an exponential decay curve consisting of different components. The long lifetime component may arise from some radiative transitions of different deeply trapped states. After stopping the laser irradiation of the as-grown and annealed  $\text{SrTiO}_3$  crystals, we frequently observed faint phosphorescence lasting for several seconds, with the naked eye. Unfortunately, the decay time of such a phosphorescence component ( $t \gg 10^{-3}$  s) cannot be determined from the decay curve analysis, because the phosphorescence contribution to the decay curve is too small.

### 3.4. Photoluminescence spectra of $\text{SrTiO}_3$ under intense excitation

We have measured the PL spectra of the same  $\text{SrTiO}_3$  single crystal at different excitation laser fluences. A typical result is shown in figure 4(a). In figure 4(b), the peak intensities of the

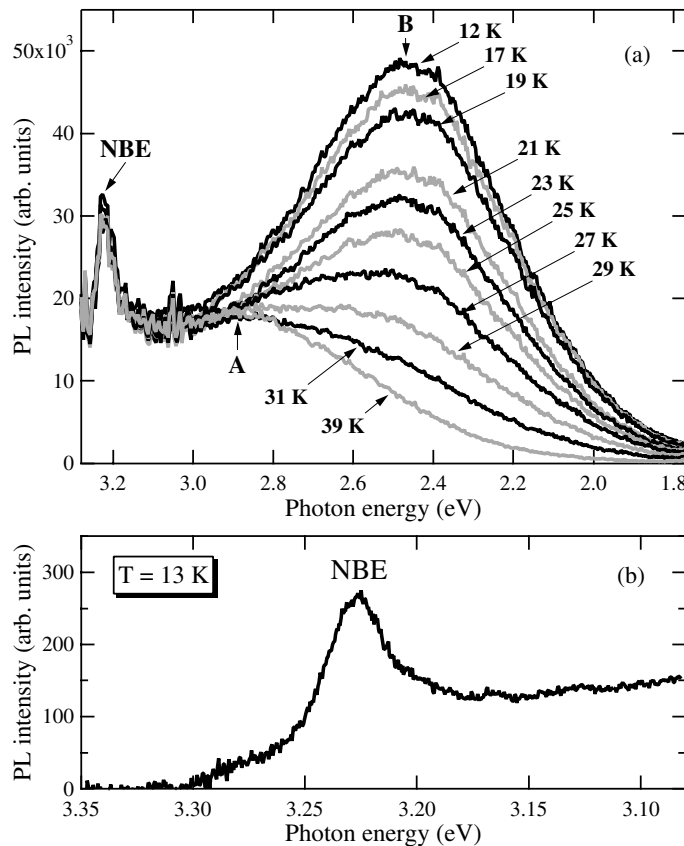


**Figure 5.** The photoluminescence of SrTiO<sub>3</sub> under intense photoexcitation: (a) photoluminescence spectra at different temperatures ( $T \leq 39$  K). The 355 nm excitation laser fluence was  $0.93 \text{ mJ cm}^{-2}$ . (b) Near-band-edge (NBE) emission at 13 K. The 355 nm excitation laser fluence was  $12 \text{ mJ cm}^{-2}$ .

NBE and the B luminescence bands are plotted against laser fluence. Solid squares and hollow circles correspond to the NBE luminescence and the B luminescence, respectively. Under weak excitation, only a B luminescence band is observed. With increasing laser fluence, the B luminescence intensity increases monotonically, and the NBE and A luminescence bands appear. On the laser fluence further increasing up to  $4 \text{ mJ cm}^{-2}$ , the B luminescence attains a maximum, while both the NBE luminescence and the A luminescence become prominent. On laser fluence exceeding  $4 \text{ mJ cm}^{-2}$ , the B luminescence intensity begins to decrease monotonically, while both the NBE luminescence band and the A luminescence band continue to grow, degrading the B luminescence band. Incidentally, we have found that the B luminescence intensity maximum appeared at  $0.4 \text{ mJ cm}^{-2}$  for the sintered SrTiO<sub>3</sub> powder compact. This suggests that most of the B luminescence centres are at the specimen surface.

In order to study the NBE, A and B luminescence bands in detail, we have measured the PL spectra at different temperatures under an intense excitation of  $0.93 \text{ mJ cm}^{-2}$ . This excitation intensity is enough to show up all of the luminescence bands. The results are shown in figures 5(a), 6(a) and (b). We subtract the spectrum measured at 297 K from the spectrum measured at 12 K, in an attempt to extract the B luminescence component. The difference spectrum is given in figure 6(c). By comparing this spectrum with the spectrum (figure 1(a)) observed at the same temperature under a weak photoexcitation, it was found that the spectral

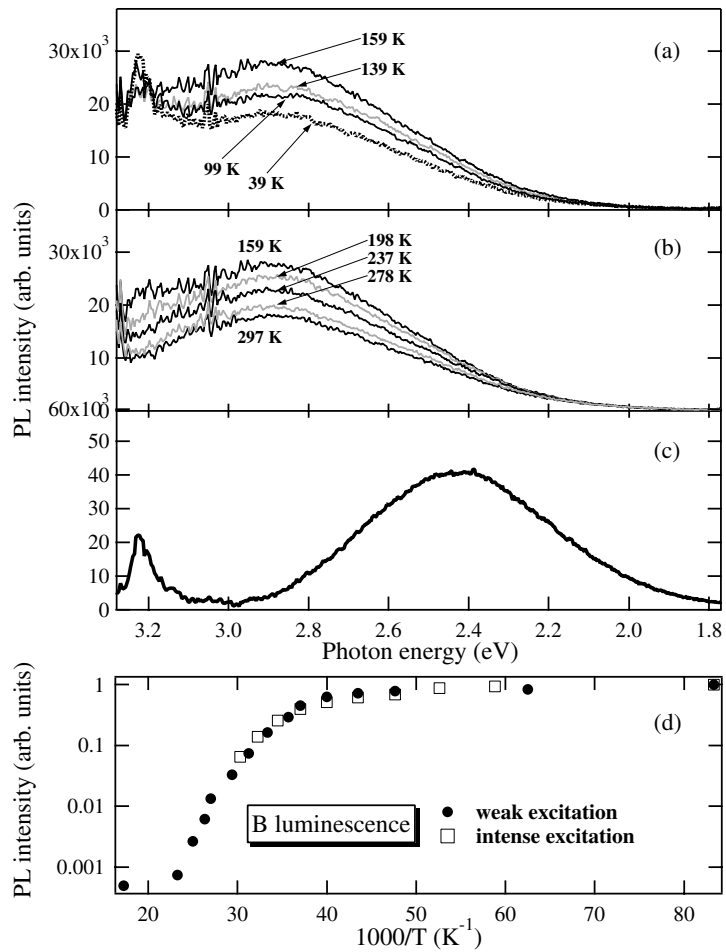


**Figure 6.** The photoluminescence of  $\text{SrTiO}_3$  under intense photoexcitation ( $0.93 \text{ mJ cm}^{-2}$ ): (a) photoluminescence spectra at different temperatures ( $39 \text{ K} \leqslant T \leqslant 159 \text{ K}$ ); (b) photoluminescence spectra at different temperatures ( $159 \text{ K} \leqslant T \leqslant 297 \text{ K}$ ); (c) the difference spectrum; (d) the temperature dependence of the integrated intensity of the B luminescence band for weak and intense excitations which were  $0.079$  and  $0.93 \text{ mJ cm}^{-2}$ , respectively. The spectral integration was performed in a photon region between  $2.9$  and  $1.77 \text{ eV}$ .

shape of the B luminescence band is almost independent of the photoexcitation intensity. With temperature increasing up to  $39 \text{ K}$ , the B luminescence intensity decreases and then it disappears at  $39 \text{ K}$ , while the NBE and A luminescence intensities are almost constant. With temperature increasing above  $39 \text{ K}$ , the A luminescence band continues to grow more without changing the spectral shape and then it attains a maximum at  $159 \text{ K}$ , while the NBE luminescence band becomes weak with the spectral broadening and is merged in the A luminescence band at  $198 \text{ K}$ . At present, it is not clear why such a phonon-assisted nature of the A luminescence band arose. With the temperature further increasing above  $159 \text{ K}$ , the A luminescence intensity decreases. This intensity decrease may be due to non-radiative traps. The PL spectrum measured at  $297 \text{ K}$  was subtracted from that measured at different temperatures, and then the spectral integration was performed over a photon energy range between  $2.9$  and  $1.77 \text{ eV}$ . The integrated intensities thus obtained for the B luminescence band are plotted against inverse temperature, as hollow

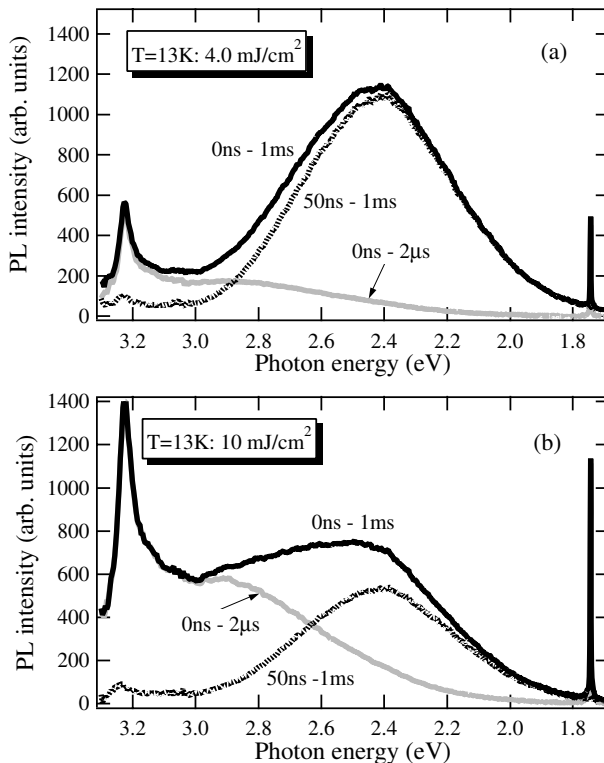


**Figure 7.** The time-resolved photoluminescence spectra of SrTiO<sub>3</sub> at 13 K: (a) laser fluence =  $4.0 \text{ mJ cm}^{-2}$ ; (b) laser fluence =  $10 \text{ mJ cm}^{-2}$ .

squares, in figure 6(d). The data obtained for weak excitation, which are already shown in figure 1(c), are also plotted as solid circles in this figure.

Under a high laser fluence ( $12 \text{ mJ cm}^{-2}$ ), more detailed measurements were performed also on the NBE luminescence and the A luminescence, using a high resolution monochromator. This laser fluence is enough to show up the NBE and A luminescence bands. The result obtained at 13 K is given in figure 5(b). As seen in this figure, the NBE luminescence band is on the rise of the A luminescence band. The NBE luminescence peak is about 77 meV lower in energy than the onset energy of the A band, and it is about 34 meV lower than the PLE edge energy. The NBE luminescence band and the A luminescence have similar temperature and excitation intensity dependences. This suggests that the NBE luminescence and the A luminescence have the same origin.

Most of luminescent metal oxides show some photo-darkening effects under intense photoexcitation. It is found that the PL spectrum and PL intensity of the SrTiO<sub>3</sub> single crystal used were almost unchanged, in spite of such intense 355 nm photoexcitation ( $14 \text{ mJ cm}^{-2}$ ).

### 3.5. Time-resolved photoluminescence spectra of SrTiO<sub>3</sub>

Time-resolved photoluminescence spectra of the same SrTiO<sub>3</sub> single crystal have been measured at 13 K under different excitation intensities. To study the time evolutions of all of the luminescence bands, the measurements were performed under intense excitation. The spectra obtained under excitations of  $4.0$  and  $10 \text{ mJ cm}^{-2}$  are shown in figures 7(a) and (b), respectively. The measurement times,  $t_d$  and  $t_g$ , are given by each curve. At the

initial stage of photoexcitation, the laser light pulse is seen at twice the wavelength, 710 nm ( $=355\text{ nm} \times 2 = 1.745\text{ eV}$ ), of each spectrum, which is common to every grating monochromator. Both the NBE luminescence and the A luminescence disappear rapidly within 50 ns after excitation. Taking account of the parasitic delay, timing jitter times of the apparatus used and the actual laser pulse duration ( $\leqslant 10\text{ ns}$ ), the lifetimes of the NBE and A luminescences are estimated to be less than 10 ns. The B luminescence band is growing over time between 50 ns and 1 ms, and the spectral shape is almost unchanged with further increase in time. The B luminescence observed between 50 ns and 1 ms is slightly shifted toward the lower energy side of the B luminescence observed between 0 ns and 1 ms, as shown in figure 7(a). The shift is due to the time integration effect on the PL intensity. The measured intensity between  $t_d$  and  $t_g$  is expressed as follows:

$$I(t) = \sum_j \int_{t_d}^{t_g} \eta_j N_j(t=0) e^{-t/\tau_j} dt, \quad (3)$$

where  $\eta_j$ ,  $N_j(t=0)$  and  $\tau_j$  are the quantum yield, number and lifetime of  $j$ th luminescence centre including the extrinsic and intrinsic luminescence centres, respectively. If the luminescence centres responsible for the B luminescence band differ slightly in energy, a small shift may be anticipated, as is in fact observed.

Both the PLE spectrum shown in figure 2 and these time-resolved spectra show clearly that the B luminescence follows the NBE and A luminescence. The long lifetime luminescence, continuing for more than several tens of milliseconds, like the B luminescence, is not peculiar to SrTiO<sub>3</sub> but such long lasting luminescence is frequently observed for different metal oxides, for example, ZrO<sub>2</sub> (Fujishiro and Mochizuki 2005). This indicates that the B luminescence cannot necessarily be connected with the nature of the quantum paraelectric state. Such long lifetime luminescence observed for different oxides is thought to arise from accidental recombination of shallowly trapped electrons with distant holes localized around defects. In such a case, the luminescence has slightly different long lifetimes, as seen in figures 3(a) and (b), and the B luminescence spectral shape is almost unchanged with time, as seen in figures 7(a) and (b).

### 3.6. Reversible photo-induced spectral change in SrTiO<sub>3</sub>

When the same SrTiO<sub>3</sub> single crystal is irradiated with a CW 325 nm laser light at room temperature in an evacuated chamber, the B luminescence intensity is enhanced to about twice. Then, introducing oxygen gas into the specimen chamber, the intense PL state returns to the original weak one under the same laser light irradiation, with increasing irradiation time. Through many successive experiments, it was found that the spectral change is nearly reversible under 325 nm laser light irradiation. After removing the 325 nm laser light irradiation, each PL state is stored for a long time at room temperature under room light, regardless of any changes of atmosphere. A typical example of the photo-induced spectral change obtained is shown in figure 8. The experiments were carried out in the following order: (a)  $\rightarrow$  (b)  $\rightarrow$  (c)  $\rightarrow$  (d). Irradiation times  $t_{ir}$  under a given atmosphere and the kind of atmosphere are indicated by each curve. Irradiating under oxygen gas considerably decreases the PL intensity of the specimens. In figure 9, the difference spectrum, curve 7 – curve 8, is shown. The PL spectral change observed for the SrTiO<sub>3</sub> single crystal is mainly characterized by an intensity change of the B luminescence band. A slight degradation of the PL intensity is observed, which may be caused by some photo-induced non-radiative centres. The same experiments were carried out by changing the wavelength of the irradiating laser light. No spectral change was observed except for the CW 325 nm laser light. It was found that the speed of the change accelerates on increasing the power density of the activating light.

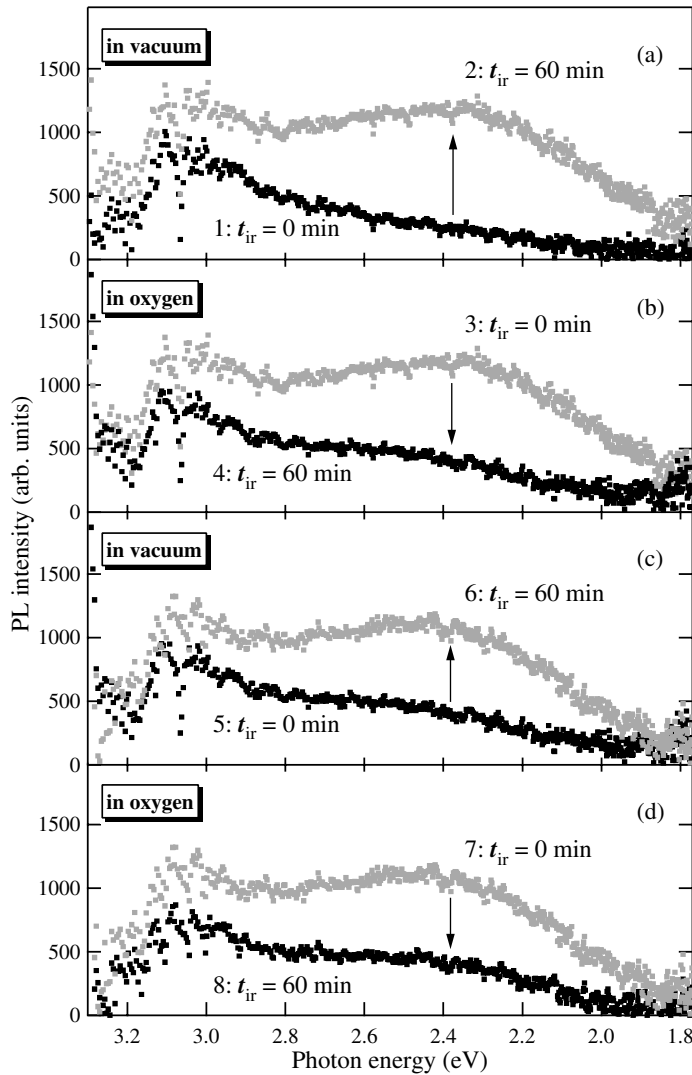


**Figure 8.** The photo-induced reversible spectral change of SrTiO<sub>3</sub> at room temperature: (a) in vacuum, (b) in oxygen gas, (c) in vacuum, (d) in oxygen gas. The experiments were carried out in the following order: (a) → (b) → (c) → (d). Each irradiation was carried out for 60 min under a given atmosphere. Each spectral change is indicated by an arrow. The 325 nm laser fluence was  $0.79 \text{ W cm}^{-2}$ .

Similar photo-induced spectral change has been observed at different temperatures from 13 K to room temperature. The result obtained at 13 K in vacuum under irradiation with 325 nm laser light is shown in figure 10(a), as a typical result. The  $t_{ir}$  in vacuum is indicated by each curve. The peak intensity is plotted against  $t_{ir}$  in figure 10(b). With increasing  $t_{ir}$ , the intensity increases and then tends to saturate at 90 min. The intensity increase is proportional to  $t_{ir}^n$  ( $n < 1$ ). It has been found that the magnitude of the spectral change for 60 min is nearly independent of temperature. After stopping the laser light irradiation, the photoluminescence intensity decreases slightly with increasing time and then reaches a steady state value, which is a photomemory phenomenon.

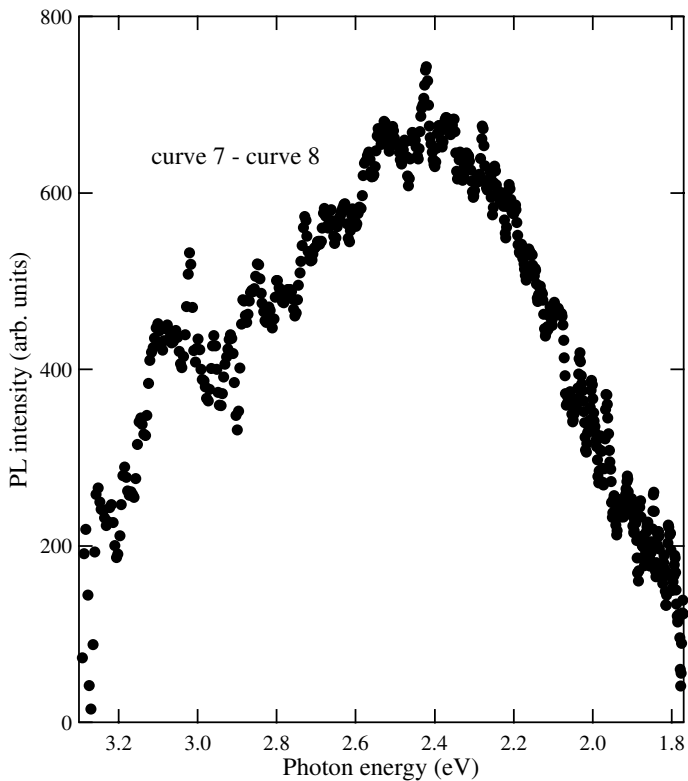


**Figure 9.** The difference spectrum for curve 7 and curve 8. Curves 7 and 8 are shown in figure 8.

Like for  $\text{Sm}_2\text{O}_3$  (Mochizuki 2003),  $\text{Eu}_2\text{O}_3$  (Mochizuki *et al* 2001), anatase  $\text{TiO}_2$  (Mochizuki *et al* 2003) and vitreous  $\text{SiO}_2$  (Mochizuki and Araki 2003b), the observed spectral transition may arise from photo-induced oxidation and photo-induced reduction.

### 3.7. Photoluminescence properties of as-grown $\text{SrTiO}_3$

In order to elucidate the crystal defect effects on the photoluminescence more directly, we have studied the reversible photo-induced spectral transition for an as-grown Verneuil  $\text{SrTiO}_3$  crystal at room temperature. The as-grown  $\text{SrTiO}_3$  crystal is dark blue. The luminescence was excited also with a 325 nm laser line of the He–Cd laser. The result is shown in figure 11(a). Curve 1 is the spectrum of the as-grown crystal. The PL intensity of the as-grown crystal is stronger than several thousands times that of the annealed crystal. The spectrum consists of at least three luminescence bands, at 2.9, 2.3 and 2.2 eV. Curve 2 is the spectrum measured after irradiating in oxygen gas for 60 min. Under 325 nm laser light irradiation in oxygen gas, the PL intensity is decreased considerably. The degradations of the 2.3 and 2.2 eV luminescence bands are especially prominent. The specimen chamber is evacuated again. Curve 3 and curve 4 are the spectra measured at 60 and 480 min after beginning irradiation in vacuum, respectively. Then, oxygen gas was introduced again into the specimen chamber. Curve 5 is the spectrum measured at 840 min after beginning irradiation in oxygen gas. The integrated PL intensity of curve 4 is increased more than 16 times compared with that of curve 5. In figure 11(b), curve 4 is compared after rescaling curve 5 so as to fit to curve 4 at photon energies higher than 2.8 eV. The rescaled curve is shown as curve 5'. Like for the annealed transparent

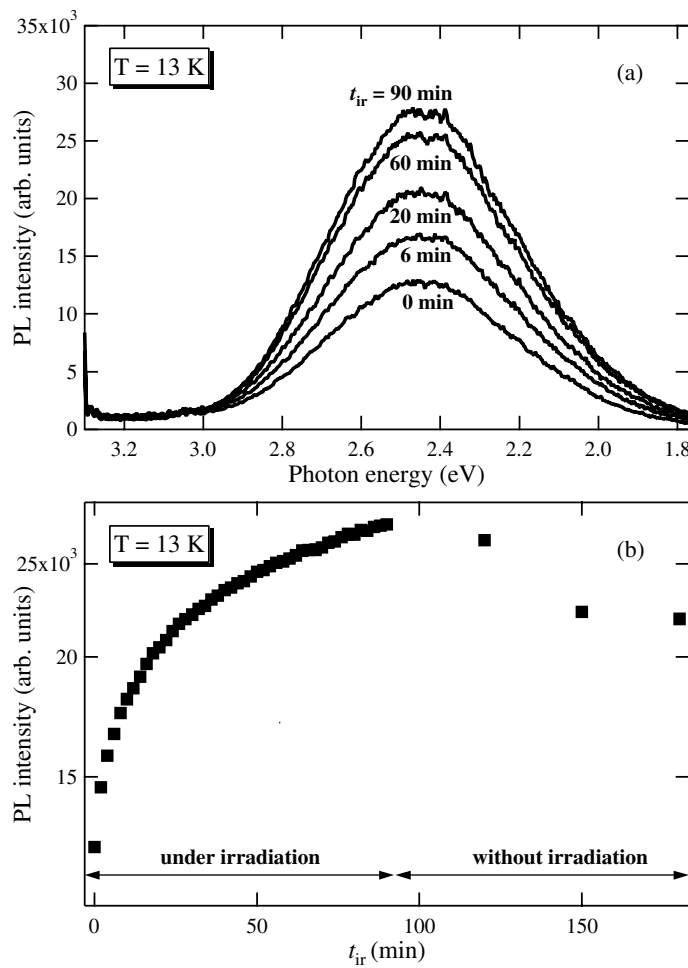


**Figure 10.** The photo-induced spectral change of SrTiO<sub>3</sub> at 13 K in vacuum: (a) photoluminescence spectra for 325 nm laser light irradiation; the irradiation time is indicated by each curve; (b) the irradiation time dependence of the peak intensity of the photoluminescence. The 325 nm laser fluence was  $0.79 \text{ W cm}^{-2}$ .

SrTiO<sub>3</sub> crystal, an A-like luminescence appears in the as-grown crystal: compare curve 5 in figure 11(a) with curve 8 in figure 8(d) and the curve observed at 297 K in figure 6(b). To deduce the information on the B luminescence observed in the annealed SrTiO<sub>3</sub> crystal, the difference spectrum (curve 4 – curve 5') was calculated; it is shown in figure 11(b). We can find a broad luminescence band centred at 2.3 eV, which is slightly shifted to the lower energy side of the B luminescence band of the annealed crystal. It is noted that the B luminescence intensity for the as-grown and the annealed crystals can be varied by 325 nm laser light irradiation in vacuum and in oxygen gas. Since the light penetration depth is very small at 325 nm for SrTiO<sub>3</sub> (Zollner *et al* 2000), the observed spectral change of the B luminescence band could be closely related to the change of surface electronic states.

Using the same as-grown crystal, we have measured the photoluminescence spectra at different temperatures under an intense excitation ( $14 \text{ mJ cm}^{-2}$ ). As a typical result, the spectrum obtained at 12 K is shown in figure 12. The spectrum obtained at 13 K under the

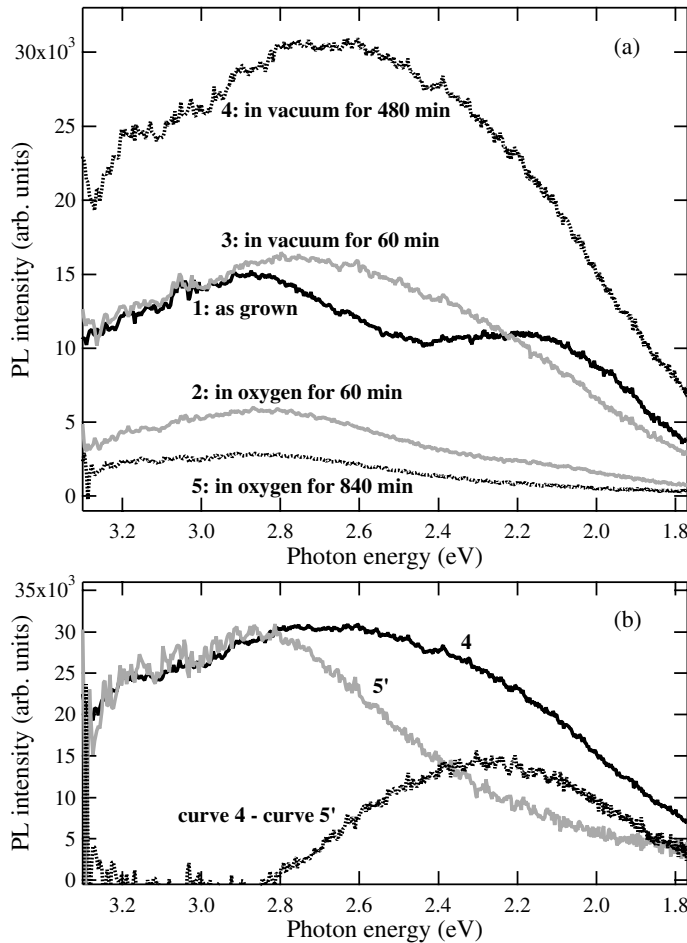


**Figure 11.** The photo-induced reversible spectral change of as-grown SrTiO<sub>3</sub> at room temperature: (a) photo-induced spectral change for replacing specimen atmosphere, (b) comparison of curve 4 with curve 5'. The 325 nm laser fluence was  $0.79 \text{ W cm}^{-2}$ .

same excitation intensity for the annealed crystal is also shown; this was already shown in figure 4(a). The NBE and A luminescence are considerably enhanced in the as-grown crystal. The fine structure and PL intensity of the NBE luminescence band depend on the annealing time. The results suggest that the NBE and A luminescence are assisted by crystal defects.

### 3.8. Miscellaneous

We have measured the PL spectra of sintered SrTiO<sub>3</sub> powder compacts at different temperatures and different laser fluences. The powder specimens show clearly the NBE, A and B luminescences. The NBE and A luminescences remain at room temperature, while the B luminescence disappears above 40 K. Most of the PL properties were very similar to those of single-crystal specimens. Like for other luminescent oxides, the powder compacts were less luminescent and their luminescence decay lifetimes were shorter than those of the single crystals. The main difference between the cases for the powder compacts and the single crystals is that the B luminescence of the powder compacts saturates at lower laser fluence (approximately  $0.5 \text{ mJ cm}^{-2}$ ), while that of the single crystals saturates at  $4 \text{ mJ cm}^{-2}$ .

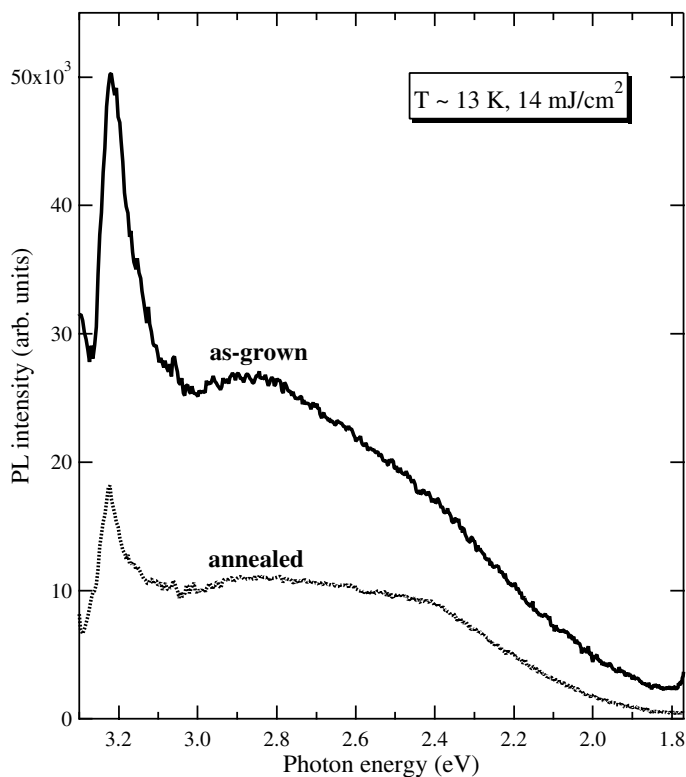


**Figure 12.** The photoluminescence spectra of the as-grown dark blue and annealed transparent SrTiO<sub>3</sub> crystals at about 13 K under an intense 355 nm photoexcitation (laser fluence = 14 mJ cm<sup>-2</sup>).

#### 4. Discussion

##### 4.1. The reversible photo-induced spectral change

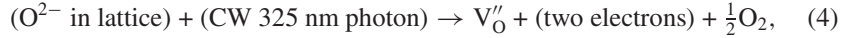
The present experimental results on the reversible photo-induced spectral change of SrTiO<sub>3</sub> single crystal may be summarized as follows.

- (1) The photo-induced reversible spectral change between weak PL and intense PL can be observed at different temperatures, from 13 K to room temperature. The spectral change takes time. The speed of the spectral change is nearly independent of temperature but it increases with increasing light intensity.
- (2) The spectral change tends to saturate at a long light irradiation time (more than 90 min).
- (3) The spectral change is induced by changing the specimen atmosphere between oxygen gas and vacuum only under a CW 325 nm laser light. On the other hand, intense pulsed 355 nm laser light (14 mJ cm<sup>-2</sup>) never induced such spectral change.
- (4) After removing the 325 nm laser light irradiation, each PL property persists for a long time even at room temperature under room light, regardless of any changes of atmosphere.

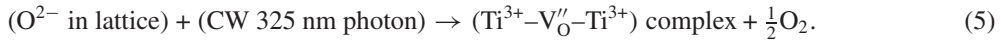
The result (1) indicates that the observed photo-induced spectral changes are purely electronic phenomena and they are not phonon-assisted ones. The result (1) indicates also that the B luminescence is an extrinsic luminescence due to the luminescence centres introduced

by a CW 325 nm laser light. Since the 325 nm (=3.81 eV) laser light never dissociates directly free O<sub>2</sub> molecules, the result (3) indicates that the phenomena arise from the photo-induced associative detachment and photo-induced dissociative adsorption of O<sub>2</sub> molecules near the SrTiO<sub>3</sub> surface. In this case, photoexcited SrTiO<sub>3</sub> crystal acts as a photocatalyst for decomposing O<sub>2</sub> molecules and also as an oxygen reservoir. The results also summarize how spectral change arises naturally from photo-activated oxidation and reduction.

Although some chemical heterogeneity on the surface has been pointed out for the surfaces of SrTiO<sub>3</sub> crystal reduced and oxidized at high temperatures (Szot *et al* 1997, Szot and Speier 1999), we discuss tentatively the observed photo-induced spectral changes at room temperature by regarding the measured SrTiO<sub>3</sub> crystal as chemically homogeneous, as follows. The chemical heterogeneity effects will be discussed in the next subsection. The reduction of the SrTiO<sub>3</sub> surface under a CW 325 nm laser light in vacuum may be accompanied by the creation of electron-captured oxygen vacancies V''<sub>O</sub>, as follows:



where Kröger–Vink notation is used (Kröger and Vink 1956). Using a local spin density approximation plane wave pseudopotential method, Astala and Bristowe (2001) have shown that the doubly positively charged state is the most stable. This is in good agreement with the experimental result that oxygen deficiency in SrTiO<sub>3</sub> enhances the electrical conductivity (Jourdan and Adrian 2003) even at low temperatures. This means that most of the electrons around oxygen vacancies are released and, therefore, such oxygen vacancy sites are relatively positively charged. Therefore, the oxygen vacancies tend to trap photo-generated electrons. On the other hand, several authors (Henrich *et al* 1978, Cord and Courths 1985, Kimura *et al* 1995) proposed another type of defect at the SrTiO<sub>3</sub> surface as follows:



In the complex, the Ti<sup>3+</sup> ions act as hole traps, while the vacancy V''<sub>O</sub> tends to trap electrons. For SrTiO<sub>3</sub> crystal, it is known that electrons determine the transport properties, for example, electrical conductivity and photoconduction, well, while no phenomena related to holes have been observed. This indicates that holes are almost trapped around crystal defects. Incidentally, the high dielectric constant (several tens of thousands) of SrTiO<sub>3</sub> crystal suppresses, creating excitons (ex). Toyozawa (1983) proposed three types of symmetry-breaking instability for excitons in the phonon field and, when the electron and the hole have deformation potentials of opposite sign, decomposition into a pair of self-trapped particles occurs. In other words, the instability of an exciton leads to lattice decomposition into an electron centre (an anion vacancy) S<sub>e</sub> and a hole centre (an anion interstitial) S<sub>h</sub>, if the exciton is formed in the bulk. On surfaces, the hole centre is emitted from the surface, thus leaving only the electron centre. Therefore, such exciton instability may result in oxygen desorption at SrTiO<sub>3</sub> surfaces in vacuum and the oxygen vacancies thus produced give rise to B luminescence. Similar desorption has already been discussed for photo-induced breaking of the Si–O bond in a silica (Shluger and Stefanovich 1990). By a quantum chemical calculation, Eglitis *et al* (2004) has demonstrated that the chemical bonding of the perovskite structure contains a considerable covalent component, like the case for silica. It is noted that CW 325 nm laser light is indispensable for spectral change due to the photo-induced oxidation and reduction in SrTiO<sub>3</sub>. The CW laser fluence in the present experiments was at most 0.8 W cm<sup>-2</sup>, and therefore any bond-breaking mechanism based on the instability under high density excitation may be excluded from the present discussion. Unlike the case for alkali halides, a single interband excitation never induces the desorption of surface atoms in semiconductors, since the binding energy of atoms is larger than the energy gap. In such photoexcited semiconductor

cases, only atoms around crystal defects at the surfaces can be released (Puchin *et al* 1993, Itoh *et al* 1995, Itoh 1995, Itoh and Stoneham 2000, Song and Williams 1993). Astala and Bristowe (2001) calculated the oxygen vacancy formation energy of about 7 eV, which is approximately twice the bulk energy gap and slightly smaller than twice the CW 325 nm He–Cd laser photon energy, at the TiO<sub>2</sub>-terminated (100) surface of SrTiO<sub>3</sub>. Both the oxygen defects (for example, Ti<sup>3+</sup>–O<sub>V</sub><sup>–</sup>–Ti<sup>3+</sup> and O<sub>V</sub><sup>–</sup>) inherent to SrTiO<sub>3</sub> surfaces and the infinite continuity of the laser light may enable the 325 nm laser photons to release O<sub>2</sub> molecules from the surface. Incidentally, pulsed 355 nm laser light (the pulse width is 4–5 ns), although the photon energy is close to that of the CW 325 nm laser light, never induced spectral change even at 14 mJ cm<sup>–2</sup>, as a result of (3). Besides the surface defects, a small amount of OH<sup>–</sup> ions introduced inevitably during crystal growth by the Verneuil method should also be taken into account for the photo-induced spectral change. Incidentally, Ohmukai *et al* (1999) have observed a 126 nm laser-induced bond breaking and some polycrystalline precipitates on a SiO<sub>2</sub> glass. We could not detect any light scattering due to precipitates on the 325 nm laser light irradiated SrTiO<sub>3</sub> crystal.

It has been said that the desorption via such an excited state occurs within 10<sup>–13</sup> s after laser pulse incidence. However, it is found that a relatively long time (more than 90 min) is taken to complete the spectral change in SrTiO<sub>3</sub>, as a result of (2). This indicates that the photo-induced oxygen desorption probability is very low at the SrTiO<sub>3</sub> surface. The observed saturation tendency with further increasing *t*<sub>ir</sub> suggests that photo-induced oxygen defects increase the potential energy of the light irradiated surface. In such a case, equilibrium may be realized in a system composed of matter (SrTiO<sub>3</sub> crystal) and a radiation field. It can be assumed that the intensity, coherency and continuity of laser light determine the degree of fluctuation in the system and the dynamics of photo-induced spectral change. Unlike the case for a pulsed laser light, the possibility of successive electronic excitation is not ignored for CW laser light. More detailed experiments with varying frequency, pulse width and duty ratio of a periodic laser light pulse are in progress in our laboratory.

In relation to the UV laser light-induced oxygen defects and white luminescence, it should be noted that the crystals (for example, LaAlO<sub>3</sub>) grown by light heating methods (for example, the floating zone methods and the arc furnace method) display intense white luminescence. During the growth, the crystals are exposed to intense ultraviolet radiation and, therefore, oxygen defects may be produced, exhibiting oxygen defect-related white luminescence between 3 and 2 eV (Kawabe *et al* 2000).

#### 4.2. The B luminescence band

The present experimental results on the B luminescence of SrTiO<sub>3</sub> single crystal may be summarized as having the following features.

- (1) The broad B luminescence band is observed well under band-to-band excitation (>3.27 eV) in SrTiO<sub>3</sub> with a large energy shift (0.80 eV). Although the quantum yield is small, the B luminescence is also observed under a 442 nm (=2.80 eV) laser light excitation.
- (2) The B luminescence intensity is considerably increased by photo-induced reduction with 325 nm (=3.81 eV) laser light irradiation in vacuum.
- (3) The PL intensity increases with progressive annealing in a reducing atmosphere. The intensity peak energy and spectral width of the B luminescence depend on annealing history.
- (4) The B luminescence decay curve consists of at least four components. The phosphorescence component lasts for at least several seconds. It is hard to fit the decay curve uniquely to a power law time (*t*<sup>–2</sup>) dependence.

- (5) With increasing temperature, the B luminescence intensity decreases, increasing the NBE and A luminescence bands. The B luminescence of both the single crystal and the powder compact disappeared above about 40 K.
- (6) With increasing excitation intensity, the B luminescence intensity increases. On further increasing the excitation intensity, the B luminescence intensity attains a maximum at about  $4 \text{ mJ cm}^{-2}$  and then decreases, increasing the NBE and A luminescence bands. The  $\text{SrTiO}_3$  power compacts display the B luminescence intensity maximum at approximately  $0.5 \text{ mJ cm}^{-2}$ .

Feature (1) indicates that the B luminescence arises from several kinds of PL mechanisms. Both feature (2) and the feature (3) indicate that oxygen deficiency is a main cause of B luminescence. Feature (4) indicates that the deviation from stoichiometry creates different types of defect which give different luminescence centres and traps. Most workers have been studying  $\text{SrTiO}_3$  crystals produced by the Verneuil method. Unfortunately, the compositional deviation of the crystals produced by the Verneuil method is known to be between  $10^{-2}$  and  $10^{-4}$  even for simple transition metal oxides ( $\text{MnO}$ ,  $\text{CoO}$ ,  $\text{NiO}$  and  $\text{TiO}_2$ ). The chemical purities and isotope separation of the constituent elements (especially strontium and titanium) are not necessarily satisfactory and therefore most of the available  $\text{SrTiO}_3$  crystals are at most 99.99% pure. These are problems common to many transition metal oxides. Moreover, since a flame consisting of  $\text{H}_2$  gas and  $\text{O}_2$  gas is used for the Verneuil crystal growth process, some contamination due to  $\text{OH}^-$  ions may be inevitable. Feature (6) indicates that most of the B luminescence centres are at the specimen surface. Ignoring the above-described chemical impurity effects and noting only the effects due to the deviation from  $\text{SrTiO}_3$  stoichiometry, we will discuss the results of the PL measurements.

We first discuss the excited states created in  $\text{SrTiO}_3$  crystal by the third harmonics (355 nm) of the pulsed  $\text{Nd}^{3+}$ :YAG laser. Unlike CW 325 nm laser light, this 355 nm laser light never induced the spectral changes discussed in the previous subsection. The valence and conduction bands of  $\text{SrTiO}_3$  mainly consist of the 2p orbits of  $\text{O}^{2-}$  ions and the 3d orbits of  $\text{Ti}^{4+}$  ions, respectively. Therefore, the fundamental absorption transfers the electron from the  $\text{O}^{2-}$  ion to the  $\text{Ti}^{4+}$  one. After such photoexcitation, some of the photo-produced electrons and holes recombine directly, displaying luminescence via some processes with short lifetime. However, perfect  $\text{SrTiO}_3$  crystal is an indirect gap semiconductor and, therefore, the PL intensity is so weak that it cannot be measured. Another portion of electrons and holes may be trapped by intrinsic crystal defects at the surface and by the defects related to the deviation from the stoichiometry. In such a case, the PL property differs with the type of defect and also with the sites of defects, as follows.

**4.2.1. Oxygen defects at the surface and in the bulk.** Stashans and Vargas (2001) have calculated structural and electronic properties of the F centres (two electrons trapped by an oxygen vacancy) in  $\text{SrTiO}_3$ , as have Astala and Bristowe (2001). The results indicate that the wavefunctions of the two extra electrons extend over the titanium atoms closest to the two vacancies and over other nearby atoms, which is the same as the  $\text{Ti}^{3+}$ -oxygen vacancy complex model proposed by Henrich *et al* (1978), Cord and Courths (1985) and Kimura *et al* (1995). In other words, most of the oxygen vacancies are  $\text{Ti}^{3+}$ -oxygen vacancy complexes in real  $\text{SrTiO}_3$  crystal. In this complex,  $\text{Ti}^{3+}$  ion is one of the candidate hole-trapping centres and the oxygen vacancy is one of the candidate electron-trapping centres. Since electrical conduction due to holes is not observed, most of the photo-generated holes may be deeply trapped at  $\text{Ti}^{3+}$  sites of the complexes. Unlike such holes, photo-generated electrons may be itinerant, experiencing repeatedly collisions with phonons and trapping by oxygen defects.

When some portions of photo-generated holes and electrons are trapped at distant complexes, a luminescence arises from accidental recombination of shallowly trapped electrons with distant holes localized around the defects, exhibiting a long lasting luminescence. Taking account of the electronic conductivity, both the absorption tail in the OD spectrum shown in the inset (a) of figure 2 and the energy difference of 0.80 eV may guarantee the existence of such deeply trapped hole states and shallowly trapped electron states. The broadness of the OD tail shown in the inset (a) of figure 2 suggests that such hole trap levels and electron trap ones arise from many slightly different defects. Using ultraviolet photoemission spectroscopy (UPS), Henrich *et al* (1978) found that the Fermi level of the fractured SrTiO<sub>3</sub> lies about 3 eV above the top of the valence band, which places it within 0.1 eV of the bottom of the conduction band. Also, they observed surface sensitive band gap emission band at energies between the top of the valence band and the Fermi level. These UPS results confirm also the existence of band gap states of the SrTiO<sub>3</sub> surface. Thus, the energy difference of 0.8 eV may correspond to the average energy difference between the shallow electron trap levels and the deep hole trap levels in the band gap. Since the observed luminescence decay curve was expressed as a multi-component exponential curve (at most four components), the overlapping between electron and hole wavefunctions is thought to be almost time independent.

With increasing laser fluence, the numbers of photo-generated electrons and holes increase and then the PL intensity may increase. With further increasing laser fluence, photo-generated electrons and holes become diffused more rapidly inside the crystal (bulk), and therefore the PL intensity decreases, as shown in figures 4(a) and (b). This is why the PL intensity maximum appears at 4 mJ cm<sup>-2</sup>. In other words, this means that most of the defect luminescence centres are at the specimen surface. Since a powder specimen has a large specific surface area, a SrTiO<sub>3</sub> powder specimen may exhibit a PL intensity maximum at the laser fluence smaller than that of the single-crystal specimen. This suggestion was certainly confirmed by the present experimental result that the PL intensity maximum of the B luminescence for the powder compacts appeared at laser fluences (approximately 0.5 mJ cm<sup>-2</sup>) lower than that (4 mJ cm<sup>-2</sup>) observed for the single crystal. On the other hand, the luminescence arising from the defects in the bulk is thought to saturate at higher laser fluence. In addition to these defect effects, it should be taken into consideration that, at higher laser fluence, the recombination of photo-generated electrons and holes is enhanced and therefore it also reduces the luminescence intensity.

**4.2.2. Chemical heterogeneity in the surface region.** As stated in the previous sections, a colourless transparent SrTiO<sub>3</sub> single crystal is obtained by thermally annealing dark blue as-grown crystal at high temperature under an appropriate reducing atmosphere. Although it is colourless and transparent, the crystal is thought to be affected to some extent by such annealing treatment. In particular, it has been reported that the surfaces of reduced and oxidized SrTiO<sub>3</sub> contain not only the above-described oxygen defects but also Ruddlesden–Popper phases (Ruddlesden and Popper 1957, 1958). The combination of x-ray diffraction analysis with surface sensitive techniques has revealed a chemical inhomogeneity in the surface region of single crystals of SrTiO<sub>3</sub> prepared under low and high partial pressures of oxygen at elevated temperatures (Szot *et al* 1997). A solid state reaction leads to the formation of a multilayer-type structure. For oxidized crystals, they observed SrO-rich Ruddlesden–Popper phases at the surface and Magnelli phases of Ti in deeper layers of the surface region. The order of the layered structure is reversed for the reduced crystals, with Ti oxides of different oxidation levels at the surface and Ruddlesden–Popper phases in lower parts of the surface region. Measurements by atomic force microscopy are also reported for the (100) and (110) surfaces of SrTiO<sub>3</sub> single crystals prepared with different oxidizing and reducing conditions at elevated temperatures (1073–1273 K) (Szot and Speier 1999). The morphology of the surfaces turns

out to be drastically altered for both oxidized and reduced crystals in comparison with the original stoichiometric surfaces. The observed changes on the surface of  $\text{SrTiO}_3$  due to the applied extensive thermal treatment cannot be explained by the formation of point defects, relaxation of the uppermost surface layer, rumpling or reconstruction due to vacancy ordering. Instead, the results have to be interpreted in terms of segregation processes and solid state reactions at elevated temperatures, which cause the formation of new chemical phases on the surface and in the region underneath. On the surface of oxygen-annealed  $\text{SrTiO}_3$ , this leads to the growth of steps perpendicular to the surface with step heights larger than the unit cell of the perovskite structure. Crystals prepared above 1173 K are shown to exhibit a step height of 1.18 nm which is attributed to the formation of a Ruddlesden–Popper phase  $\text{SrO}^*(\text{SrTiO}_3)_n$  with  $n = 1$  on the surface. In the case of reduced crystals, the topographic changes on the surface are caused by the formation of Ti-rich phases such as  $\text{TiO}$  and  $\text{Ti}_2\text{O}$  on the surface above 1173 K. The complex interplay of the processes at the surface for different temperatures, in particular its dependence on the details of the heat treatment, is discussed. The induced chemical heterogeneity of the surface and in the near-surface region is interpreted in terms of a kinetic demixing.

Certainly, as shown in figures 11(a) and (b), we observed complicated spectral change under CW 325 nm laser light irradiation in oxygen gas and vacuum for the as-grown  $\text{SrTiO}_3$  crystal, which cannot be explained entirely by the simple oxygen point defect model. Since the as-grown crystal has a higher light absorption coefficient than the colourless annealed crystal, the observed spectral change may be more affected by the surface crystal defects, including the chemical heterogeneity (for example, Ruddlesden–Popper phases) in the surface region.

Bearing these chemical heterogeneities in mind, we have measured the PL properties of the as-grown crystal at different stages of annealing in a reducing atmosphere and also measured those of a colourless transparent stepped  $\text{TiO}_2$ -terminated  $\text{SrTiO}_3$  crystal whose step height is 0.4 nm. The detailed results will be reported in a separate paper (Mochizuki and Fujishiro 2005). The results are summarized as follows. The low temperature PL spectral structures of these crystals are almost the same as those of the colourless transparent (100) faced crystal, apart from the PL intensity. However, with progressive annealing, the dark blue colour becomes weak, the intensities of the NBE, A and B luminescence bands decrease and the lower energy tail of the PLE for the B luminescence becomes weak. Moreover, the excitation laser fluence giving the B luminescence intensity maximum (we call this fluence  $F_{\max}$ ) increases with progressive annealing. Like that for the as-grown crystals, the  $F_{\max}$  for the stepped  $\text{TiO}_2$ -terminated  $\text{SrTiO}_3$  crystal decreases considerably in comparison with the  $F_{\max}$  for the colourless transparent  $\text{SrTiO}_3$  crystal. The observed change in  $F_{\max}$  may be due to the change in the probability of electron–hole pairs with surface defects arising from chemical heterogeneity. We have observed also at least five broad optical absorption bands at about 2.9 eV, about 2.4 eV, about 2.1, 1.6 eV and about 0.9 eV for the as-grown crystal at different annealing stages. The dark blue colour of the as-grown crystal is attributed to this spectral structure in which the blue colour wavelength range is a spectral window. With progressive annealing, these absorptions decrease in intensity. These optical absorption bands may be assigned to oxygen defects and some chemical heterogeneity (Szot *et al* 2002). The broad OD tail observed for the colourless transparent crystal is thought to be a trace from these absorption bands; see the inset (a) of figure 2 in the present paper and the figure 4 in the paper reported by Szot *et al* (2002). In order to clarify the optical excitation in the Ruddlesden–Popper phases, more detailed surface sensitive spectroscopic measurements (for example, reflectivity and PL measurements under total reflection conditions) and morphological and structural measurements for the as-grown crystals at different stages of annealing are now in progress in our laboratory.

Taking account of these studies on different kinds of defects in the real SrTiO<sub>3</sub> crystal grown by the Verneuil method, we thus assign the B luminescence band to the radiative decay of the crystal defect-related excited electronic states. Alternatively, it is theoretically assumed that a long lasting luminescence arises also from some forbidden transition, and therefore we cannot ignore the contribution from de-excitation of some triplet excited states. Previously, many workers have discussed the long lasting B luminescence on the basis of intrinsic self-trapped electronic (exciton) states, ignoring the effects of crystal defects. As discussed above, it should now be apparent that defect effects are important for such self-trapping, and more careful consideration of them is necessary for deducing the intrinsic nature of SrTiO<sub>3</sub> from experimental data.

#### 4.3. The NBE and A luminescence bands

Both the NBE luminescence and the A band luminescence have the following features:

- (α) Both luminescences become prominent under higher excitation intensity and do not saturate under intense excitation ( $14 \text{ mJ cm}^{-2}$ ). They grow to the detriment of the B luminescence with increasing excitation intensity.
- (β) With increasing temperature, both luminescences become prominent to the detriment of the B luminescence and survive even at high temperatures. The spectral structures of the two luminescences at room temperature are hardly changed by changing the excitation laser wavelength from 325 to 355 nm.
- (γ) Both luminescences are considerably enhanced in the as-grown crystal.
- (δ) Both luminescences appear near the band edge energy region and have very short decay times ( $\ll 50 \text{ ns}$ ).

Feature (α) indicates that both the NBE luminescence and the A luminescence arise not from a small number of impurities and crystal defects, but from numerous luminescent species. Feature (β) indicates also that the NBE and A luminescence centres are stable at high temperatures, without any thermal exhaustion. This feature indicates that both luminescences are assisted by phonons. Feature (γ) indicates that the luminescence is emission assisted by crystal defects. Together with the features (α), (β) and (γ), feature (δ) suggests that the two luminescences arise from the same origin and are assignable to some kind of electron–hole recombination emission assisted by crystal defects and phonons.

We discuss these luminescence bands from two different viewpoints as follows. The frequency shift of the NBE luminescence band from incident 355 nm laser light is about  $2207 \text{ cm}^{-1}$ . This is too large for assigning this band to non-resonant Raman scattering (Sirenko *et al* 1999). Non-resonant Raman scattering in a cubic centrally symmetric crystal is forbidden by the odd parity of the optical phonons of F<sub>1u</sub> symmetry, and therefore cubic SrTiO<sub>3</sub> crystal displays weak broad Raman spectrum due to second-order Raman scattering in which two phonons are involved in the scattering process. In the tetragonal phase below 105 K, the phonon mode splits into two Raman-inactive modes of A<sub>2u</sub> and E<sub>u</sub> symmetry. When crystal defects (impurities and vacancies) are introduced (Kleemann *et al* 1997) or when uniaxial external fields (electric field and stress) are applied (Akimov *et al* 2000, Worlock and Fleury 1967), these first-order Raman-inactive modes can be observed only below  $1000 \text{ cm}^{-1}$ . They cannot explain the observed large frequency shift (about  $2207 \text{ cm}^{-1}$ ) of the NBE luminescence. On the other hand, since the photon energy of the incident 355 nm ( $=3.49 \text{ eV}$ ) laser light is close to the reported direct gap energy ( $=3.47 \text{ eV}$ ; Capizzi and Frova 1970) and the observed PLE edge energy ( $=3.26 \text{ eV}$ ), we have to take account of the resonant Raman scattering effects. In this case, the Raman spectrum may display several resonance lines due to the scattering by different phonons near the direct and indirect gap energies, together with other critical points of

the interband transitions (Cardona 1982). As is well known theoretically, the resonant Raman process involves effects due to different intraband and interband scatterings, which display a broad resonance. If we regard the NBE and A luminescences as a result of such resonance Raman scattering, the phonon energy may be estimated from the difference between the indirect band edge energy (PLE edge energy = 3.26 eV) and the NBE luminescence peak energy (= 3.23 eV): the estimated value is 30 meV ( $=242\text{ cm}^{-1}$ ), which is comparable to the transverse optical phonon frequency. Further discussion on the basis of such resonant Raman scattering requires measurements at different incident wavelengths and information about the chemical heterogeneity and defect effects on the Raman scattering.

Next, we discuss the NBE and A luminescence bands as follows. The NBE and the A luminescences were seen even at high temperatures, and they do not exhibit any PL intensity saturation under higher excitation intensity. Although an explanation with so-called donor-acceptor pair (D–A pair) luminescence due to unwanted impurities is frequently given for the intense broad luminescence band with intensity peaks for semiconductors, such D–A pair luminescence related to inevitable impurities may saturate under intense photoexcitation because of the limited numbers of donors and acceptors. Moreover, the luminescence intensity decreases remarkably with increasing temperature. Moreover, such a luminescence spectrum for D–A pairs related to unwanted impurities is thought to be time resolved, since separations between donors and acceptors differ. Therefore, we can ignore the contribution from the impurity-related D–A pair luminescence in the present discussion.

Now, we note that, since ideal  $\text{SrTiO}_3$  crystal has an indirect gap, the crystal does not exhibit directly any intense intrinsic edge emission. When crystal defects giving shallow levels are introduced at the surface, a PL process becomes possible. We note moreover that the NBE and A luminescence bands are observed even at high temperatures under intense excitation and that these luminescence bands are considerably enhanced for the as-grown crystal, as seen in figure 12. Therefore, we regard the observed NBE and A luminescence bands as defect-induced edge luminescence (emission) ones, in which processes different phonons are created. The NBE luminescence band having a shift of  $242\text{ cm}^{-1}$  may be assigned to one of the optical phonon lines. A zero-phonon line anticipated at 3.26 eV is thought to be buried in the rise of the A luminescence band. The full width at half-maximum (FWHM) of the NBE band is about 30 meV. Such a large FWHM is thought to be due to some structural inhomogeneity and damping. It is noted that the A luminescence displays an almost smooth and continuous band. This suggests that, besides optical phonons, many longitudinal and transverse acoustic phonons are created during electron–hole recombination.

## 5. Conclusion and remarks

In summary, we have investigated the reversible PL spectral change and the basic PL properties of as-grown and annealed  $\text{SrTiO}_3$  single crystals, together with sintered  $\text{SrTiO}_3$  powder compacts, at different temperatures from 12 K to room temperature. Three luminescence bands, NBE, A and B, are observed around 3.2, 2.9 and 2.4 eV, respectively. The B luminescence intensity changes with CW 325 nm laser light irradiation in oxygen gas and a vacuum. This result indicates that the B luminescence is not intrinsic luminescence but results from radiative decays of the oxygen defect-related photoexcited states and the chemical heterogeneity in the surface region. The NBE and A luminescences remain at high temperatures and they do not saturate under high density photoexcitation (at least  $14\text{ mJ cm}^{-2}$ ). Their PL properties (temperature dependence, excitation intensity dependence and time dependence) suggest that the NBE luminescence and the A luminescence arise from the same origin. Taking account of crystal defects, the NBE and the A luminescence are discussed qualitatively from two

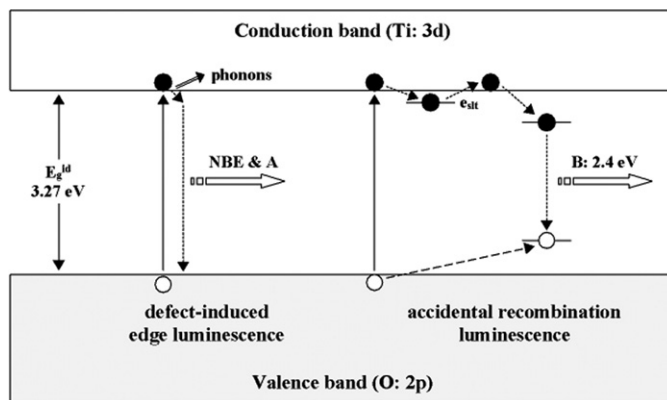


**Figure 13.** Some of the possible photoluminescence processes in real SrTiO<sub>3</sub> crystal. The solid arrow and dotted arrow indicate the optical absorption and radiative transition, respectively. The hollow arrow and double arrow indicate the luminescence and phonon creation, respectively.  $E_g^{id}$  and  $e_{slt}$  denote the indirect gap energy and the shallow electron trap level, respectively. For the accidental recombination model, the short dotted arrow and the broken arrow indicate the electron trapping and hole trapping, respectively.

different viewpoints: defect-induced resonant Raman scattering and defect-induced electron–hole recombination luminescence accompanying creation of phonons. At present, we do not exclude the possibility of other explanations. Although it constitutes a difficult problem, the surface defect structure and the defect-induced effects on the resonant Raman scattering and the edge luminescence (edge emission) should be considered in more detail.

A tentative energy diagram showing some of the possible PL processes in real SrTiO<sub>3</sub> crystal containing crystal defects is given in figure 13. The solid arrow and dotted arrow indicate the optical absorption and radiative transition, respectively. The hollow arrow and double arrow indicate the luminescence and phonon creation, respectively.  $e_{slt}$  indicates a shallow electron trap. For the accidental recombination model, the short dotted arrow and the broken arrow indicate the electron trapping and hole trapping, respectively.

Incidentally, Pontes *et al* (2002) found intense PL in amorphous SrTiO<sub>3</sub> at room temperature under 488 nm (=2.539 eV) radiation from an Ar<sup>+</sup> ion laser. They ascribed the PL excited by low energy photons to non-bridging oxygen defects, for example, TiO<sub>5</sub>. Study of how the non-bridging oxygen defects enhance the PL in amorphous SrTiO<sub>3</sub> is also helpful in discussing the PL properties of real SrTiO<sub>3</sub> crystal surfaces.

Finally, more detailed PL measurements, with excitation laser wavelengths varying around the band gap energies, on different annealing stages of SrTiO<sub>3</sub> crystals are now progress in our laboratory. Experiments with chopped laser light with different duty ratios on the reversible photo-induced spectral change are also now in progress. The results will be reported in a separate paper.

### Acknowledgments

This work was partially supported by a Grant-in-Aid for Scientific Research from the Ministry of Education, Science, Sports, Culture and Technology, Japan. This work was supported by an Interdisciplinary General Joint Research Grant for Nihon University. This work was also partially supported by a Project Research Grant from The Institute of Information Sciences of the College of Humanities and Sciences (Nihon University) and by a Cooperative Research Grant from The Institute of Natural Sciences (Nihon University).

## References

- Akimov I A, Sirenko A A, Clark A M, Hao J-H and Xi X X 2000 *Phys. Rev. Lett.* **84** 4625  
 Astala R and Bristowe P D 2001 *Modelling Simul. Mater. Sci. Eng.* **9** 415  
 Blazey K W 1971 *Phys. Rev. Lett.* **27** 146  
 Capizzi M and Frova A 1970 *Phys. Rev. Lett.* **25** 1298  
 Capizzi M, Frova A and Dunn D 1972 *Solid State Commun.* **10** 1165  
 Cardona M 1965 *Phys. Rev.* **140** A651  
 Cardona M 1982 *Light Scattering in Solids II* (Berlin: Springer)  
 Cohen M I and Blunt R F 1968 *Phys. Rev.* **168** 929  
 Cord B and Courths R 1985 *Surf. Sci.* **162** 34  
 Eglitis R I, Kotomin E A and Borstel G 2004 *Comput. Mater. Sci.* **30** 376  
 Fujishiro F and Mochizuki S 2005 in preparation  
 Grabner L 1969 *Phys. Rev.* **177** 1315  
 Hasegawa T, Mouri S, Yamada Y and Tanaka K 2003 *J. Phys. Soc. Japan* **72** 41  
 Hasegawa T, Shirai M and Tanaka K 2000 *J. Lumin.* **87–89** 1217  
 Henrich V E, Dresselhaus G and Zeiger H J 1978 *Phys. Rev. B* **17** 4908  
 Itoh N 1995 *Butsuri* **50** 704 (in Japanese)  
 Itoh N, Kansaki J, Okano A and Nakai Y 1995 *Annu. Rev. Mater. Sci.* **25** 97  
 Itoh N and Stoneham A M 2000 *Material Modification by Electronic Excitation* (Cambridge: Cambridge University Press)  
 Jourdan M and Adrian H 2003 *Physica C* **388/389** 509  
 Katsu H, Tanaka H and Kawai T 2001 *J. Appl. Phys.* **90** 4578  
 Kawabe Y, Yamanaka A, Hanamura E, Kimura T, Takiguchi Y, Kan H and Tokura Y 2000 *J. Appl. Phys.* **88** 1175  
 Kimura S, Yamauchi J and Tsukada M 1995 *Phys. Rev. B* **51** 11049  
 Kleemann W, Albertini A, Kuss M and Linder R 1997 *Ferroelectrics* **203** 57  
 Kröger F A and Vink H J 1956 *Solid State Physics* vol 3 (New York: Academic) p 307  
 Mochizuki S 2003 *Physica B* **340–342** 944  
 Mochizuki S and Araki H 2003a *Physica B* **340–342** 913  
 Mochizuki S and Araki H 2003b *Physica B* **340–342** 969  
 Mochizuki S, Nakanishi T, Suzuki Y and Ishi K 2001 *Appl. Phys. Lett.* **79** 3785  
 Mochizuki S, Shimizu T and Fujishiro F 2003 *Physica B* **340–342** 956  
 Mochizuki S and Fujishiro F 2005 in preparation  
 Müller K A, Berlinger W and Tosatti E 1991 *Z. Phys. B* **84** 277  
 Müller K A and Burkard H 1979 *Phys. Rev. B* **19** 3593  
 Nasu K 2004 *Rep. Prog. Phys.* **67** 1607  
 Ohmukai M, Takigawa Y and Kurosawa K 1999 *Appl. Surf. Sci.* **137** 78  
 Pontes F M, Longo E, Leite E R, Lee E J H, Varela J A, Pizani P S, Campos C E M, Lanciotti F, Mastellaro V and Pinheiro C D 2002 *Mater. Chem. Phys.* **77** 598  
 Puchin V E, Shluger A L and Itoh N 1993 *Phys. Rev. B* **47** 10760  
 Ruddlesden S N and Popper P 1957 *Acta Crystallogr.* **10** 538  
 Ruddlesden S N and Popper P 1958 *Acta Crystallogr.* **11** 54  
 Shluger A and Stefanovich E 1990 *Phys. Rev. B* **42** 9664  
 Sirenko A A, Akimov I A, Fox J R, Clark A M, Li H C, Si W and Xi X X 1999 *Phys. Rev. Lett.* **82** 4500  
 Song K S and Williams R T 1993 *Self-Trapped Excitons* (Berlin: Springer)  
 Stashans A and Vargas F 2001 *Mater. Lett.* **50** 145  
 Szot K and Speier W 1999 *Phys. Rev. B* **60** 5909  
 Szot K, Speier W, Carius R, Zastrow U and Beyer W 2002 *Phys. Rev. Lett.* **88** 075508-1  
 Szot K, Speier W, Herion J and Freiburg C 1997 *Appl. Phys. A* **64** 55  
 Takesada M, Yagi T, Itoh M and Koshihara S 2003 *J. Phys. Soc. Japan* **72** 37  
 Toyozawa Y 1983 *Physica B* **112 & 118** 23  
 Tsang C and Street R A 1979 *Phys. Rev. B* **19** 3027  
 Worlock J M and Fleury P A 1967 *Phys. Rev. Lett.* **19** 1176  
 Zollner S, Demkov A A, Liu R, Fejes P L, Gregory R B, Alluri P, Curless J A, Yu Z, Ramdani J, Droopad R, Tiwald T E, Hilfiker J N and Woollam J A 2000 *J. Vac. Sci. Technol. B* **18** 2242



Available online at [www.sciencedirect.com](http://www.sciencedirect.com)



Journal of Luminescence 112 (2005) 71–74

JOURNAL OF  
LUMINESCENCE

[www.elsevier.com/locate/jlumin](http://www.elsevier.com/locate/jlumin)

# Photoluminescence studies on AgI–ZrO<sub>2</sub> composites

Fumito Fujishiro\*, Shosuke Mochizuki

Department of Physics, College of Humanities and Sciences, Nihon University, 3-25-40 Sakurajosui, Setagaya-ku, Tokyo 156-8550, Japan

---

## Abstract

AgI–ZrO<sub>2</sub> fine particle composites were fabricated over a wide composition range of AgI. We have measured the X-ray diffractograms and photoluminescence properties of the composites, together with those of pristine AgI and pristine ZrO<sub>2</sub> fine particles. The results give the information about the atomic structure of AgI/ZrO<sub>2</sub> interfaces, which may provide the pathway for the high ionic conduction.

© 2004 Elsevier B.V. All rights reserved.

PACS: 78.55.-m; 61.72.-y; 66.10.Ed

Keywords: Exciton; Photoluminescence; Ionic conductor; Interface; Oxygen defect

---

The ionic conductivity of AgI is considerably enhanced by adding oxide fine particles [1,2]. It is frequently assumed that highly conductive layers are created at AgI/oxide fine particle interfaces. However, it is difficult to clarify experimentally the atomic structure of the interfaces. In order to investigate such interface structure, the photoluminescence (PL) study is effective. Besides AgI [3], most oxides also show structure-sensitive PL. Very recently, we have fabricated AgI–ZrO<sub>2</sub> composites and observed considerable conductivity enhancement [4]. In the present paper, we report the structural and PL studies on AgI–ZrO<sub>2</sub> compo-

sites, and we discuss the structure of AgI/ZrO<sub>2</sub> fine particle interfaces.

AgI–ZrO<sub>2</sub> composites were prepared by mixing AgI powder (99.999%, Alfa) and ZrO<sub>2</sub> powder (>98%, Aldrich) with an average diameter of 26 nm, compressing uniaxially the mixture under 0.2 GPa for 30 min into pellets and then heating the pellets in the lidded crucible at 673 K in air for 12 h. The composite pellets were characterized by the X-ray diffraction analysis with Cu K $\alpha_1$  radiation. The third harmonics,  $\lambda = 355$  nm (= 3.49 eV), of a pulsed Nd<sup>3+</sup>-YAG laser light was used to excite PL.

Fig. 1 shows the X-ray diffractograms of different  $(x)$ AgI– $(1-x)$ ZrO<sub>2</sub> composites. All of the diffraction lines observed for a pristine ZrO<sub>2</sub> ( $x=0$ ) specimen are assigned to the monoclinic

---

\*Corresponding author. Tel./fax: +81 3 5317 9771.

E-mail address: [fumito@phys.chs.nihon-u.ac.jp](mailto:fumito@phys.chs.nihon-u.ac.jp)  
(F. Fujishiro).

phase, except for the tetragonal phase line at  $30.2^\circ$ . Since the diffraction line widths are hardly changed with adding AgI, the average size of  $\text{ZrO}_2$  particles in the composites is thought to be almost the same as that of the starting material powder. On further increasing  $x$ , the AgI diffraction lines become pronounced. The diffraction intensities of the  $\beta\text{AgI}(100)$  line at  $22.3^\circ$  and  $\beta\text{AgI}(200)$  line at  $45.6^\circ$  are considerably enhanced

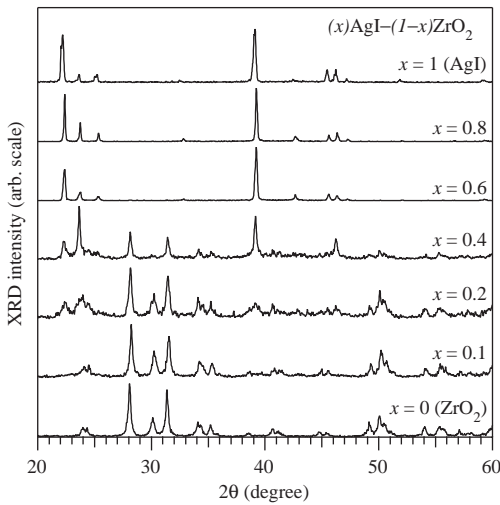


Fig. 1. The X-ray diffractograms for different  $(x)\text{AgI}-(1-x)\text{ZrO}_2$  composites at 297 K.

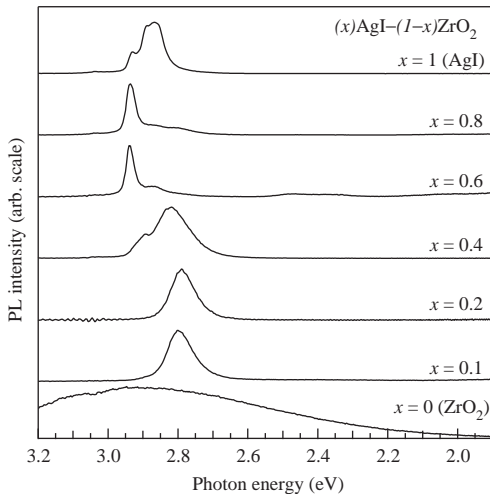


Fig. 2. The PL spectra for different  $(x)\text{AgI}-(1-x)\text{ZrO}_2$  composites at 12 K.

in comparison with other AgI-based composites [1], which may be due to preferred-orientations.

The PL spectra for different  $(x)\text{AgI}-(1-x)\text{ZrO}_2$  composites at 12 K are shown in Fig. 2. The excitation laser fluence  $I_{\text{ex}}$  was  $0.066 \text{ mJ/cm}^2$ . Pristine  $\text{ZrO}_2$  shows a broad PL band centered at about 2.9 eV. The PL peak energy depends on the excitation photon energy  $E_{\text{ex}}$ , as shown in Figs. 3(a) and (b). Adding small amount ( $0.1 \leq x \leq 0.2$ ) of AgI, the intensity of the broad PL band decreases extremely, and a new PL band appears at about 2.80 eV. At  $x = 0.4$ , two PL bands appear at 2.89 and 2.83 eV. On further adding AgI ( $0.6 \leq x \leq 0.8$ ), another new sharp PL band appears at 2.94 eV, accompanying by some weak PL bands at its lower energy side. The 2.94 eV band is assigned to the radiative decay of free excitons (FE) in AgI domain [3]. At  $x = 1$ ,

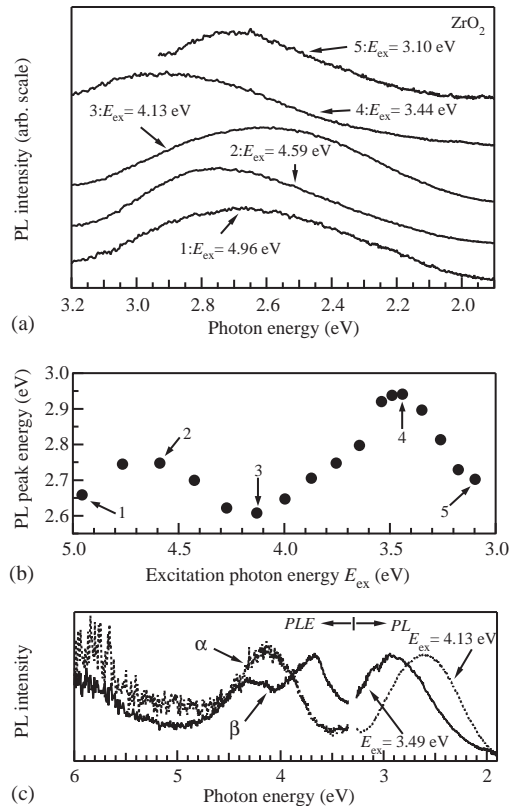


Fig. 3. (a) The PL spectra of pristine  $\text{ZrO}_2$  excited with various  $E_{\text{ex}}$  at 13 K; (b) the PL peak energy plotted against  $E_{\text{ex}}$ ; (c) the PL and PLE spectra for pristine  $\text{ZrO}_2$  at 13 K.

namely, pristine AgI, besides the free exciton emission, more intense PL bands grow at 2.89 and 2.86 eV. These intense PL bands are assigned to radiative decays of excitons trapped around defects and grain boundaries in AgI specimen.

In pristine  $ZrO_2$  ( $x=0$ ), we have found that the PL intensity peak energy depends on  $E_{ex}$ , as shown in Fig. 3(a). The PL intensity peak energy is plotted against  $E_{ex}$  in Fig. 3(b). It is noted that each PL spectrum is considerably Stokes-shifted, which indicates that there are different localized electronic states in the energy gap (5.8 eV) of  $ZrO_2$ . The PL and PL excitation (PLE) spectra are also shown in Fig. 3(c). The PLE curve  $\alpha$  is monitored at 2.99 eV, which corresponds to the PL intensity peak energy for the excitation  $E_{ex}=3.49$  eV, while the PLE curve  $\beta$  is monitored at 2.53 eV which corresponds to the PL intensity peak energy for the excitation  $E_{ex}=4.13$  eV. The PLE spectra ascertain the existence of the luminescent localized electronic states in the energy gap. Since the PL intensity of  $ZrO_2$  was decreased remarkably by adding AgI, as shown in Fig. 2, such luminescence centers may be at  $ZrO_2$  particle surfaces.

The temperature dependence of PL spectra for different  $(x)AgI-(1-x)ZrO_2$  composites was measured. The results are shown in Figs. 4(a) and (b). Each spectrum is normalized in intensity at each maximum. In small  $x$  range ( $0.1 \leq x \leq 0.2$ ), with increasing temperature, the 2.80 eV band is considerably weakened and almost disappears above about 100 K. The broad PL band observed at 99 K may arise from  $ZrO_2$ . However, the PL spectral shape above 2.85 eV is affected by the optical absorptions due to AgI [3]. At  $x=0.4$ , the PL intensity of the 2.83 eV band decreases, while the PL intensity of the 2.89 eV band increases in comparison with that of the 2.83 eV band, with increasing temperature. It suggests that phonon-assisted reverse transition from the 2.83 eV luminescence center to the 2.89 eV luminescence center occurs. In large  $x$  range ( $0.6 \leq x \leq 0.8$ ), with increasing temperature, free exciton emission decreases in intensity, while another PL band appears at 2.90 eV. This indicates that the 2.90 eV band arises from radiative decay of excitons trapped around thermally ionized defects or thermally ionized impurities.

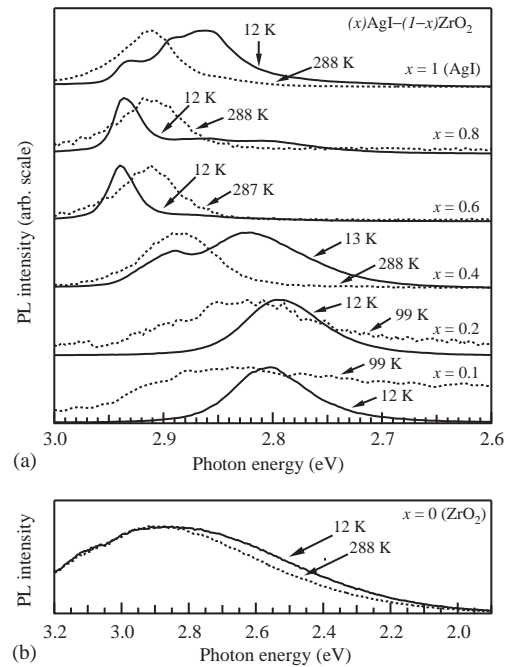


Fig. 4. The temperature dependence of the PL spectra: (a) for different  $(x)AgI-(1-x)ZrO_2$  composites; (b) for pristine  $ZrO_2$ .

Figs. 5(a) and (b) show the  $I_{ex}$  dependence of the PL spectra for different  $(x)AgI-(1-x)ZrO_2$  composites at 12 K. Each spectrum is normalized in intensity at each maximum. Labels, I and W, indicated by the curves denote intense ( $\geq 1.0 \text{ mJ/cm}^2$ ) and weak ( $\leq 0.1 \text{ mJ/cm}^2$ ) excitations, respectively. For small  $x$  region ( $\leq 0.2$ ), the PL component below 2.80 eV saturates at intense excitation, which indicates that the luminescence center giving this PL component is limited in number, though it has high quantum yield. We note the  $x$  dependence of the spectra for weak excitation. With adding AgI, the 2.80 eV band shifts to 2.78 eV at  $x=0.2$  and, with further adding AgI, it shifts to 2.81 eV at  $x=0.4$ . At both  $x=0.6$  and 0.8, the band remains as a shoulder of AgI-related PL bands. Since adding AgI to  $ZrO_2$  induces the oxygen defects,  $Zr_{1-x}Ag_xO_{2-3x/2}(V_O)_{3x/2}$  [5], the shift may be connected with the change in the electronic states at AgI/ $ZrO_2$  interfaces. On further adding AgI, the shoulders at 2.94 and 2.86 eV become prominent.

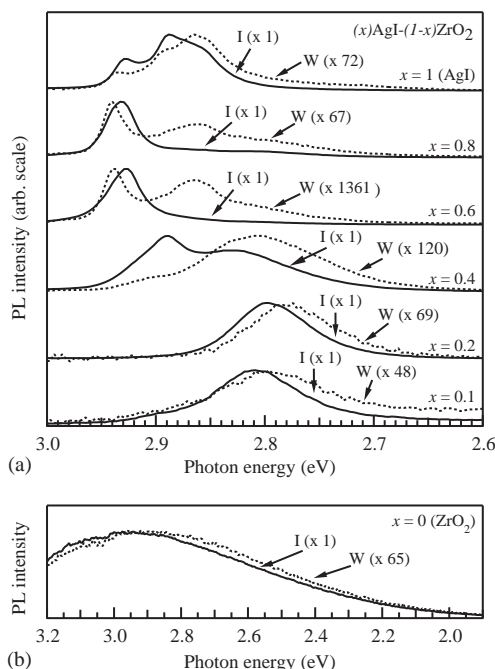


Fig. 5. The  $I_{ex}$  dependence of the PL spectra: (a) for different  $(x)\text{AgI}-(1-x)\text{ZrO}_2$  composites; (b) for pristine  $\text{ZrO}_2$  at 12 K.

The spectral transition with adding AgI is explained as follows. For small  $x$  region, the free excitons generated in AgI domain collides frequently with AgI surfaces, and they are trapped at AgI/ZrO<sub>2</sub> interfaces, creating bound excitons. With increasing  $x$ , the size of AgI domain increases and free excitons are able to propagate in a long distance. Therefore, before trapping at AgI/ZrO<sub>2</sub> interfaces, a part of free exciton decays spontaneously with generating the 2.94 eV luminescence, and other part of free exciton is trapped at crystal defects and impurities within AgI domain. The radiative decay of these trapped excitons generates the 2.93 and 2.86 eV luminescence.

Besides the above PL properties, we have found also a reversible photo-induced PL spectral change in the present AgI-ZrO<sub>2</sub> composites at room temperature. One of the results is shown in Fig. 6, as a typical example. After fully irradiating with CW 325 nm laser light in an evacuated specimen chamber for 10 min, the specimen shows a broad PL band at 2.57 eV. Oxygen gas is then

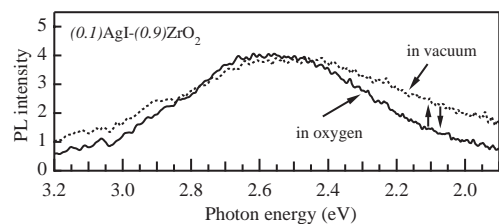


Fig. 6. Reversible photo-induced PL spectral change of  $(0.1)\text{AgI}-(0.9)\text{ZrO}_2$  composite at 295 K.

introduced into the specimen chamber and, with increasing irradiating time, the PL component below 2.45 eV decreases in intensity. Through many successive experiments, it is found that such spectral changes appear repeatedly. The observed spectral changes may originate from excitation-energy exchange between the photo-induced oxygen vacancies on ZrO<sub>2</sub> particle and AgI. The spectral transitions yield materials for optical sensor devices.

In summary, we have studied the PL properties of  $(x)\text{AgI}-(1-x)\text{ZrO}_2$  ( $0 \leq x \leq 1$ ) composites. The PL spectra have shown well the behavior of free and trapped excitons at AgI/ZrO<sub>2</sub> interfaces where Ag<sup>+</sup> ions may move with high-ionic conductivity. The specimen fabrications using different starting-material ZrO<sub>2</sub> powders and more detailed studies are now in progress.

This work is supported by a Grant-in-Aid for Scientific Research from the Ministry of Education, Science, Sports, Culture and Technology, Japan. This work is partially supported by Interdisciplinary General Joint Research Grant for Nihon University.

## References

- [1] S. Mochizuki, F. Fujishiro, J. Phys.: Condens. Matter 15 (2003) 5057.
- [2] M.C.R. Shastry, K.J. Rao, Solid State Ionics 51 (1992) 311.
- [3] S. Mochizuki, F. Fujishiro, J. Phys.: Condens. Matter 16 (2004) 3239.
- [4] F. Fujishiro, S. Mochizuki, in preparation.
- [5] F.A. Kröger, H.J. Vink, Solid State Phys. 3 (1956) 307.



Available online at [www.sciencedirect.com](http://www.sciencedirect.com)



Journal of Luminescence 112 (2005) 267–270

JOURNAL OF  
LUMINESCENCE

[www.elsevier.com/locate/jlumin](http://www.elsevier.com/locate/jlumin)

# The reversible UV-laser-light-induced spectral change and origin of the 2.4 eV luminescence band in SrTiO<sub>3</sub>

Shosuke Mochizuki\*, Seiko Minami, Fumito Fujishiro

Department of Physics, College of Humanities and Sciences, Nihon University, 3-25-40 Sakurajosui, Setagaya-ku, Tokyo 156-8550, Japan

Available online 24 November 2004

---

## Abstract

In order to clarify the origin of the 2.4 eV luminescence band in SrTiO<sub>3</sub>, as-grown and annealed SrTiO<sub>3</sub> single crystals are irradiated with a continuous-wave ultraviolet laser light ( $\lambda = 325$  nm) in different atmospheres at room temperature. Under the laser light irradiation in a vacuum, the 2.4 eV luminescence band grows with increasing irradiation time, while it returns to the original weak-luminescence state under the same laser light irradiation in oxygen gas. The excitation-intensity, temperature and time dependences of the photoluminescence spectra are also measured for the crystals. All the results indicate that the 2.4 eV luminescence band arises not from intrinsic self-trapped excitons but from extrinsic excitons trapped around oxygen defects. Near-band-edge emissions have been observed, for the first time, at 3.2 and 2.9 eV under intense excitation.

© 2004 Elsevier B.V. All rights reserved.

PACS: 71.35.-y; 78.55.-m; 82.50.-m; 61.72.-y

Keywords: Quantum paraelectric state; Photo-induced defects

---

A large number of the optical studies have been devoted to clarify the quantum paraelectric state in strontium titanate (SrTiO<sub>3</sub>). Grabner [1] measured the photoluminescence (PL) properties of doped and undoped SrTiO<sub>3</sub> crystals, and observed a near-infrared luminescence band around approximately 1.6 eV and a visible luminescence band

around 2.4 eV. These PL bands were Stokes-shifted considerably. He assigned them to intrinsic defects or intrinsic excitons. Recently, Hasegawa et al. [2] measured the optical absorption and PL properties of SrTiO<sub>3</sub> crystal. They assigned the Stokes-shifted long-lasting luminescence around 2.4 eV to the radiative decay of intrinsic self-trapped excitons. However, many metal oxides display the similar visible PL, which are related to oxygen defects [3–6]. Unfortunately, such oxygen defect effect has been accorded too low evaluation in the optical study of SrTiO<sub>3</sub> and it has led many researchers

---

\*Corresponding author. Tel.: +81 3 5317 9771; fax: +81 3 5317 9771.

E-mail address: [motizuki@physics.chs.nihon-u.ac.jp](mailto:motizuki@physics.chs.nihon-u.ac.jp)  
(S. Mochizuki).

astray. Very recently, we have observed that the 2.4 eV luminescence band of  $\text{SrTiO}_3$  grows under a continuous wave (CW) 325 nm-laser-light irradiation in a vacuum, while it disappears under the same laser light irradiation in oxygen gas [7]. It was found that the observed phenomenon relates closely to the creation and annihilation of oxygen defects under the laser light. Taking account of the oxygen defects in real  $\text{SrTiO}_3$  crystals [8–10], the PL properties of  $\text{SrTiO}_3$  should be now restudied in detail. In the present paper, we report the PL properties and reversible photo-induced spectral change of as-grown and annealed  $\text{SrTiO}_3$  single crystals.

$\text{SrTiO}_3$  single crystals were grown by the Verneuil method. As-grown crystals are dark blue and they become transparent by annealing in an appropriate atmosphere. During CW 325 nm laser-light irradiation, we have measured the PL spectra of these as-grown and annealed crystals as a function of irradiation time  $t_{\text{ir}}$ . Fig. 1 shows the photo-induced PL spectral change of the as-grown  $\text{SrTiO}_3$  crystal at room temperature in a vacuum as a function of  $t_{\text{ir}}$  (in min). As seen in this figure, the initial PL spectrum ( $t_{\text{ir}} = 0$ ) is very broad, and it has an intensity peak at about 2.8 eV and two faint kinks at about 2.4 and 2.15 eV. With increasing  $t_{\text{ir}}$ , the intensity increases, growing the PL component below 2.8 eV. With  $t_{\text{ir}}$  increasing further, the rate of the spectral change becomes decreased. The spectrum at  $t_{\text{ir}} = 0$  min is rescaled,

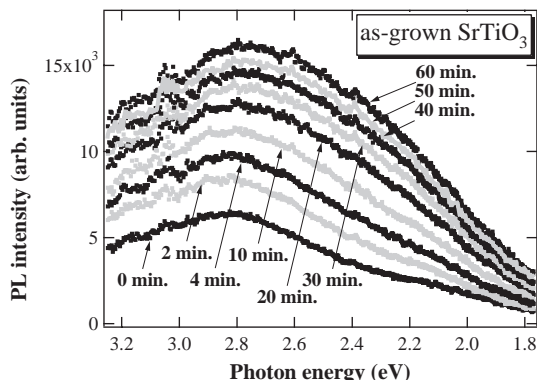


Fig. 1. The CW 325 nm laser light-induced spectral change of an as-grown  $\text{SrTiO}_3$  crystal at room temperature in vacuum. The  $t_{\text{ir}}$  is given in min.

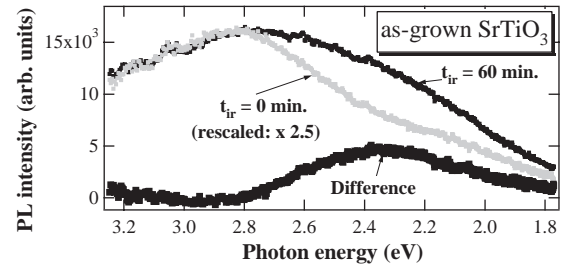


Fig. 2. The CW 325 nm laser light-induced PL component of an as-grown  $\text{SrTiO}_3$  crystal at room temperature.

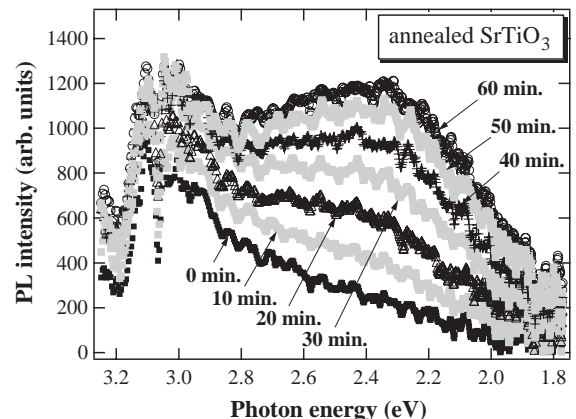


Fig. 3. The CW 325 nm laser light-induced spectral change of an annealed  $\text{SrTiO}_3$  crystal at room temperature in vacuum. The  $t_{\text{ir}}$  is given in min.

and then a difference between the spectrum at  $t_{\text{ir}} = 60$  min and the rescaled spectrum is calculated, which is shown in Fig. 2. This figure shows clearly that a broad PL band grew at 2.4 eV under 325 nm laser light irradiation in a vacuum. Fig. 3 shows the photo-induced PL spectral change of the annealed  $\text{SrTiO}_3$  crystal at room temperature in a vacuum. It is noted that the annealing treatment reduces the PL intensity to about one-tenth. The PL component below 2.8 eV grows with increasing  $t_{\text{ir}}$ . With  $t_{\text{ir}}$  increasing further, the rate of the spectral change becomes decreased. As done for the results of the as-grown crystal, the difference spectrum is also calculated, which is given in Fig. 4. It indicates clearly that a broad PL band of the annealed crystal grew at 2.4 eV under 325 nm laser light irradiation in a vacuum. The same spectral change in the 2.4 eV band was observed

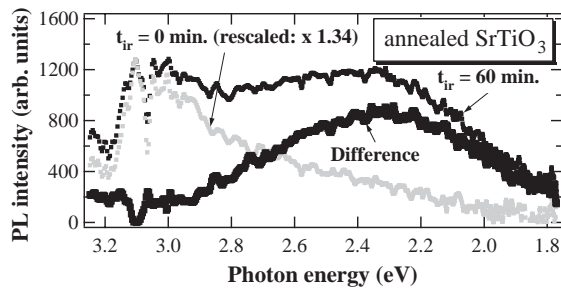


Fig. 4. The CW 325 nm laser light-induced PL component of an annealed  $\text{SrTiO}_3$  crystal at room temperature.

also at 12 K in our previous study [7]. As well as the as-grown crystal, it is found, under the same laser light irradiation in oxygen gas, the 2.4 eV band disappears, returning to the original weak PL state. Since the 325 nm laser light never dissociates directly free  $\text{O}_2$  molecule, the observed spectral changes arise from the photo-induced associative detachment and photo-induced dissociative adsorption of  $\text{O}_2$  molecules near the  $\text{SrTiO}_3$  surfaces [6].

We have studied the PL spectra of the as-grown and annealed  $\text{SrTiO}_3$  crystals at 13 K as a function of excitation laser fluence of the third harmonics ( $\lambda = 355 \text{ nm}$ ) of a  $\text{Nd}^{3+}$ -YAG laser. The results are shown in Figs. 5 and 6. We have confirmed that, unlike CW 325 nm laser light, the pulsed 355 nm laser light cannot induce any reversible spectral change even at  $14 \text{ mJ/cm}^2$ . At the lowest laser fluence, both crystals exhibit only the intense 2.4 eV band. However, the center energy for the as-grown crystal is slightly smaller than that for the annealed crystal. We compare the PL spectra observed at  $4 \text{ mJ/cm}^2$ , before and after annealing. The annealed crystal displays more intense 2.4 eV luminescence than that for the as-grown crystal. This may be due to decrease in the number of non-radiative trap by the annealing treatment. With increasing laser fluence, two new PL bands appear at 3.2 eV, which is near indirect gap of  $\text{SrTiO}_3$  and at 2.9 eV. On the contrary to the 2.4 eV band, the 3.2 and 2.9 eV bands for the as-grown crystal are more intense than those of the annealed crystal. This indicates that the 3.2 eV luminescence and 2.9 eV one are enhanced by oxygen defects. As seen from Fig. 5, with increasing laser fluence, the 2.4 eV band for the as-grown crystal grows and

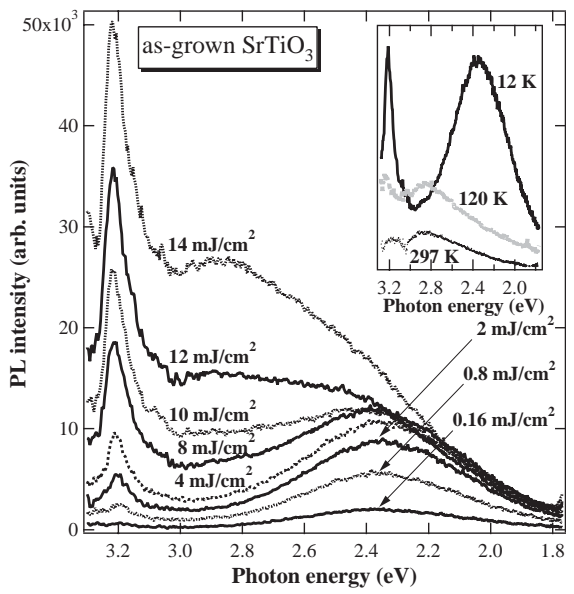


Fig. 5. The excitation laser intensity dependence of the PL spectra of an as-grown  $\text{SrTiO}_3$  crystal at 12 K. The temperature dependence of the PL spectrum is shown in the inset.

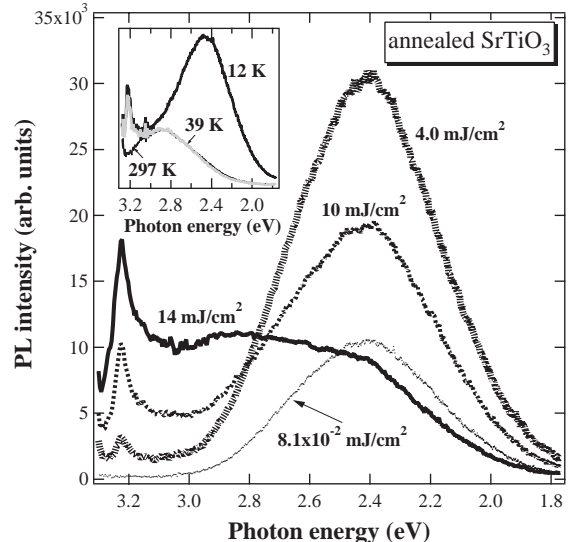


Fig. 6. The excitation laser intensity dependence of the PL spectra of an annealed  $\text{SrTiO}_3$  crystal at 12 K. The temperature dependence of the PL spectrum is shown in the inset.

then becomes saturated at  $8 \text{ mJ/cm}^2$ , while the 3.2 and 2.9 eV bands continue to grow without any saturation. As seen in Fig. 6, the PL intensity of the 2.4 eV band for the annealed crystal increases

also with increasing laser fluence, and then it reaches a maximum at  $4\text{ mJ/cm}^2$ , while the 3.2 and 2.9 eV bands continue to grow without displaying any maximum. Besides these measurements, the PL spectra were measured at different temperatures between 12 and 297 K. Of them, the PL spectra at 12, 120 and 297 K for the as-grown crystal are given in the inset of Fig. 5, and the PL spectra at 12, 39 and 297 K for the annealed crystal are given in the inset of Fig. 6. As seen from these insets, the 3.2 and 2.9 eV bands grow deteriorating the 2.4 eV band with increasing temperature. The 2.4 eV band observed for the as-grown and annealed crystals disappeared at 120 and 39 K. The 3.2 eV band becomes weak and broad with increasing temperature. The 2.9 eV band remains even at room temperature. We have also measured the time-resolved spectra and found that the 2.4 eV luminescence has long lifetime ( $\geq 1\text{ ms}$ ), while both the 3.2 luminescence and the 2.9 eV one have short lifetime ( $\ll 50\text{ ns}$ ), at 12 K [7].

Finally, the experimental results obtained in the present study are summarized and discussed as follows. Since the PL intensity of the 2.4 eV band is affected considerably by oxygen defects and it saturates under intense excitation, the 2.4 eV band is assigned to the radiative decay of extrinsic excitons trapped around oxygen defects. The excitation intensity dependences of the PL shown in Figs. 5 and 6 indicate that, with increasing laser fluence, the 3.2 and 2.9 eV bands grow deteriorating the 2.4 eV band. This intensity relation among these PL bands at 2.4, 3.2 and 2.9 eV with increasing excitation intensity may arise from two causes: (1) finite number of the 2.4 eV luminescence centers, and (2) electron–hole recombination enhanced with higher laser fluence. Since the recombination rate increases with increasing carrier density, the near-band edge emissions at 3.2 and 2.9 eV increase linearly with increasing laser fluence, while the rate of electron (including hole) migration to the 2.4 eV luminescence centers decreases with increasing laser fluence. The excitation-intensity and temperature dependences of the 3.2 and 2.9 eV bands also indicate that two PL bands occur from the same origin. We measured also the PL excitation (PLE) spectrum for the 2.4 eV band and found a sharp

PLE edge at 3.26 eV. This edge corresponds well to the indirect gap of  $\text{SrTiO}_3$ . Generally, an indirect-gap-type semiconductor crystal does not exhibit intense PL. However, some impurities and crystal defects activate the PL of indirect excitons, exhibiting intense PL band near band edge. Therefore, the intense PL at 3.2 and 2.9 eV may be assigned to the radiative decay of indirect excitons affected by oxygen defects, creating phonons. The energy difference ( $271\text{ cm}^{-1}$ ) between the PLE edge and the peak energy of the 3.2 eV band is close to the transverse optic (TO) phonon frequency [11]. Thus, the 3.2 eV band is assigned to the one TO phonon sideband, while the broad 2.9 eV band is also assigned to a continuum consisting of other phonon sidebands.

## Acknowledgements

This work is supported by a Grant-in-Aid for Scientific Research from the Ministry of Education, Science, Sports, Culture and Technology, Japan. This work is partially supported by Interdisciplinary General Joint Research Grant for Nihon University.

## References

- [1] L. Grabner, Phys. Rev. 177 (1969) 1315.
- [2] T. Hasegawa, M. Shirai, K. Tanaka, J. Lumin. 87–89 (2000) 1217.
- [3] S. Mochizuki, T. Shimizu, F. Fujishiro, Physica B 340–342 (2003) 956.
- [4] Y. Kawabe, A. Yamanaka, E. Hanamura, T. Kimura, Y. Takiguchi, H. Kan, Y. Tokura, J. Appl. Phys. 88 (2000) 1175.
- [5] S. Mochizuki, H. Araki, Physica B 340–342 (2003) 969.
- [6] S. Mochizuki, T. Nakanishi, Y. Suzuki, K. Ishi, Appl. Phys. Lett. 79 (2001) 3785.
- [7] S. Mochizuki, S. Minami, F. Fujishiro, J. Phys.: Condens. Matter., submitted for publication.
- [8] S. Kimura, J. Yamauchi, M. Tsukada M, Phys. Rev. B 51 (1995) 11049.
- [9] V.E. Henrich, G. Dresselhous, H.J. Zeiger, Phys. Rev. B 17 (1978) 4908.
- [10] R. Astala, P.D. Bristowe, Modell. Simul. Mater. Sci. Eng. 9 (2001) 415.
- [11] R.A. Cowley, Phys. Rev. 134 (1964) A981.